A perturbative model for the feedback cooling of finite temperature Bose gases

Matthew J. Blacker

A thesis submitted for the degree of
Bachelor of Philosophy with Honours in Physics, at
The Australian National University

October, 2020

Declaration

The research presented in this thesis has been completed on the lands of the Ngunnawal and Ngambri people, the traditional owners of the land of the ANU. I acknowledge that this land was stolen and sovereignty was never ceded, and pay my respects to the elders past, present, and emerging.

This thesis is an account of research undertaken between February 2020 and October 2020 at The Department of Quantum Science, Research School of Physics, The Australian National University, Canberra, Australia.

Except where acknowledged in the customary manner, the material presented in this thesis is, to the best of my knowledge, original and has not been submitted in whole or part for a degree at any university.

Matthew J. Blacker
October, 2020

Acknowledgements

I have, for a long time, dreamed of becoming a theoretical physicist and studying the secrets of the universe. As the minutes tick down towards the deadline for this thesis, I realise that somewhere along the way this year that dream became a reality — and there are many people I have to thank for that.

First, to my supervisors Stuart Szigeti and Joe Hope. Stuart, thank you for tolerating my poorly formatted twenty-page long derivations, my "scheduled send" emails, and for constantly challenging my ideas. Joe, thank you for always asking "why", the spontaneous life advice, and the occasional surprises when my headphones are too loud. I've learnt so much from you both, and am genuinely keen to get stuck into the "Future Work" of this thesis (after a short break).

Second, to everyone at the Department of Quantum Science. Thank you Simon, Angela and Ruvi for the insightful discussions and feedback, and Yosri for being terrible at ping pong (and keeping me company when I was working late). Thank you to Zain for always being happy to answer questions and discuss ideas. And thank you to Matt, for being an awesome mentor throughout the last four years, and for convincing me to sacrifice my soul to the gods of feedback cooling.

To my fellow Honours students, in particular Tom, Maddie, Owen and Ben for sharing your music taste (both good and Tom's). And to Cas and Jodie, who've meant I've always had a friend in the physics classroom at ANU.

To my friends at Bruce Hall, for making Canberra home. In particular, to Josh and Jayanth for always having my back, making me laugh and sharing my enthusiasm for this research. And to Rachael, for riding every up and down of this thesis with me.

A special thanks to Caspian Nicholls, Kate Curtis, James Dingley and Rachael Piggott, who I somehow convinced to read this document in its entirety.

To Joseph Audino, for your passion for teaching, and making me believe that I could become a physicist. I hope you can enjoy reading this over a scotch on the rocks.

Finally, to my parents. Thank you for you unwavering support in my education, and always encouraging me to make my dreams a reality.

Abstract

Ultra-cold atomic gases are an ideal platform for precision measurement devices and analogue quantum simulators, which will prove instrumental in unlocking the secrets of quantum gravity and high-temperature superconductivity. However, current experimental techniques cannot cool atomic gases to simulatenously both the low entropies and high particle numbers necessary for these applications. A promising alternative is feedback cooling: using continuous-measurement feedback control to damp out energy fluctuations and cool a gas. So far, feedback cooling has been primarily studied at zero temperature, with the only finite temperature simulation achieved via a computationally expensive numerical method restricted to bosons. This thesis develops a perturbative model for the feedback cooling of a finite temperature condensed Bose gas using Bogoliubov theory, with the aim of deriving dynamic equations for the system that are both analytically tractable, and allow for fast numerical prototyping of new feedback control schemes. Using the measurement-feedback model of Szigeti *et al.* [1, 2], we derive a low temperature perturbative model for feedback cooling of a Bose gas in an arbitrary trapping and control potential. Using this general model, we then derive a model for the dynamics of a Bose gas in a hard box trap being cooled with an energy damping control. We complete preliminary simulations of this model in the no-backaction conditional measurement limit, damping out density fluctuations in a gas of 90% condensate fraction and cooling it to $93.5 \pm 1\%$. We find that, in this limit, the dynamics of the gas are largely independent of number but significantly depend on the inter-particle interaction. We also find an optimal energy damping control strength in this limit. However, our model is not very efficient for simulation, particularly for a large number of particles and measurement strength. As an alternative, we propose an approximation scheme in which steady-state analytic solutions could be obtained from the model. Finally, we propose two methods to develop a Bogoliubov model for the feedback cooling of fermions, which would be the first finite temperature model for the Fermi gas case.

Contents

List of Figures

Chapter 1

Introduction

The experimental realisation of Bose Einstein Condensates (BECs) at the end of the 20th century [3, 4, 5] sparked an explosion in the study of ultra-cold atom physics. In the years since, ultra-cold atoms of both Bose and Fermi species have found uses in a broad range of disciplines of physics: as qubits in quantum computers [6], completing analogue studies of quantum field theory in curved spacetime [7], and as platforms to build Josephson junctions [8]. Perhaps the most exciting future application of ultra-cold Bose gases is to enhance the precision of inertial measurements made by atom interferometers [9], measurements necessry to complete tests of theories of quantum gravity [10]. On the other hand, ultra-cold Fermi gases have the potential to be analogue quantum simulators, enabling the study of exotic quantum phenomena including high temperature superconductivity [11, 12].

However, atom interferometers and analogue quantum simulators are yet to be applied to their full potential. This is because the most common method for cooling atomic gases to the ultra-cold ($< 1\mu$ K) regime a) discards most of the atoms which are being cooled and b) relies upon the scattering properties of atoms, which are species dependent [13]. In this thesis, we consider an alternative method which does not have these limitations: *continuous-measurement feedback control*.

In Section 1.1, we review in detail the application of atom interferometers as precision measurement devices, and the potential improvement offered by larger atom number BECs. Similarly, in Section 1.2 we discuss the potential use of ultra-cold Fermi gases as anologue quantum simulators. To understand why these applications are yet to be realised, we summarise current cooling techniques and their inherent limitations in Section 1.3. We then present feedback cooling in Section 1.4 as an alternative procedure to overcome these challenges. Finally, having motivated an interest in feedback cooling and the study of ultra-cold atomic gases, we outline the structure of this thesis in Section 1.5.

1.1 Ultra-cold Bose gases: a platform for precision measurement devices

It is impossible (even for theoretical physicists) to construct a complete description of the universe without some measurement of the surrounding world, whether it be of length, time, or any other quantity. From the fruitless hunt for a luminous aether by Michelson and Morley [14], to the first observation of gravitational waves in 2016 [15],

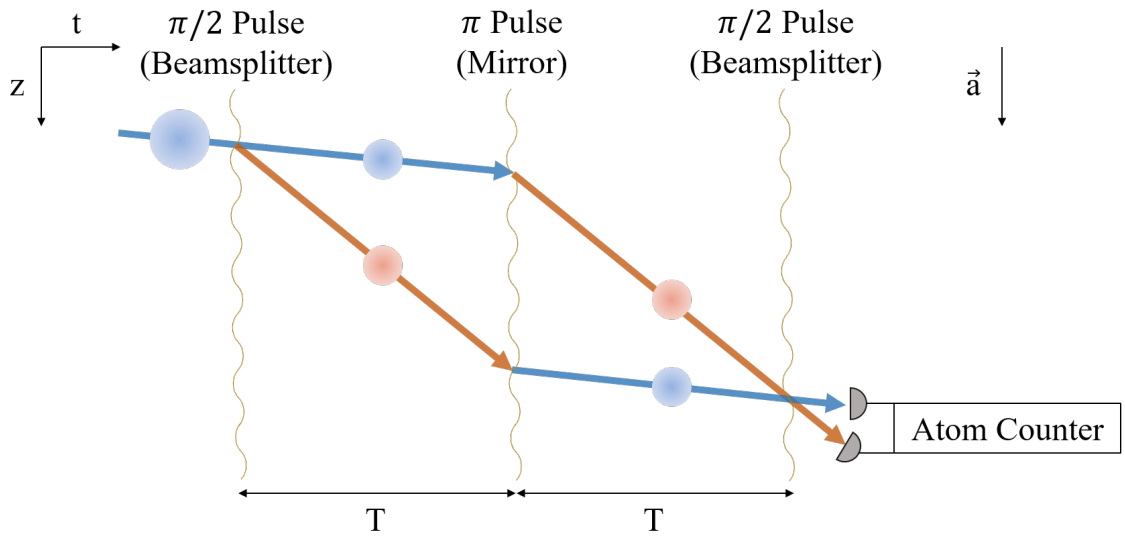

Figure 1.1: Space-time diagram of an atom interfereometer in the Mach-Zender configuration. A colleciton of atoms is hit with a light pulse, so that some of the atoms travel through a different region of the accelerating field $\vec{a}$. After time T, a second pulse provides a momentum kick to the other atoms, and a third pulse recombines the atom, before detection at an atom detector. For a reader unfamiliar with space-time diagrams, see Ref. [17] for an introduction.

many ground-breaking discoveries in physics have been made using precise measurements of distance with optical interferometers. Fundamentally, an interferometer measures the phase shift of two waves which have interfered after travelling through two different paths in space, guided by beamsplitters which separate the light based on its polarisation.

The discovery that matter can also behave as a wave - first proposed by De Broglie [16] - has inspired the development of interferometers with a matter-wave source: *atom interferometers*. We provide a basic schematic for an atom interferometer in a Mach-Zender configuration in Figure 1.1. In an atom interferometer, a coherent laser is the analogue for the beamsplitter, shining upon a collection of atoms under some free acceleration $\vec{a}$.[1] This laser light stimulates either the absorption or emission of a photon, giving the atom a momentum kick between one of two states. Two laser pulses, separated by a time T, guide the two states through different paths in space-time, before a third laser pulse recombines the two states. When the atoms recombine, the phase shift of their interfered waves contains information about the accelerating field they passed through.[2]

1.1.1 Applications of precision measurement

Atom interferometers using Bose gas sources have the potential to be applied as *inertial sensors*; devices which precisely measure accelerations and angular velocities [9]. These inertial sensors have the potential to advance fundamental physics by completing tests of the *weak equivalence principle*. The weak equivalence principle states that a body's

[1] In a *gravimeter*, the atoms are in free-fall, and the acceleration g is due to the gravitational field.

[2] For a more detailed introduction to the mechanics of atom interferometers, the interested reader should consult a text on atom optics, such as Ref. [18].

inertial mass m_i (the mass measured by resistance to acceleration) and gravitational mass m_g (the mass measured by gravitational attraction to other bodies) are equivalent [17]. Whilst a key tenant of Einstein's theory of general relativity in four space-time dimensions, the equivalence principle theoretically breaks down in a higher number of dimensions (i.e. $m_g/m_i \neq 1$) [19]. Some theories of quantum gravity, such as string theory [20], require more than four space-time dimensions; so measuring violations of the weak equivalence principle could be used to rule in or out candidate theories of quantum gravity. The challenge, however, is that these violations are expected to be of the order of 10^{-18} [21] — well beyond the 10^{-10} achieved by existing experimental techniques [22]. One solution is atom interferometers using a BEC as the matter wave source: at experimentally achievable sizes, they are predicted to observe changes in gravity necessary to measure violations in m_g/m_i of the order of $10^{-15} - 10^{-17}$ [23]. Whilst this is still below the precision desired, creating Bose gases of even larger number is a possible way to overcome that final hurdle (for reasons that will be discussed in Section 1.1.2).

Atom interferometers also have the potential to be a powerful tool in a number of other low-energy tests of theories of quantum gravity — for a detailed review, see Ref. [10].[3]. Beyond the realms of quantum gravity tests, atom interferometers have possible applications to fundamental physics in the space-based detection of gravitational waves [23, 27] and refining the definition of the kilogram [28].

Inertial sensors also have a number of potential practical applications outside of fundamental physics. In particular, due to their ability to make precise measurements of gravity gradients [29, 30], atom interferometers can make accurate density measurements of the Earth's crust. These density measurements are indicative of ore deposits which could be used to optimise mineral discovery for resource companies, and are useful for models of plate tectonics, magma flows, and other areas of geophysics. Devices mounted in aeroplanes have demonstrated the feasibility of atom interferometry for these studies [31, 32]. Measurements of gravity gradients are also a powerful tool in climate modelling: they have already been used to measure the melting rate of icesheets in Greenland [33] and study variation in groundwater levels in the Murray-Darling basin [34]. Additionally, the precise measurements of accelerations possible with an atom interferometer have been proposed to improve navigation technologies [35, 36], with applications to navigation of aircraft [37] and missiles [38].

1.1.2 Atom interferometry and Bose-Einstein Condensation

Whilst exciting and diverse in scope, these applications require a precision beyond that of the current generation of atom interferometers. There are three key limits to the precision of an atom interferometer:

1. **Particle number**. Each measurement of the number of particles is uncorrelated, so the sensitivity of the measurement of phase Φ is limited by shot noise. Shot noise is proportional to the inverse square root of the number of particles N (i.e. $\Delta\Phi \propto 1/\sqrt{N}$) [39], so increasing particle number increases the precision of the device.

[3] Particularly exciting are two independent proposals [24, 25] that use the interaction between two adjacent atom interferometers to measure quantum mechanical contributions to the gravitational force between masses. This effect is 10^{10} times smaller than that of a weak equivalence principle violation, so would require even larger Bose gas sources [26].

2. **Separation time**. A longer separation time T allows for a greater accumulation of phase, so that the relative error $\Delta\Phi/\Phi$ is smaller [40].[4]

3. **Momentum distribution width**. A narrower distribution of atom momenta means that the light pulses can give a momentum kick to more of the atoms [42]. This increases the contrast, and thus sensitivity, of the interferometer.

Atom interferometry is presently completed with (relatively) hot atoms, in the $10-100\mu K$ temperature regime [30, 32]. However, these hotter sources have a broad momentum width[5] and low coherence times. Since their experimental realisation at the end of the 20th century [3, 4, 5], BECs have emerged as a possible alternative source for atom interferometers. We review BECs in more detail in Chapter 2; but essentially, BECs are a collection of ultra-cold (usually in the nanokelvin regime) atoms that are nearly all in one low energy state. Crucially, BECs have a high coherence time and a narrow momentum width because of their low temperature [43]. They are to cold atoms what lasers are to light.

The disadvantage of BEC sources is that they are 25-50 times smaller in atom number than hotter Bose gases. In the shot noise limit, $\Delta\Phi \propto 1/\sqrt{N}$, so this size difference reduces the sensitivity of an atom interferometer by a factor of 10. The relatively small size of BECs is a consequence of existing cooling techniques being non-number conserving, as will be elaborated upon in Section 1.3. However, by generating larger BEC sources, it will be possible to build atom interferometers with the higher sensitivity needed for weak equivalence principle tests and other inertial sensing applications.

1.2 Ultra-cold Fermi gases: a platform for analogue quantum simulation

Ultra-cold Fermi gases, on the other hand, have the potential to advance our ability to simulate many-body quantum systems. The ability of computers to simulate classical systems has proved a powerful tool for theoretical modelling in physics, biology, and numerous other disciplines. However, classical computers can only simulate very small quantum mechanical systems, because the complexity of a quantum system scales exponentially with its size. Simulation of fermionic systems is particularly challenging; the anti-symmetric nature of fermionic wavefunctions leads to oscillatory integrals which cannot easily be solved numerically [44].

Feynman [45] proposed a simple solution: why not simulate quantum systems on a platform that is itself quantum? Lloyd [46] subsequently proved[6] that a set of qubits (quantum bits) can overcome the scaling problem, and perform a *digital* simulation of any Hamiltonian: functioning as a *quantum computer*. Whilst the development of a universal quantum computer is a broad and active area of research (see Ref. [48] for a

[4] This is a particularly strict limit for some applications, such as in aircraft based navigation, where the devices have to be very compact [36, 41].

[5] This simply follows from hotter sources being at a higher temperature, and thus having a wider energy distribution.

[6] Technically, Lloyd's proof was only for local systems. However, most systems of interest fall into this class, and recent research has extended the result to other classes of Hamiltonians [47].

detailed introduction), developments in useful[7] quantum computers has been hindered by the short lifetimes of qubits [50, 51] and difficulties in scaling beyond $\sim$ 50 qubits [49]. An alternative, more immediately achievable, route to quantum simulation is to construct a device which mimics the Hamiltonian of a system of interest. This process is known as *analogue quantum simulation* — for a more detailed introduction, see Ref. [52].

Ultra-cold atoms in lattices are an ideal platform for analogue simulation. Firstly, they are a relatively pure system: that is, they are free of unwanted dopants or defects, and easily isolated from the environment [11, 12, 53]. Secondly, they can be easily trapped and controlled in a variety of optical potentials [54, 55, 56] and their interaction strength effectively freely manipulated by a Feshbach resonance [57, 58], meaning that their Hamiltonian can be easily controlled. Finally, it is feasible to observe and study the dynamics of an ultra-cold atomic gas, as there are a swathe of measurement techniques for both Bose [59, 60] and Fermi [61, 62] species.

It is theoretically possible for ultra-cold Bose [63] and Fermi [64] atoms, acting as an analogue quantum simulator, to realise their respective forms of the *Hubbard model*. The Hubbard model describes particles in a periodic lattice, where particles hop between fixed sites, and can interact with particles at the same fixed point. Further details of the Hubbard model are not relevant to this thesis[8], but what is crucial is that the Hubbard model for fermions has emerged as a leading candidate to decribe the behaviour of high-temperature superconductors [69, 70]. High temperature superconductivity is presently unexplained by the standard Bardeen-Cooper-Schieffer theory of superconductivity [71].[9] Being able to understand, and ultimately stably[10] create, high-temperature superconductors would advance fields as diverse as quantum computing [49, 50] and Maglev train technology [74]. To that end, analogue quantum simulations of the Hubbard model using ultra-cold fermions have been proposed to study high-temperature superconductivity [75]. However, these simulations require fermions at an entropy per particle 2-4 times lower than that achievable with current cooling techniques [13]. To understand why this limit exists, we will now review existing cooling techniques for atomic gases.

1.3 Creating ultra-cold atomic gases

To reach the micro- or nano- kelvin regimes required for these diverse applications, a number of procedures are used to cool atomic gases (see Refs. [13] and [76] for a detailed review). The most common approach is to cool gases from room temperature to the microkelvin regime using laser (Doppler) cooling, then reach the nanokelvin regime with

[7] In 2019, Google used a 53-qubit quantum computer to complete a calculation 1000 times faster than possible on the worlds most powerful supercomputer [49]. However, the task completed has no known application.

[8] For more details of the Fermi-Hubbard model, see Hubbard's original paper [65] and the two concurrently published papers deriving the same model [66, 67]. For more details on the Bose-Hubbard model, see Ref. [68].

[9] The standard theory of superconductivity is equivalently derived by Bogoliuobv in Ref. [72]. As will be discussed in Chapter 2, Bogoliubov's perturbative approach is only valid at low temperatures. It is therefore not surprising that the cooper-pair description of superconductivity is insufficient for superconductors at relatively high temperature ($T \approx 90K$).

[10] There has been recent experimental realisation of a superconductor at room temperature ($\sim 15^{\circ}$C) [73]. However, the device in question only enters the superconducting phase at $\sim 10^6$ times atmospheric pressure.

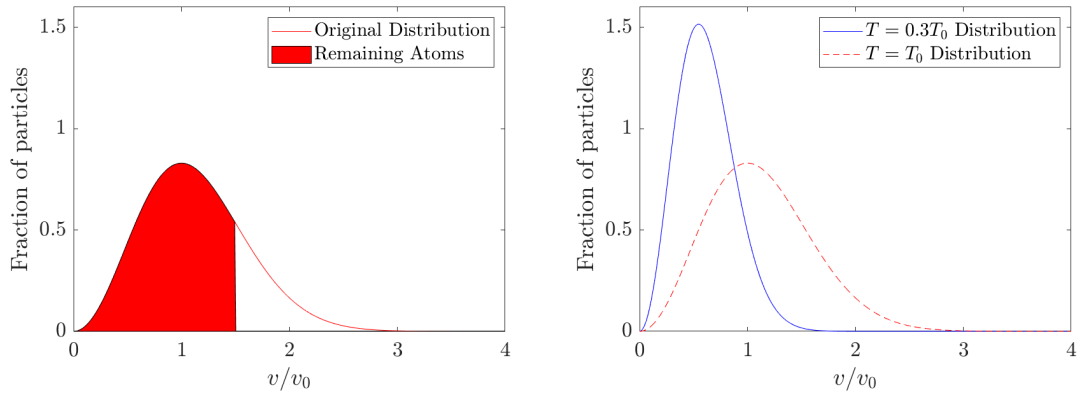

(a) Removing hot tail from $T = T_0$ distribution

(b) $T = T_0$ vs $T = 0.3T_0$ distribution

Figure 1.2: Demonstration of the effect of evaporative cooling for a ensemble of atoms obeying a Maxwell-Boltzmann distribution at $T_0 = mv_0^2/2k_B$, where v_0 is some energy scale. In Figure 1.2a, all particles with $v/v_0 > 1.5$ are removed (for atoms in a trap, this is achieved by lowering the walls of the trap). This removes the hottest $\sim 1/3$ atoms. The remaining atoms collide, redistributing the leftover energy, and obey the new distribution in Figure 1.2b. Note that this lower distribution is narrower, meaning that the distribution of possible energy states is effectively lower - reducing the entropy of the atomic ensemble.

evaporative cooling. This two-stage process achieved the first experimental realisation of BEC [3, 4, 5] and the creation of degenerate Fermi gases [77, 78]. We do not discuss the details of laser cooling here, other than noting it can cool large numbers of atoms ($\sim 10^{10}$) from room temperature to the microkelvin regime with effectively no particle loss (see Ref. [79] for a more detailed review). It is the next stage in the cooling process — evaporating cooling — which is of interest to us.

An evaporative cooling scheme lowers the temperature of a gas by continuously removing the highest energy atoms from the system. The remaining atoms then collide and redistribute the remaining energy, lowering the temperature and entropy of the gas (as in Figure 1.2). These details are sufficient to understand the two key limitations of evaporative cooling[11]. Firstly, it is inherently non-number conserving — up to 99.9% of the atoms are lost from the gas [82] — limiting the capacity of evaporative cooling to produce large atom-number BECs needed for atom interferometry. Secondly, the procedure relies upon strong inter-atomic scattering, so is highly species-dependent. This is particularly problematic for fermions, which do not scatter strongly in the energy regime of evaporative cooling [81].[12] This means that evaporative cooling cannot cool fermions to the low entropies needed for analogue quantum simulations of high temperature superconductivity.

One alternative to evaporative cooling, which is particularly useful for fermions, is sympathetic cooling. In a sympathetic cooling scheme for fermions, a Fermi gas is coupled to a Bose gas that is being cooled. The scattering between the fermions and bosons exchanges heat, simultaneously cooling the fermions. Sympathetic cooling has

[11] A reader interested in a more thorough introduction to evaporative cooling should consult Ref. [80] or Chapter 4.6 of Ref. [81].

[12] Specifically, at low temperatures, s-wave scattering dominates (this will be discussed in more detail in Chapter 2). For fermions, the s-wave cross section at low energies vanishes, as a consequence of the asymmetry of the fermionic wavefunction.

experimentally reached the low microkelvin regime for Fermi gases [83, 84], however cannot overcome the limits of evaporative cooling for fermions for a number of reasons (for a detailed summary, see Ref. [85]). Firstly, it relies upon strong interactions between the Bose and Fermi species being cooled. More critically, it requires continuous cooling of the coupled Bose species, which is typically done by evaporative cooling. In that case, the Fermi gas can only be sympathetically cooled for a short time before the Bose gas is completely depleted. Therefore, the most promising alternative to evaporative cooling for fermions is still constrained by the limits of cooling for bosons.[13]

We are therefore motivated to develop an alternative technique to evaporative cooling; in particular, one which is number-conserving and does not rely upon the scattering properties of the atomic species being cooled.

1.4 An exciting alternative: feedback cooling

In this thesis, we consider *continuous-measurement feedback control* as a promising solution to the limitations of evaporative cooling. In a feedback control scheme, a system is measured to obtain an estimate of the system state. Based on that estimate, an observer then perturbs the system to drive it towards a desired state. We theoretically apply the principle of feedback control to a quantum gas, with the desired state being the ground state. We refer to this control as *feedback cooling*, as the feedback control is driving the gas to its minimum energy configuration and therefore cooling it.

The feedback control of quantum systems has grown into a broad field since emerging three decades ago. A reader interested in a recent, detailed review of quantum control should consult Ref. [86]; here, we focus on the application of quantum control to cold atoms. The first studies were motivated by using BECs as a source for atom lasers, and used perfect knowledge of the system state. In particular, Wiseman and Thomsen developed a single-mode quantum model for a feedback control to damp number fluctuations in a Bose gas [87, 88]. Feedback cooling - specifically using feedback control to reduce the total energy of a Bose gas - was then first introduced by Haine *et al.*, who demonstrated with a mean-field model[14] that a time-dependent feedback control could damp out fluctuations in the density of a Bose gas [89]. Johnsson *et al.* demonstrated the robustness of this model in the presence of experimental factors relevant to the atom laser, such as continuous outcoupling of atoms from the BEC [90].

By assuming perfect knowledge of the system state, these models ignored a crucial effect of quantum mechanics: that measuring a quantum system collapses it into a random state. Thus, in a quantum feedback control scheme, obtaining an estimate of the system state also alters that very state. This effect is termed *measurement backaction*, and in closed-loop quantum feedback control leads to a trade-off between information and unwanted changes to the state.

Wilson *et al.* first demonstrated the effectiveness of feedback cooling whilst accounting for measurement backaction, damping out density excitations of a single (Bose)

[13] Indeed, similar limitations arise for boson-boson sympathetic cooling.

[14] A mean-field model approximates the full quantum state with a classical function. We discuss mean-field theory in more detail in Chapter 2.

atom in a harmonic trap. The authors used the model of Doherty and Jacobs [91], which assumed measurement by an optical wavelength greater than the trap size — an assumption that breaks down for a BEC of more than a few atoms. Szigeti *et al.* developed a full quantum dynamical theory for a BEC under an experimentally realisable measurement of number density [1], and subsequently demonstrated feedback cooling via simulation using a mean-field approximation [2]. This model was then extended to Fermi gases, and feedback cooling completed using a mean-field approximation in a recent Honours thesis by Goh [64]. The full quantum model of Szigeti *et al.* is reviewed in more detail in Chapter 3.

A mean-field approximation of the full quantum dynamical theory only considers the average state, so it ignores a) quantum correlations between possible states and b) the distribution of energy states present at finite (non-zero) temperature. Mean-field models therefore only study feedback cooling of zero temperature energy fluctuations, and neglect the finite temperature effects present in real atomic gases.

The first alternative to mean-field theory used to model the full quantum theory of Szigeti *et al.* was the *number-phase Wigner* (NPW) simulation method developed in Refs. [92, 93]. Essentially, the NPW method randomly samples particles from an initial state distribution, evolves those particles under a full quantum model[15] and then averages the behaviour of those random samples. Hush *et al.* [94] implemented the NPW method to feedback cool a BEC from a zero temperature initial state with quantum correlations, and Taylor [95] used the NPW method to feedback cool a BEC initially in a thermal state. Specifically, Taylor and unpublished work by Goh *et al.* demonstrated that feedback cooling could increase the fraction of atoms in the condensate from $\sim 10\%$ to $\sim 90\%$. Despite these successes, there are three limitations to the NPW method:

1. It is a computationally intensive approach, which makes it inefficient for rapidly characterising how different feedback control schemes behave at finite temperature.

2. It is a completely computational method, so is difficult to obtain intuition for *why* different control schemes have particular behaviours.

3. There is no extension of the NPW method for fermions.

A reader interested in further details of the NPW method should see Ref. [92, 93], but an understanding of the above limitations is sufficient to read this thesis. In particular, these limits motivate developing a finite temperature model for feedback cooled atomic gases that a) is analytically tractable for different feedback potentials and b) can model fermions. The former will allow for the rapid proposal and prototyping of different analytic forms for feedback control, which can then be fully characterised with the NPW method.

A promising approach is the perturbation theory of Bogoliubov, which analytically describes thermal excitations in low (but finite) temperature Bose [96] and Fermi [72] gases. We provide a more detailed introduction to Bogoliubov theory in Chapter 2, but the essential idea is that excitations are treated as perturbations around a mean-field. Using Bogoliubov theory, Wade *et al.* modelled the use of feedback control to damp

[15] Specifically, it evolves the sampled particles under the *stochastic master equation* for the system, such as the full quantum model of Szigeti *et al.* in Refs. [1, 2]. Stochastic master equations will be introduced in detail in Chapter 3.

individual excitations in a Bose gas [97, 98], and Hurst *et al.* modelled the feedback control of excitations induced by measurement backaction [99]. Notably, Wade *et al.* used Bogoliubov theory to develop analytic steady-state solutions for their feedback control. Schemmer *et al.* then used a Bogoliubov approach to model the cooling of a 1D quasi-condensed Bose gas [100]. However, their approach considered a measurement scheme where atoms are removed from the condensate and spatially measured, which is not only experimentally challenging, but is also inherently non-number conserving.

These works demonstrate the capacity of Bogoliubov theory in extending models of feedback control beyond mean-field theory. As a semi-analytic model that works for both bosons *and* fermions, Bogoliubov theory has the potential to overcome the limitations of the NPW method in modelling the feedback cooling of atomic gases. However, it has not yet been used to model feedback cooling in an experimentally feasible measurement scheme, such as phase-contrast imaging [5, 101]. In this thesis, we complete the first investigation into the use of Bogoliubov theory to model the cooling of a Bose gas with feedback control based on a phase-constrast imaging measurement scheme. As well as developing an alternative to the NPW method with possible analytic solutions, this thesis acts as a feasibility test for using Bogoliubov theory to model the feedback cooling of finite temperature Fermi gases.

1.5 Outline of this thesis

The primary aim of this thesis is to derive a model for the feedback cooling of a Bose gas using Bogoliubov theory. Broadly speaking, Chapters 2 and 3 contain the background theory necessary to build our model. Chapters 4 and 5 then focus on derivation and model building. Chapter 6 focuses on preliminary numeric simulation to validate the model. In Chapter 7, we discuss the conclusions from this thesis, and propose avenues for future work.

More specifically, in Chapter 2 we present a pedagogical introduction to the quantum field theory of cold atoms and Bogoliubov theory. We first recap the basics of bosons and fermions, before introducing the quantum field theory needed to understand them. We then introduce bosonic Bogoliubov theory. In Chapter 3, we review conditional measurement theory, and place feedback cooling on an analytic foothold, in order to present the full quantum model of Szigeti *et al.* [1, 2]. Using this conditional measurement theory, we apply the Bogoliubov theory covered in Chapter 2 to develop a low temperature model for the feedback cooling of a Bose gas in an arbitrary control and trapping potential in Chapter 4. We then study this model for specifically the energy damping control in a hard box trap in Chapter 5. Preliminary characterisation of this model is completed in Chapter 6, via numeric simulation in the no-backaction conditional measurement limit. Finally, we review the limits of our model in Chapter 7, and propose future approaches for developing analytic solutions to our model and an equivalent model for Fermi gases.

Chapter 2

Background I: An introduction to cold atom physics

In this chapter, we present a pedagogical introduction to the techniques used in this thesis to model cold Bose gases at non-zero temperature. We begin by summarising the statistical properties of bosons and fermions in Section 2.1. In Section 2.2, we summarise the techniques of quantum field theory necessary to then construct a quantitative model of cold Bose gases in Section 2.3, where we introduce a zero temperature model for these Bose gases. In Section 2.4 we then consider a first approach for modelling Bose gases at finite temperature: symmetry-breaking Bogoliubov theory. This will prepare us to then introduce number-conserving Bogoliubov theory in Section 2.5.

2.1 The statistical mechanics of bosons and fermions

In contemporary particle physics, all fundamental particles are classified as bosons or fermions. This arises out of our understanding of quantum mechanics. Let us briefly recap why, and qualitatively describe the differences between the two.

In classical mechanics, after observing two "identical" particles — those which share each defining property such as charge or mass — we can map out their unique trajectories. Conversely, in quantum mechanics there is always uncertainty in measurement, so an observer cannot continually keep track of two particles. Instead, you have to measure them at some point in time. Therefore, if two particles have the same value for every defining quantum number (and are therefore identical), under measurement these particles are indistinguishable.

To understand the consequences of this seemingly innocuous statement, let us consider the position measurement of two identical particles with positions $\mathbf{r}_1$ and $\mathbf{r}_2$ and wavefunction $\Psi(\mathbf{r}_1, \mathbf{r}_2)$. As the particles are indistinguishable, exchanging their positions cannot change the outcome of the measurement. Therefore, exchanging their position must only change the wavefunction up to a global phase

$$\Psi(\mathbf{r}_1, \mathbf{r}_2) = e^{i\alpha}\Psi(\mathbf{r}_2, \mathbf{r}_1), \tag{2.1}$$

where α is a real constant, so that

$$|\Psi(\mathbf{r}_1, \mathbf{r}_2)|^2 = |\Psi(\mathbf{r}_2, \mathbf{r}_1)|^2 . \tag{2.2}$$

That is, the probability density function of the wavefunction (which is what quantum mechanical observables are defined in terms of), is unchanged under particle exchange. To see what values for α are possible, we can define the permutation operator $\hat{P}$ which exchanges the two particles as

$$\hat{P}\Psi(\mathbf{r}_1, \mathbf{r}_2) = \Psi(\mathbf{r}_2, \mathbf{r}_1). \tag{2.3}$$

Swapping the particles twice obtains the original state, so $\hat{P}^2 = \hat{1}$. Equivalently, $e^{i2\alpha} = 1$, which is solved by $\alpha = 0$ or $\alpha = \pi$. There are therefore two possibilities for our wavefunction:

$$\Psi(\mathbf{r}_1, \mathbf{r}_2) = \pm\Psi(\mathbf{r}_2, \mathbf{r}_1). \tag{2.4}$$

The positive (symmetric) solution describes *bosons*, and the negative (anti-symmetric) solution describes *fermions*. Bosons are particles with integer spin, and fermions have half-integer spin[1]. If $\mathbf{r}_2 = \mathbf{r}_1$, the anti-symmetric solution to equation (2.4) must be zero (i.e. $\Psi(\mathbf{r}_1, \mathbf{r}_2) = 0$). Thus, there is a fundamental difference between bosons and fermions: identical bosons can be in the same state, where as identical fermions cannot. This constraint is known as the *Pauli exclusion principle*. Qualitatively, this constraint is the main reason Fermi gases are more difficult to theoretically study.[2]

The Pauli exclusion principle means that bosons and fermions produce vastly different physics. Using statistical mechanics (specifically the microcanonical ensemble), the average number of non-interacting indistinguishable particles in an energy state ϵ_j can be determined as a function of temperature T (see Chapter 14 of Ref. [39] for a full derivation). Bosons obey the Bose-Einstein distribution

$$\bar{n}_j^{(B)} = \frac{1}{e^{(\epsilon_j - \mu)/k_B T} - 1}, \tag{2.5}$$

and fermions, constrained by the Pauli exclusion principle, obey the Fermi-Dirac distribution

$$\bar{n}_j^{(F)} = \frac{1}{e^{(\epsilon_j - \mu)/k_B T} + 1}. \tag{2.6}$$

Here, μ refers to the chemical potential of the particles and k_B is the Boltzmann constant[3]. A full derivation of equations (2.5) and (2.6) can be found in Chapter 8 of Huang [39]. A comparison of each distribution at a range of temperatures is included in Figure 2.1. In the high temperature limit ($T \gg \epsilon_j/k_B$), both distributions tend to $\bar{n}_j \to e^{-(\epsilon_j - \mu)/k_B T}$; the Maxwell-Boltzmann statistics describing an ideal gas.

As $T \to 0$, the Fermi-Dirac distribution becomes the step function

$$\bar{n}_j^{(F)} = \begin{cases} 1 & \text{if } \epsilon_j < \mu, \\ 0 & \text{if } \epsilon_j > \mu. \end{cases} \tag{2.7}$$

[1] The reason for this is is actually quite nuanced, and is a consequence of the *spin-statistics theorem*. A reader interested in a technical discussion of this should turn to Chapter 5 of Ref. [102].

[2] That is why this thesis also functions as an important feasibility test for Bogoliubov theory as a finite temperature description of feedback cooling for fermions. If the Bogoliubov approach is intractable for bosons, it will certainly not be any easier for fermions.

[3] These results assume that the energy states are non-degenerate; that is, only one state corresponds to each energy. We've made this assumption because we only care about the qualitative differences between the two cases.

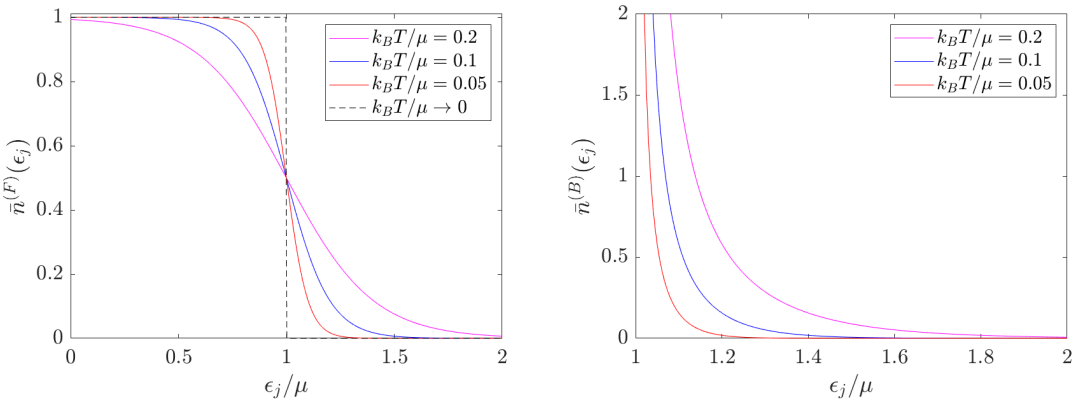

(a) Fermi-Dirac Distribution (b) Bose-Einstein Distribution

Figure 2.1: Bose-Einstein and Fermi-Dirac distributions for the non-degenerate, continuous energy spectra from equations (2.5) and (2.6). In a), as $T \to 0$, the distribution approaches a step function, with all particles occupying states below the Fermi energy $\epsilon = \mu$. In b), as $T \to 0$, the distribution approaches a delta function at $\epsilon = \mu$, indicating that all particles occupy the ground state.

As can be seen in Figure 2.1a, each state below a particular energy (the Fermi energy $\epsilon_j = \mu$) is occupied, and every state above this energy is empty. This creates a "Fermi sea", where all the fermions are packed as tightly as possible into discrete energy levels in order to obey the Pauli exclusion principle. When T is small but non-zero, individual fermions are excited to states above the Fermi energy, leaving a "hole" in the Fermi sea. Associating each excited particle with the hole left behind — as a "particle-hole pair" — is a useful qualitative understanding of thermal excitations in a cold Fermi gas.

The story is significantly different for bosons. As can be seen in Figure 2.1b, the most densely occupied states are those close to the ground state. As temperature T decreases, fewer and fewer particles inhabit the excited states. Once a critical temperature T_C is reached, particles begin to move into the ground state. Below this temperature, the gas has formed a BEC: a state of matter where a singular energy state is macroscopically occupied. This phenomenon was first predicted by Einstein in 1925 [103] based on the statistical approach of Bose [104], before being experimentally observed in 1995 in rubidium [3] and sodium [4]. For a gas of N non-interacting bosons in a three-dimensional harmonic trap[4], below T_C the fraction of particles in the condensate (condensate fraction) is [81]

$$\frac{N_C}{N} = 1 - \left(\frac{T}{T_C}\right)^3, \tag{2.8}$$

where N_C is the number of particles in the condensate. Equation (2.8) indicates that condensate fraction can be used as a proxy for temperature.

2.2 Important tools of quantum field theory

The statistical picture we have just painted describes the equilibrium properties of Bose and Fermi gases. In this thesis, we are concerned with the *dynamic* properties of atomic

[4]Note that this corresponds to a discrete energy spectrum, unlike that plotted in Figure 2.1b.

gases. To that end, it is necessary to introduce some tools of quantum field theory (QFT); which, amongst other things, allows us to study quantum systems of a large number of particles. A detailed introduction to QFT can be found in Refs. [105] and [106], and a brief but useful summary in the context of cold atoms can be found in Ref. [107].

2.2.1 A brief review of second quantisation

When working with an arbitrary number of particles, specifying the individual state of each particle as in Section 2.1 becomes laborious. However, as particles in quantum mechanics are indistinguishable, the state of each individual particle no longer matters - what matters is the number of particles in each mode. Each mode can have a discrete (such as spin) or continuous (such as position) index, or can have both.

Specifically, QFT deals with *Fock space*. Conceptually, Fock space is the set of states which are each occupied by a discrete number of particles[5]. We will first write states in Fock space using *Fock states*, which are those with a well defined number of particles n_j in each mode single particle state $|\phi_j\rangle$. Together, the set $\{|\phi_j\rangle\}$ forms the single-particle basis. A Fock state is then written as $|n_1, n_2, \dots\rangle$, and Fock states span Fock space. We can therefore write a general state $|\Psi(t)\rangle$ as a sum of Fock states

$$|\Psi(t)\rangle = \sum_{n_1,n_2,\cdots=0}^{\infty} C_{n_1,n_2,\dots}(t)\,|n_1, n_2, \dots, \rangle\,, \tag{2.9}$$

where $C_{n_1,n_2,\dots}(t)$ is the normalised weight of each of these states.

As our basis elements (Fock states) have a well-defined number of particles in each mode, it makes sense to define operators which can change that number. These are the *annihilation* ($\hat{a}_j$) and *creation* ($\hat{a}_j^\dagger$) operators, defined as

$$\hat{a}_j\,|n_1, \dots, n_j, \dots\rangle = \sqrt{n_j}\,|n_1, \dots, n_j - 1, \dots\rangle\,, \tag{2.10a}$$

$$\hat{a}_j^\dagger\,|n_1, \dots, n_j, \dots\rangle = \sqrt{n_j + 1}\,|n_1, \dots, n_j + 1, \dots\rangle\,. \tag{2.10b}$$

These operators then obey

$$\left[\hat{a}_j, \hat{a}_k^\dagger\right] = \delta_{jk}, \;\; [\hat{a}_j, \hat{a}_k] = \left[\hat{a}_j^\dagger, \hat{a}_k^\dagger\right] = 0. \tag{2.11}$$

Note that crucially, if the vacuum state is defined as $|0, \dots, 0\rangle$,

$$\hat{a}_j\,|0, \dots, 0\rangle = 0, \tag{2.12}$$

so it is impossible to create a state with negative number. The creation and annihilation operators are convenient for modelling the dynamics of a system, because they can be used to write any operator[6].

[5] More rigorously, Fock space is the Hilbert space spanned by N-particle states, including each possible value of N. A Hilbert space is a vector space with a complex domain and an inner product.

[6] The nuances behind why this is the case are beyond the scope of this thesis, and cannot be accurately summarised in a footnote. For a detailed discussion of why the claim is true, the interested reader should see Chapter 4 of Ref. [106] or Chapter 1 of Ref. [108].

As the set of single particle states $|\phi_i\rangle$ and annihilation operators $\hat{a}_i$ is an arbitrary basis, we can move to another discrete basis with modes $|\chi_j\rangle$ and operators $\hat{b}_j$ via the following transformation

$$\hat{b}_j = \sum_i \langle \chi_j | \phi_i \rangle \, \hat{a}_i. \tag{2.13}$$

It is also possible to move into a continuous basis, such as the position basis

$$\hat{\psi}(\mathbf{x}) = \sum_i \phi_i(\mathbf{x}) \hat{a}_i. \tag{2.14}$$

In the position basis, the annihilation and creation operators are referred to as *field operators*. A field operator $\hat{\psi}(\mathbf{x})$ annihilates a particle at position $\mathbf{x}$. It follows from equations (2.11) and (2.14) that

$$\left[\hat{\psi}(\mathbf{x}), \hat{\psi}^\dagger(\mathbf{y})\right] = \delta(\mathbf{x}-\mathbf{y}), \quad \left[\hat{\psi}(\mathbf{x}), \hat{\psi}(\mathbf{y})\right] = \left[\hat{\psi}^\dagger(\mathbf{x}), \hat{\psi}^\dagger(\mathbf{y})\right] = 0. \tag{2.15}$$

Note that the preceding formalism is specific to bosons; fermionic creation and annihilation operators obey anti-commutator relations. There is a more general formalism for particles with multiple internal modes (such as different spin states); however, that procedure is not relevant to this thesis.

2.2.2 Dynamics in quantum field theory

In quantum mechanics, we are ultimately concerned with the expectation values of operators. The expectation value of an operator $\hat{\mathcal{O}}$ on a state evolves in time, and for a state $|\Psi\rangle$ is defined

$$\left\langle \hat{\mathcal{O}} \right\rangle (t) = \left\langle \Psi \left| \hat{U}^\dagger(t,t_0) \hat{\mathcal{O}} \hat{U}(t,t_0) \right| \Psi \right\rangle, \tag{2.16}$$

where $\hat{U}(t,t_0)$ is the time evolution operator corresponding to evolving the state from t_0 to t. For the expectation value to evolve in time, it follows that some combination of the state and operator must also evolve in time. Two immediate choices are the *Heisenberg picture* and the *Schrödinger picture*. In the Heisenberg picture, operators evolve in time and states are static. In particular, operators are defined as $\hat{\mathcal{O}}(t) = \hat{U}^\dagger(t,t_0)\hat{\mathcal{O}}\hat{U}(t,t_0)$ and obey the *Heisenberg equation of motion*

$$\frac{d\hat{\mathcal{O}}}{dt} = -\frac{i}{\hbar}\left[\hat{\mathcal{O}}, \hat{H}\right] + \frac{\partial \hat{\mathcal{O}}}{\partial t}, \tag{2.17}$$

where $\hat{H}$ is the system Hamiltonian. In this thesis, we only consider operators without explicit time dependence, so $\partial\hat{\mathcal{O}}/\partial t = 0$. Alternatively, in the Schrödinger picture, operators are static and states are defined as $|\Psi(t)\rangle = \hat{U}(t,t_0)|\Psi(t_0)\rangle$ to evolve in time. In particular, they evolve under the Schrödinger equation as

$$i\hbar \frac{\partial}{\partial t} |\Psi(t)\rangle = \hat{H} |\Psi(t)\rangle. \tag{2.18}$$

Importantly, both the Heisenberg and Schrödinger pictures return equivalent physics. In this thesis, we use the Heisenberg picture to demonstrate why feedback cooling works in Chapter 3 and justify our choice of Bogoliubov theory in Chapter 4, and the Schrödinger picture in Chapter 4 to derive our model for an arbitrary trapping and control potential.

2.3 Quantum field theory of cold atoms

We now have the tools of QFT necessary to understand the theory of cold Bose gases and BECs. In particular, we can now introduce the standard cold atom Hamiltonian, and consider dynamics of a collection of bosons. Little knowledge of atomic physics is necessary to understand this thesis. A reader concerned with the details of atomic physics relevant to cold atom physics, or interested in a more detailed introduction to the QFT of cold atoms, should consult Ref. [81].

2.3.1 The cold atom Hamiltonian

In this thesis, we are concerned with cooling ensembles of atoms, which themselves are not single particles. Instead, they are made up of protons, neutrons, and electrons - which are all fermions. However, sufficiently low temperatures correspond to energy scales well below the ionisation energy of atoms, so their component fermions are effectively bound together. The atoms themselves can therefore be treated as single particles, and the parity of the number of composite fermions determines if the atom is bosonic (even) or fermionic (odd)[7].

Treating each atom as a single particle, we can now write a Hamiltonian for a collection of cold bosonic atoms in terms of bosonic field operators $\hat{\psi}(\mathbf{x})$. This thesis is primarily concerned with the simplest dynamics for a collection of bosons, so does not consider internal degrees of freedom such as spin[8]. Therefore, for a collection of bosons each of mass m in a trapping potential $V_{\text{ext}}(\mathbf{x},t)$

$$\hat{H} = \overbrace{\int d\mathbf{x}\hat{\psi}^\dagger(\mathbf{x})\left(-\frac{\hbar^2}{2m}\nabla^2_{\mathbf{x}} + V_{\text{ext}}(\mathbf{x},t)\right)\hat{\psi}(\mathbf{x})}^{\text{Single-particle dynamics}} + \underbrace{\frac{1}{2}\int d\mathbf{x}\int d\mathbf{y}\hat{\psi}^\dagger(\mathbf{x})\hat{\psi}^\dagger(\mathbf{y})V_{\text{int}}(\mathbf{x}-\mathbf{y})\hat{\psi}(\mathbf{y})\hat{\psi}(\mathbf{x})}_{\text{Inter-particle interactions}}. \tag{2.19}$$

Each individual particle evolves due to its kinetic energy ($-(\hbar^2/2m)\nabla^2_{\mathbf{x}}$) and the trapping potential ($V_{\text{ext}}(\mathbf{x},t)$). Each particle at a position $\mathbf{x}$ interacts with a particle at position $\mathbf{y}$ via the potential $V_{\text{int}}(\mathbf{x}-\mathbf{y})$. Qualitatively, this interaction is only strong when atoms are close together. However, ultra-cold atomic gases are typically dilute, and the energy scales are significantly small such that only the lowest order scattering effects (s-wave scattering) contribute. Therefore, the standard approach in the literature is to approximate the interaction as two atoms scattering off each other like billiard balls [43, 107]. That is, $V_{\text{int}}(\mathbf{x}-\mathbf{y})$ is approximated by the contact potential

$$V_{\text{int}}(\mathbf{x}-\mathbf{y}) = g\delta(\mathbf{x}-\mathbf{y}), \tag{2.20}$$

[7] An actual proof of this is nuanced and well beyond the scope of this thesis, and indeed difficult to find in the literature. However, the experimental observation of BECs [3, 4] is sufficient evidence that it is possible for a collection of fermions to act as a boson.

[8] Our model therefore holds for a spin zero boson, or a spin polarized gas where the spin is fixed by a strong magnetic field.

where g is the interaction strength defined as

$$g = \frac{4\pi\hbar^2 a}{m}. \tag{2.21}$$

Here, a is the scattering length of the s-wave scattering. For a more detailed discussion of the approximation in equation (2.20), the interested reader should consult Chapter 5 of Ref. [81].

The interaction strength g varies signficantly in the vicinity of a Feshbach resonance, an inter-atomic coupling effect that arises at particular magnetic field strengths.[9] By varying an external magnetic field, Feshbach resonances can be exploited to precisely tune g for many atomic species [57, 58]. Therefore, in this thesis we essentially treat g as a free parameter, and in particular only consider repulsive interactions ($g > 0$), where the interaction between two atoms pushes them away from each other. Although attractive interactions ($g < 0$) are experimentally possible [111], they are less experimentally accessible than repulsive interactions, and most atomic species naturally[10] have strong repulsive interactions [3, 4].

Equation (2.19) is for a three-dimensional system; however, theoretical investigation is more tractable in one or two dimensions. For a harmonically trapped gas, with a potential $\mathbf{V}(\mathbf{x}) = \frac{1}{2}m\left(\omega_x^2 x^2 + \omega_y^2 y^2 + \omega_z^2 z^2\right)$, it is theoretically possible to confine the gas to one dimension if the trap is much stronger along that direction than the other two — in particular, if $\omega_y, \omega_z \gg \omega_x$ [112].[11] It is standard to assume that the gas is in its ground state along the other two dimensions, so the dynamics of the system are effectively confined to one dimension [115]. As this behaviour has been experimentally observed [116, 117], it is standard to construct theoretical models for effective 1D Boses gases as they are simpler to model and give a good approximation to 3D dynamics. That is indeed the approach we take in this thesis. Under this approximation and equation (2.20), our Hamiltonian becomes[12]

$$\hat{H} = \int dx \hat{\psi}^\dagger(x)\left(-\frac{\hbar^2}{2m}\nabla_x^2 + V_{\text{ext}}(x,t)\right)\hat{\psi}(x) + \frac{g}{2}\int dx \hat{\psi}^\dagger(x)\,\hat{\psi}^\dagger(x)\,\hat{\psi}(x)\,\hat{\psi}(x)\,. \tag{2.22}$$

This effective 1D Hamiltonian will be the focus of this thesis. With this Hamiltonian, we can begin to study the dynamics of an ultra-cold Bose gas.

[9] Feshbach resonances arise because of the *Zeeman effect*: when an external magnetic field is applied to an atomic gas, the energy levels of the internal states shift [81]. This means that the energy levels of a pair of individual atoms can become the same as the energy levels of a molecule of those two atoms combined. When this degeneracy occurs, the two atoms can momentarily couple, which vastly changes their scattering properties and thus the interaction strength g. This effect was first predicted by Feshbach in Ref. [109] and is often experimentally manipulated in atomic physics [110].

[10] By naturally, we mean without manipulation of Feshbach resonances.

[11] This is only the condition for a non-interacting Bose gas. As repulsive interactions increase, atoms can "pop out" into other dimensions. The conditions for creating a 1D Bose gas are therefore more complicated in an interacting gas, but it is sufficient for this thesis to understand that is is still possible to construct an effective 1D system with repulsive interactions [113, 114].

[12] Note that the interaction strength g in equation (2.22) now refers to an *effective* interaction strength in 1D. Therefore, it is not equivalent to that defined in equation (2.21).

2.3.2 Mean-field dynamics: the Gross-Pitaevskii equation

The evolution of the field operator $\hat{\psi}(x)$ can be found using the Heisenberg equation of motion, equation (2.17). Under the Hamiltonian in equation (2.22), the field operator evolves as

$$i\hbar\frac{d\hat{\psi}(x)}{dt} = \left[\left(-\frac{\hbar^2}{2m}\nabla_x^2 + V_{\text{ext}}(x,t)\right) + g\hat{\psi}^\dagger(x)\,\hat{\psi}(x)\right]\hat{\psi}(x)\,. \tag{2.23}$$

Hypothetically, solving this equation of motion would give the dynamics of the quantum field of an ultra-cold Bose gas. However, even numeric integration is intractable for the full quantum field. This is because $\hat{\psi}(x)$ lives in a Hilbert space which is a tensor product of all its basis functions $\phi_i(x)$, and for more than a few modes this requires more bytes of computing power than atoms in the observable universe. The exponential scaling of quantum Hilbert spaces is an inherent challenge of QFT, and it is therefore necessary to make approximations so that solving equations such as equation (2.23) is possible.

The simplest approach is *mean-field theory*. We only review the basics here; a reader curious for a more general introduction should see Chapter 4 or Ref. [108], and specifically in the context of cold atoms Chapter 6 of Ref. [81].

In a mean-field theory, we assume that the majority of the particles in a system are in one particular state, such as a number state or a coherent state. A single function $\phi(x)$ — termed an *order parameter* or a *classical field* — describes that state. Expectation values of operators are then written in terms of that order parameter. For example, for some state $|\Psi\rangle$ if we assume a) that there is always a basis where all particles are in a single mode, and b) that single mode is a coherent state, we can prove (see Appendix A.1)

$$\hat{\psi}(x)|\Psi\rangle = \phi(x)|\Psi\rangle, \tag{2.24}$$

where the order parameter $\phi(x)$ is some function defined in terms of the single-mode basis and the eigenvalues of the coherent state. Equation (2.24) and its complex conjugate are used to write the expectation value of any combinations of field operators; for example, $\langle\hat{\psi}(x)\rangle = \phi(x)$, and $\langle\hat{\psi}^\dagger(y)\hat{\psi}(x)\hat{\psi}(y)\rangle = |\phi(y)|^2\,\phi(x)$.

Recall that in Figure 2.1b, we saw that as $T \to 0$, the majority of atoms in a Bose gas occupy one state, forming a BEC. In a coherent state approximation, we assume that the system is in a coherent state of that single mode. Taking the expectation value of equation (2.23), and applying the coherent state approximation (equation (2.24)) obtains

$$i\hbar\frac{d\phi(x,t)}{dt} = \left[\left(-\frac{\hbar^2}{2m}\nabla_x^2 + V_{\text{ext}}(x,t)\right) + g\,|\phi(x,t)|^2\right]\phi(x,t). \tag{2.25}$$

Equation (2.25) was first proposed by Gross [118, 119] and Pitaevskii [120], and is termed the *Gross-Pitaevskii Equation* (GPE). Alternatively, readers may be familiar with equation (2.25) as the non-linear Schrödinger equation [121]. At dynamic equilibrium, the condensate wavefunction $\phi(x)$ will only evolve by rotating in phase space [122]. Thus, the condensate wavefunction is separable in time and position, and can be written

$$\phi(x,t) = \phi_0(x)e^{-i\frac{\mu t}{\hbar}}, \tag{2.26}$$

where μ is the chemical potential. Substituting equation (2.26) into equation (2.25) obtains

$$\mu\phi_0(x) = \left[\left(-\frac{\hbar^2}{2m}\nabla_x^2 + V_{\text{ext}}(x,t)\right) + g\left|\phi_0(x)\right|^2\right]\phi_0(x), \tag{2.27}$$

known as the *time-independent GPE* (TIGPE). Some authors therefore refer to equation (2.25) as the *time-dependent GPE* (TDGPE).

The GPE is our lowest-order description of the dynamics of a BEC. As the GPE assumes effectively all of the atoms are in the condensate, it therefore assumes $T = 0$. However, the GPE can provide a sufficient description as hot as half the critical temperature ($T \approx T_C/2$), provided the gas is weakly interacting [123, 124]. Even when multiple energy states are occupied, the GPE can be an accurate description of the dynamics of the lowest energy state [107].

Recall again Figure 2.1b, and observe that as temperature increases above $T = 0$, a greater number of energy states have non-negligible occupation, so not all the atoms are behaving in the same way. It is therefore no longer accurate to estimate the quantum behaviour by a single order parameter. This means that the further we get from $T = 0$, the mean-field dynamics described by the GPE break down, and a new theory is needed.[13].

2.4 An introduction to symmetry-breaking Bogoliubov theory

In this thesis, we model the finite (non-zero) temperature behaviour of ultra-cold Bose gases, so the GPE alone is insufficient. Our model will be inspired by the approach of Bogoliubov in his seminal work on superfluidity [96].

The key aim of Bogoliubov theory is to diagonalise the cold atom Hamiltonian in order to obtain tractable equations of motion for the collective excitations of the gas. In particular, these collective excitations are represented by quasiparticle modes. In Section 2.4.1, we discuss in detail the two key assumptions of Bogoliubov's original theory; that it is a perturbation theory about the mean-field, and that it treats the condensate as a classical field. We then work through the steps of diagonalising the cold atom Hamiltonian in Section 2.4.2. We develop a further intuition for the properties of Bogoliubov excitations by studying a particular analytic solution in Section 2.4.3, before discussing the important effect of quantum depletion in Section 2.4.4.

In our summary of symmetry-breaking Bogoliubov theory, we only introduce the basic tools relevant to this thesis. A reader interested in a more detailed introduction should consult Ref. [107].

[13] A similar effect occurs when the repulsive interaction strength g increases: different particles can couple to each other, and not all particles behave the same. Rigorously, increasing T and g induces *quantum correlations* in the quantum field, so $\hat{\psi}(x)$ is no longer separable.

2.4.1 A conceptual introduction

At low but non-zero temperatures, the majority of atoms in a cold Bose gas are in the condensate, but the remaining particles occupy a small number of other low energy modes. Let us describe the macroscopically occupied condensate by the annihilation operator $\hat{a}_0$ and all other modes by the field operator $\hat{\delta}(x)$. We can separate out the condensate mode from the rest of the field operator as

$$\hat{\psi}(x) = \chi_0(x)\hat{a}_0 + \hat{\delta}(x), \tag{2.28}$$

where $\chi_0(x)$ is the wavefunction of the condensate mode. As the occupation of non-condensate modes is small, $\hat{\delta}(x)$ is small, and can be thought of as a perturbation about the condensate wavefunction. Indeed by expanding the field operator in this way, we will ultimately be able to complete a perturbative expansion of the cold atom Hamiltonian, and obtain simple approximate dynamics for the excitations of the gas.[14] But first, let us turn our attention to the condensate.

Consider respectively the operation of $\hat{a}_0\hat{a}_0^\dagger$ and $\hat{a}_0^\dagger\hat{a}_0$ upon the state vector of a Bose gas. Let us represent the state vector as $|N_c, \vec{v}\rangle$, where N_C is the number of particles in the condensate, and $\vec{v}$ the state vector of particles in other modes. We therefore have that

$$\hat{a}_0^\dagger\hat{a}_0 |N_c, \vec{v}\rangle = N_C |N_C, \vec{v}\rangle , \ \hat{a}_0\hat{a}_0^\dagger |N_C, \vec{v}\rangle = (N_C + 1) |N_C, \vec{v}\rangle . \tag{2.29}$$

As $N_C \gg 1$, $N_C+1 \approx N_C$ and therefore $[\hat{a}_0\hat{a}_0^\dagger - \hat{a}_0^\dagger\hat{a}_0] |N_c, \vec{v}\rangle \approx 0$. Bogoliubov's assumption is then that $[\hat{a}_0, \hat{a}_0^\dagger] = 0$ and that the annihilation operator can be replaced by a complex number. In particular, $\hat{a}_0 = \sqrt{N_C} \approx \sqrt{N}$, so that equation (2.29) remains true. If $\chi_0(x)$ is normalised to $\sqrt{N_C}$, the field operator for the Bose gas becomes

$$\hat{\psi}(x) = \chi_0(x) + \hat{\delta}(x). \tag{2.30}$$

The key concept of this procedure is that the condensate is treated as a classical degree of freedom, unlike the excitations $\hat{\delta}(x)$. Indeed, an equivalent model follows from defining $\hat{\delta}(x)$ as

$$\hat{\psi}(x) = \left\langle \hat{\psi}(x) \right\rangle + \hat{\delta}(x) = \phi(x) + \hat{\delta}(x), \tag{2.31}$$

where $\phi(x)$ is the mean-field (typically modelled by the GPE). It follows from each equations (2.30) and (2.31) that

$$\left[\hat{\delta}(x), \hat{\delta}^\dagger(y)\right] = \delta(x-y), \ \left[\hat{\delta}(x), \hat{\delta}(y)\right] = \left[\hat{\delta}^\dagger(x), \hat{\delta}^\dagger(y)\right] = 0. \tag{2.32}$$

From equation (2.31), it is also apparent that $\langle\hat{\delta}(x)\rangle = 0$. This makes sense, because $\hat{\delta}$ is a perturbation around a large value (the condensate wavefunction).

A clear consequence of the approximation $N_C \approx N_C + 1$ is that the number of particles in the condensate is fixed. This means that if an excitation is destroyed it does not appear in the condensate, so the total number of particles in the gas is not fixed. More rigorously, the classical field approximation fixes the phase of $\hat{a}_0$, and the field

[14] Readers unfamiliar with perturbation theory should see Chapters 6 and 9 of Ref. [125]. It is the quantum mechanical analogue of the Taylor expansion.

operator $\hat{\psi}(x)$ is no longer invariant under the $U(1)$ gauge symmetry[15] [107, 126]. We will therefore refer to this approach as *symmetry-breaking Bogoliubov theory.*

The other significant consequence of approximating $N_C \approx N_C + 1$ is that it restricts the regime in which the symmetry-breaking Bogoliubov theory is valid. Rigorously, the theory is only valid in the regime where $N_C/N \gg 1/N$. For this reason, most literature applying symmetry-breaking Bogoliubov theory to moderately sized BECs (10^4 - 10^6 atoms) does not consider below $\sim 90\%$ condensate fraction.[16]

2.4.2 Diagonalising the cold atom Hamiltonian

We now have the tools to study the dynamics of the system using the Hamiltonian. We will first simplify the cold atom Hamiltonian with a perturbation using the approximation in equation (2.29). Then, we will introduce the *Bogoliubov transformation* in order to diagonalise our Hamiltonian, since dynamics of operators are more tractable under a diagonal Hamiltonian.

Perturbation Theory in $\hat{\delta}(x)$

The approximation $N_C \approx N_C + 1$ effectively means that particles can move between the condensate and some reservoir, so we are implicitly working in the grand canonical ensemble[17]. This makes it necessary to introduce the term $-\mu\hat{N}$ to the Hamiltonian, where $\hat{N} = \int dx \hat{\psi}^\dagger(x)\hat{\psi}(x)$ is the number operator. This term accounts for the energy change when a particle is exchanged with the particle reservoir, so the Hamiltonian in equation (2.22) becomes

$$\hat{H} = \int dx \hat{\psi}^\dagger(x) \left(-\frac{\hbar^2}{2m}\nabla_x^2 + V_{\text{ext}}(x,t) - \mu \right) \hat{\psi}(x) + \frac{g}{2} \int dx \hat{\psi}^\dagger(x)\, \hat{\psi}^\dagger(x)\, \hat{\psi}(x)\, \hat{\psi}(x) . \tag{2.33}$$

Substituting in equation (2.29) into equation (2.33), we obtain

$$\hat{H} = H_0 + \sum_{i=1}^{4} \hat{H}_i, \tag{2.34}$$

where

$$H_0 = \int dx \left[\chi_0^*(x) \hat{h}_0(x) \chi_0(x) + \frac{g}{2} |\chi_0(x)|^4 \right], \tag{2.35a}$$

$$\hat{H}_1 = \int dx \left[\hat{\delta}^\dagger(x) \left(\hat{h}_0(x) + g|\chi_0(x)|^2 \right) \chi_0(x) + \chi_0^*(x) \left(\hat{h}_0(x) + g|\chi_0(x)|^2 \right) \hat{\delta}(x,t) \right], \tag{2.35b}$$

$$\hat{H}_2 = \int dx \left[\hat{\delta}^\dagger(x) \left(\hat{h}_0(x) + 2g|\chi_0(x)|^2 \right) \hat{\delta}(x) \right] + \frac{g}{2} \int dx \left[(\chi_0^*(x))^2 \hat{\delta}(x)\hat{\delta}(x) + (\chi_0(x))^2 \hat{\delta}^\dagger(x)\hat{\delta}^\dagger(x) \right] \tag{2.35c}$$

[15] For an introduction to gauge symmetries in QFT, see Chapters 14 and 20 of Ref. [106].

[16] Technically, the regime of validity depends upon the particular system being studied. For example, Hurst *et al.* in Ref. [99] consider a minimum condensate fraction of 99%.

[17] For a review of the details of the grand canonical ensemble, the interested reader should see Ref. [39].

$$\hat{H}_3 = g \int dx \left[\chi_0^*(x)\hat{\delta}^\dagger(x)\hat{\delta}(x)\hat{\delta}(x) + \chi_0(x)\hat{\delta}^\dagger(x)\hat{\delta}^\dagger(x)\hat{\delta}(x) \right] \tag{2.35d}$$

$$\hat{H}_4 = \frac{g}{2} \int dx \hat{\delta}^\dagger(x)\hat{\delta}^\dagger(x)\hat{\delta}(x)\hat{\delta}(x). \tag{2.35e}$$

Here, we have introduced the shorthand

$$\hat{h}_0(x) = -\frac{\hbar^2}{2m}\nabla_x^2 + V_{\text{ext}}(x,t) - \mu \tag{2.36}$$

Equations (2.35a) - (2.35e) are essentially an expansion of $\hat{H}$ in increasing order of the small parameter $\hat{\delta}(x)$. Whilst this Hamiltonian appears intractable, we can obtain simple approximate dynamics by considering a perturbation theory in $\hat{\delta}(x)$.

First, note that H_0 is not operator valued (not an operator), so it is a constant offset that we can minimise. We would normally do this using calculus; however, H_0 is not defined in terms of a continuous variable, but rather a function $\chi_0(x)$. This means that H_0 is a *functional*. Fortunately, the rules of calculus for functionals are essentially the same as regular calculus, except continuous variables are replaced by complex functions (see Chapter 12 of Ref. [127] for more details). If H_0 is a functional in χ_0^*, the functional derivative with respect to χ_0^* is

$$\frac{\delta H_0\left[\chi_0^*(x)\right]}{\delta \chi_0^*(x)} = \left(\hat{h}_0(x) + g\left|\chi_0(x)\right|^2\right)\chi_0(x). \tag{2.37}$$

H_0 is minimised if the right-hand side of equation (2.37) is equal to zero, which is exactly the TIGPE (equation (2.27)) for $\chi_0(x)$.[18] If $\chi_0(x)$ obeys equation (2.27), because $\hat{h}_0$ is hermitian, $\hat{H}_1 = 0$. Therefore, if we describe the condensate by the TIGPE, $\hat{H}_2$ is the lowest order operator-valued contribution to the Hamiltonian, so in our perturbation theory we approximate $\hat{H} \approx \hat{H}_2$.

The Bogoliubov transformation

Recall that that the goal of our perturbation theory is to diagonalise the Hamiltonian. In order to do this, we will do this by representing collective excitations of the condensate as effective particles, or *quasiparticles*. Mathematically, that goal is achieved by making the linear transformation

$$\hat{\delta}(x) = \sum_{j>0} \left[u_j(x)\hat{\beta}_j + v_j^*(x)\hat{\beta}_j^\dagger \right], \tag{2.38}$$

where $\hat{\beta}_j$ and $\hat{\beta}_j^\dagger$ are quasiparticle annihilation and creation operators obeying

$$\left[\hat{\beta}_j, \hat{\beta}_k^\dagger\right] = \delta_{jk}, \quad \left[\hat{\beta}_j, \hat{\beta}_k\right] = \left[\beta_j^\dagger, \hat{\beta}_k^\dagger\right] = 0. \tag{2.39}$$

The functions $\{u_j, v_j\}$ are normalised coefficients of the quasiparticle operators. In order for both equations (2.32) and (2.39) to hold, these coefficients must obey the orthonor-

[18] Rigorously, we are assuming that a minimum solution exists, which is equivalent to assuming the condensate has a fixed phase. Assuming the condensate has a fixed phase is exactly equivalent to breaking the $U(1)$ symmetry, as discussed in Section 2.4.1. Therefore, assuming a minimum solution exists is consistent with the previous assumptions of the symmetry-breaking approach [107].

mality conditions

$$\int dx \left(u_j^*(x)u_k(x) - v_j^*(x)v_k(x)\right) = \delta_{jk}, \tag{2.40a}$$

$$\int dx \left(u_j(x)v_k(x) - v_j(x)u_k(x)\right) = 0. \tag{2.40b}$$

Here, each quasiparticle pair $\hat{\beta}_j$ and $\hat{\beta}_j^\dagger$ represents the collective excitation of particles in the Bose gas. The basis for those quasiparticles is not chosen until we specify a particular form for the coefficients $\{u_j, v_j\}$.

Substituting equation (2.38) into equation (2.35c) yields, after some simplification, the unwieldy expression

$$\begin{aligned}
\hat{H}_2 = &\frac{1}{2}\sum_{jk}\int dx \left[v_j(x)\left(\hat{\mathcal{L}}(x)v_k^*(x) + C(x)u_k^*(x)\right)\hat{\beta}_j\hat{\beta}_k^\dagger + \text{h.c.}\right] \\
&+ \frac{1}{2}\sum_{jk}\int dx \left[u_j^*(x)\left(\hat{\mathcal{L}}(x)u_k(x) + C(x)v_k(x)\right)\hat{\beta}_j^\dagger\hat{\beta}_k + \text{h.c.}\right] \\
&+ \frac{1}{2}\sum_{jk}\int dx \left[v_j(x)\left(\hat{\mathcal{L}}(x)u_k(x) + C^*(x)v_k(x)\right)\hat{\beta}_j\hat{\beta}_k + \text{h.c.}\right] \\
&+ \frac{1}{2}\sum_{jk}\int dx \left[\left(\hat{\mathcal{L}}(x)v_k^*(x) + C(x)u_j^*(x)\right)^\dagger u_j(x)\hat{\beta}_j\hat{\beta}_k + \text{h.c.}\right],
\end{aligned} \tag{2.41}$$

where $\hat{\mathcal{L}}(x) = \hat{h}_0 + 2g\left|\chi_0(x)\right|^2 = \hat{\mathcal{L}}^\dagger(x)$ and $C(x) = g\left(\chi_0(x)\right)^2$ and we use h.c. to refer to "Hermitian conjugate". However, this substitution presents a sensible choice of basis for the quasiparticles:

$$\hat{\mathcal{L}}(x)u_j(x) + C(x)v_j(x) = \epsilon_j u_j(x), \tag{2.42a}$$

$$\hat{\mathcal{L}}(x)v_j(x) + C^*(x)u_j(x) = -\epsilon_j v_j(x), \tag{2.42b}$$

where ϵ_j is the energy of the jth quasiparticle. These coupled equations are the *Bogoliubov-de Gennes equations*. When substituted into equation (2.41), and using the orthonormality conditions (equation (2.40)), one obtains (after some effort)

$$\hat{H}_2 = \sum_{j>0}\epsilon_j\left[\hat{\beta}_j^\dagger\hat{\beta}_j - \int dx \left|v_j(x)\right|^2\right]. \tag{2.43}$$

Thus, $\hat{H}_2$ is diagonal in the Bogoliubov modes, up to an energy offset. Physically, this means that Bogoliubov excitations behave as harmonic oscillator modes (to second order perturbation theory). Moreover, it means that finding the commutator $[\hat{A}, \hat{H}]$ is simple for any operator $\hat{A}$ expressed in terms of the Bogoliubov modes. That makes computing the dynamics of operators in the Heisenberg picture (using equation (2.17)) straightforward, either analytically or numerically. This diagonalisation is at the heart of what makes Bogoliubov theory so useful, and hence why it has been applied in fields beyond cold atom physics as diverse as the study of black holes [128] and the structure of atomic nuclei [129].

2.4.3 Analytic solutions to the Bogoliubov spectrum

In order to develop intuition for how Bogoliubov quasiparticles behave, it is instructive to solve the Bogoliubov-de Gennes equations for $\{u_j(x), v_j(x)\}$ and the Bogoliubov energy spectrum ϵ_j. In particular, we will consider an analytic solution of the equations in a "box" (infinite square well) potential. In Chapter 3, we will discuss this solution in comparison with analytic solutions for the Bogoliubov-de Gennes equations in a harmonic trapping potential[19]. More generally, solutions to the Bogoliubov-de Gennes equations can be found via perturbation theory [130] and numeric integration [131]. For more detailed reviews of approaches for solving for Bogoliubov modes in different traps, the interested reader should see Refs. [132] and [133].

Solving the Bogoliubov-de Gennes equations requires having the form of $\chi_0(x)$. As $\chi_0(x)$ obeys the TIGPE, we first must solve equation (2.27) for a given $V_{\text{ext}}(x,t)$. The TIGPE is most simply solved by a uniform condensate. Consider the box potential

$$V_{\text{ext}}(x,t) = \begin{cases} 0, & \text{if } -L/2 < x < L/2, \\ \infty, & \text{if elsewhere.} \end{cases} \tag{2.44}$$

We then solve the TIGPE by assuming that the kinetic energy of the atoms is small relative to the interactions between them. This approximation holds when the number of atoms is large, since more inter-atomic interactions can occur, and agrees well with experiment [134]. Neglecting the kinetic energy, equation (2.27) becomes

$$|\chi_0(x)|^2 = \frac{\mu - V(x)}{g}. \tag{2.45}$$

Equation (2.45) is known as the *Thomas-Fermi* approximation. For the box potential, it is solved by

$$\chi_0(x) = \begin{cases} \sqrt{\mu/g}, & \text{if } -L/2 < x < L/2, \\ 0, & \text{if elsewhere.} \end{cases} \tag{2.46}$$

so the condensate is uniform. Because the wavefunction $\chi_0(x)$ is normalised as $\int dx\, |\chi_0(x)|^2 = N_C \approx N$, so $\sqrt{\mu/g} = \sqrt{N/L}$. For a uniform condensate, one set of solutions to the system of equations (2.42) are the *plane-wave* solutions.[20] In 1D, these are

$$u_j(x) = \frac{1}{\sqrt{L}} \cosh r_j e^{i\frac{2\pi}{L}jx}, \text{ and } v_j(x) = \frac{1}{\sqrt{L}} \sinh r_j e^{i\frac{2\pi}{L}jx}, \tag{2.47}$$

where $r_j = \ln\left[\epsilon_j/\epsilon_j^{(0)}\right]/2$, and $\epsilon_j^{(0)}$ is the energy of a free quasiparticle. In particular,

$$\epsilon_j = \sqrt{\epsilon_j^{(0)}\left(\epsilon_j^{(0)} + 2gn\right)}, \text{ and } \epsilon_j^{(0)} = \frac{2\pi^2\hbar^2 j^2}{mL^2}, \tag{2.48}$$

where n is the density of atoms. We will often refer to equation (2.48) as the Bogoliubov *energy spectrum*, and it tells us that each excitation behaves like a free particle with its energy "dressed" by the interaction between atoms. This is a valuable feature of the Bogoliubov approach: the basis choice inherently accounts for the interactions between

[19] Note that hereafter we use "trapping potential" and trap interchangeably.

[20] Technically, these solutions have continuous boundary conditions, so actually physically correspond to a 1D ring of circumference L. We will discuss this subtle difference in more detail in Chapter 5.

atoms. For the lowest energy excitations ($\epsilon_j^{(0)} \ll 2gn$), the energy spectrum approaches $\epsilon_j \to \sqrt{2gn\epsilon_j^{(0)}}$, resembling the dispersion relation of phonons in a crystal lattice [135]. This similarity further illustrates how the Bogoliubov modes are collective excitations of our atomic ensemble.

2.4.4 Quantum depletion

The presence of interactions in the Bogoliubov modes makes it easier to study the effect of interactions upon the behaviour of an atomic gas. In particular, recall from equation (2.8) that condensate fraction is a useful proxy for temperature in a BEC. Using the plane-wave solution in equation (2.47), it is possible to show that this proxy breaks down for $g \neq 0$. Under the Bogoliubov approximation, the number operator is[21]

$$\begin{aligned}\hat{N} = &\int dx \left[|\chi_0(x)|^2 + \sum_j |v_j(x)|^2 \right] \\ &+ \sum_{jk} \int dx \left[\left(u_j^*(x) u_k(x) + v_j^*(x) v_k(x) \right) \hat{\beta}_j^\dagger \hat{\beta}_k + \left(v_j(x) u_k(x) \hat{\beta}_j \hat{\beta}_k + \text{h.c.} \right) \right].\end{aligned} \tag{2.49}$$

Recall that $\langle \hat{N} \rangle = N$ and that the condensate wavefunction is normalised to N_C. At $T \to 0$, the population of real Bogoliubov excitations tends towards zero[22], so equation (2.49) can be solved for the condensate fraction

$$\frac{N_C}{N} \approx 1 - \frac{1}{N} \sum_j \int dx \, |v_j(x)|^2 . \tag{2.50}$$

Note that $v_j \neq 0$ for $g > 0$. That is, the condensate is not fully occupied at $T = 0$ for an interacting Bose gas. Physically, the weakly repulsive interactions between atoms push some of them out of the ground state into Bogoliubov modes. This effect is termed *quantum depletion*, and was first experimentally reported in Ref. [137]. The integral in equation (2.50) can be evaluated in the box approximation, by making the low energy approximation $\epsilon_j \approx \sqrt{2gn\epsilon_j^{(0)}}$ and only summing over modes satisfying $\epsilon_j^{(0)} \ll 2gn$. This gives

$$\frac{N_C}{N} = 1 - \frac{8}{3\sqrt{\pi}} \sqrt{na^3} = 1 - \frac{1}{3\hbar^3} \sqrt{\frac{m^3 g^3 n}{\pi^4}}, \tag{2.51}$$

a result first obtained in Ref. [138]. The significance of equation (2.51) is that interactions deplete the condensate. For a condensed Bose gas at a typical density (such as sodium at 10^{14} cm^{-3}) the depletion of the condensate is only 0.2% [137], but for a strongly interacting gas it can be of the order of 20% [139]. Indeed, in liquid helium up to 90% of the condensate may be depleted [140].

A clear consequence of quantum depletion is that, even at $T = 0$, the symmetry-breaking approximation $(N_C + 1)/N \approx N_C/N$ may not hold for large g. In this thesis, we are concerned with lowering the entropy of Bose gases by driving particles into the

[21] This is assuming that the condensate and excited modes are orthogonal. This is a standard assumption which is safe for thermal excitations [136].

[22] That is, $\langle \hat{\beta}_j^\dagger \hat{\beta}_k \rangle, \langle \hat{\beta}_j \hat{\beta}_k \rangle \to 0$. For a more detailed discussion, see Chapter 8.1 of Ref. [81].

condensate. As quantum depletion tells us the maximum occupancy of the condensate, it quantifies what the lowest entropy state is.

2.5 Number-conserving Bogoliubov theory

Symmetry-breaking Bogoliubov theory has proved a powerful tool for modelling various phenomena in ultra-cold Bose gases. When proposing the approach in Ref. [96], Bogoliubov provided the first description of superfluidity as a phenomena of BECs[23], which successfully modelled the significant quantum depletion observed in Helium II [140]. Beyond superfluidity, Bogoliubov theory has proved an accurate model for Hawking radiation in analogue black holes made with BECs [142, 143], and models of nuclear structure [144, 145]. Bogoliubov [72] developed an analogous symmetry-breaking theory for fermions which successfully described superconductivity, verifying the theory of Bardeen, Cooper and Schrieffer [71]. We will discuss the fermionic formulation of Bogoliubov theory in the Outlook portion of Chapter 7.

However, symmetry-breaking Bogoliubov theory is fundamentally limited in its application by the approximation that the condensate is classical. In particular, it does not allow for dynamic changes in the number of condensed atoms, and is only valid for regimes where $T \ll T_C$, and where both g and n are sufficiently small such that quantum depletion is negligible.

An alternative approach is *number-conserving Bogoliubov theory*. Number-conserving approaches treat the condensate as a quantum degree of freedom, and in doing so maintain the $U(1)$ symmetry. This section will only introduce the core principles of number-conserving Bogoliubov theory relevant to this thesis, but a reader interested in further details should consult Chapter 8 of Ref. [146].

2.5.1 A new perturbation theory

Recall the diagonalisation performed in Section 2.4.2. If we naïvely instead use equation (2.28), keeping the condensate as a quantum degree of freedom, the function $C(x)$ in equation (2.41) is replaced with $C(x)\hat{a}_0^2$. In that case, the Bogoliubov-de Gennes equations do not diagonalise $\hat{H}_2$. It is therefore not possible to complete a perturbation theory in $\hat{\delta}$ as before.

The key idea of number-conserving Bogoliubov theory is to perform a perturbation theory in a fluctuation parameter proportional to $\hat{a}_0^\dagger\hat{\delta}(x)$.[24] This operator creates a particle in the condensate when an excitation is destroyed, so it inherently conserves the number of particles in the gas. Additionally, $\langle\hat{a}_0^\dagger\hat{\delta}(x)\rangle = 0$, which can be shown using the

[23] Whilst Landau's Nobel-Prize winning description of superfluidity had come six years earlier in Ref. [141], it assumed a particular form of excitations (photons and rotons). Whilst not all superfluids are BECs, Bogoliubov's theory was the first to propose a model of superfluidity without strict restrictions on the kinds of possible excitations.

[24] Although number-conserving Bogoliubov theory was not formally developed until the end of the 20th century by Gardiner [147] and Castin and Dum [126], the idea for such a perturbation theory was actually first proposed by Girardeau *et al.* nearly 40 years earlier [148].

definitions

$$\hat{a}_0^\dagger = \int dy \hat{\psi}^\dagger(y)\chi_0(y), \text{ and } \hat{\delta}(x) = \int dy \left[\delta(x-y) - \chi_0(x)\chi_0^*(y)\right]\hat{\psi}(y), \tag{2.52}$$

and assuming $\langle\hat{\psi}^\dagger(x)\hat{\psi}(y)\rangle = \delta(x-y)$[25]. The specific choice of fluctuation parameter depends upon the number-conserving theory: S. Gardiner and Morgan define [149]

$$\hat{\Lambda}_C(x) = \frac{1}{\sqrt{N_C}}\hat{a}_0^\dagger\hat{\delta}(x), \tag{2.53}$$

whilst C. Gardiner [147] and Castin and Dum [126] define

$$\hat{\Lambda}(x) = \frac{1}{\sqrt{N}}\hat{a}_0^\dagger\hat{\delta}(x). \tag{2.54}$$

Technically, these two fluctuation parameters scale differently, but that does not affect the results of the theory relevant to this thesis[26] The Hamiltonian (equation (2.22)) is then expanded in terms of the fluctuation parameter in decreasing powers of N as

$$\hat{H} = N\mathcal{H}_0 + \sqrt{N}\hat{\mathcal{H}}_1 + \hat{\mathcal{H}}_2 + \ldots \tag{2.55}$$

where the first two terms ($\mathcal{H}_0$, $\hat{\mathcal{H}}_1$) are the same as in the symmetry-breaking approach (equations (2.35a) and (2.35b)) with $\hat{\delta}(x)$ replaced by $\hat{\Lambda}_C(x)$. All terms beyond $\hat{\mathcal{H}}_2$ are $\mathcal{O}(1/\sqrt{N})$ and so are negligible. The difference in operator-valued terms is that $\hat{\mathcal{H}}_2$ contains an additional term[27]

$$\hat{\mathcal{H}}_2 = \hat{H}_2\left[\hat{\Lambda}_C(x)\right] - \int dxdy\hat{\Lambda}_C^\dagger(y)\hat{\Lambda}_C(y)\chi_0^*(x)\left[\hat{h}_0(x) + g\left|\chi_0(x)\right|^2\right]\chi_0(x), \tag{2.56}$$

where we have used the notation $\hat{H}_2[\hat{\Lambda}_C(x)]$ to indicate equation (2.35c) with $\hat{\delta}(x) \to \hat{\Lambda}_C(x)$. Note that, in a similar manner to Section 2.4.2, the additional term in $\hat{\mathcal{H}}_2$ vanishes when $\mathcal{H}_0$ is minimised and $\chi_0(x)$ obeys the TIGPE.

The number-conserving Hamiltonian is then diagonalised by a set of modified Bogoliubov-de Gennes equations. These equations include additional terms to equation (2.42), but these additional terms vanish when the condensate is orthogonal to the excitations.[28] In this thesis we will assume the excitations and condensate modes are orthogonal, so we will use the symmetry-breaking Bogoliubov modes (solutions to equation (2.42)) to approximate the number-conserving modes.

[25]This assumption corresponds to initially being in a state of fixed temperature [126].

[26]S. Gardiner and Morgan [149] explain the difference in scaling by defining the number of thermal excitations $N_T = N - N_C$. As $\hat{a}_0 \propto \sqrt{N_C}$ and $\hat{\delta}(x) \propto \sqrt{N_T}$, the parameter $\hat{\Lambda}_C(x) \propto \sqrt{N_T}$ always. Conversely, $\hat{\Lambda}(x) \propto \sqrt{N_T(1 - N_T/N)}$, which scales with $\sqrt{N_T}$ only if $N_T << N$. Because this scaling is not constant, S. Gardiner and Morgan prefer $\hat{\Lambda}_C(x)$ because it makes their perturbation theory consistent for all N_T.

[27]There is an additional energy offset $-g/2\int dx\left|\chi_0(x)\right|^4$, however this can be treated as a zero-point energy and thus discarded.

[28]This is except for a missing energy ϵ_0 for the condensate mode. The consequence of this is that the phase of the condensate wavefunction $\chi_0(x)$ spreads in time [150]. This is a physical difference to the symmetry-breaking approach, where the condensate is assigned a fixed phase. However, this phase spreading tends to zero as $N_C \to \infty$ [126].

The key takeaway of these approaches is that it is possible to construct a diagonal Hamiltonian, which conserves number, if the condensate is treated as a quantum degree of freedom. Specifically, if we write our wavefunction as in equation (2.28)

$$\hat{\psi}(x) = \chi_0(x)\hat{a}_0 + \hat{\delta}(x), \tag{2.57}$$

there exists a perturbation theory where (up to some constant)

$$\hat{H} = \epsilon_0 \hat{a}_0^\dagger \hat{a} + \sum_j \epsilon_j \hat{\beta}_j^\dagger \hat{\beta}_j, \tag{2.58}$$

where ϵ_0 is the energy of the condensate mode and ϵ_j the Bogoliubov energy spectrum from Section 2.4. Essentially, the condensate is treated as an additional harmonic oscillator mode of freedom. With equation (2.58), we therefore have the tools needed to model a Bose gas with the condensate as a quantum degree of freedom.

Chapter 3

Background II: Conditional measurement theory and feedback cooling

In this thesis, we model continuous-measurement feedback control as a technique for cooling a finite temperature gas. Explicitly, this means that we are implementing a control which depends upon an estimate of the system we are controlling. However, measurement of a quantum system leads to backaction — spontaneous wavefunction collapse due to the measurement made. As wavefunction collapse is random, the evolution of the system will be unique to each *trajectory* — that is, each instance in which we study it. Our feedback is therefore *conditional*: it depends upon the trajectory being considered.

In this chapter we introduce the study of systems that evolve under unique trajectories: conditional measurement theory. To understand this theory, we first review open quantum systems in Section 3.1 and then stochastic calculus in 3.2. In Section 3.3, we introduce the conditional measurement theory of a system coupled to an unchanging reservoir. In Section 3.4, we then provide an analytic introduction to feedback cooling based upon a conditional measurement, and review two feedback controls which have been used to achieve cooling in past literature. Implementing this understanding of conditional measurement theory and feedback cooling, in Section 3.5 we are then prepared to review the model presented by Szigeti *et al.* in Ref. [1] for the feedback cooling of an atomic gas using phase-contrast imaging. The aim of this thesis is then to develop a low temperature perturbative theory for this full quantum model.

3.1 Open quantum systems

When we first study quantum mechanics, we are often concerned with a quantum system in isolation from the environment it lives in. In order to model the measurement of that quantum system, we have to study both the system S and the device M used to complete the measurement. Rigorously, before the measurement our system lives in a Hilbert space $\mathcal{H}_S$ and our measurement device in $\mathcal{H}_M$. When we use the device to measure our system, they now both live in $\mathcal{H}_S \otimes \mathcal{H}_M$, the tensor product of their Hilbert spaces. The challenge with such a description is that quantum Hilbert spaces scale exponentially with their dimension, so the wavefunctions living in $\mathcal{H}_S \otimes \mathcal{H}_M$ become intractable for systems with more than a few dimensions.

One approach is to ignore some degrees of freedom of the measurement device. More generally, this approach is applied when a quantum system is entangled with some large *reservoir*. Physically, ignoring degrees of freedom of the reservoir assumes it is largely unaffected by interacting with the quantum system. This is analogous to, when studying the gravitational interaction between the Earth and the Sun, ignoring the effect upon the Sun's dynamics. When we make this approximation, we are studying an *open quantum system*.

In representing an ensemble of many quantum states, it is more efficient to introduce the *density matrix*. In this section, we will use the density matrix to model a quantum system coupled to a large reservoir. For a pedagogical introduction to open quantum systems under continuous measurement, the interested reader should consult Ref. [151]. For a more detailed introduction to open quantum systems more generally, the reader should see Ref. [152].

3.1.1 The density matrix

Consider a quantum system which can be described by one particular state $|\Psi\rangle$ — this is a *pure state*. For a pure state, the density matrix $\hat{\rho}$ is defined

$$\hat{\rho} = |\Psi\rangle\langle\Psi|. \tag{3.1}$$

The density matrix is more generally used to describe *mixed states*; where a system can be in a number of different states $|\psi_a\rangle$ in a different Hilbert space, each with probability P_a. As they are probabilities, $0 \leq P_a \leq 1$ and $\sum_a P_a = 1$. For a mixed state, the density matrix is defined as

$$\hat{\rho} = \sum_a P_a |\psi_a\rangle\langle\psi_a|. \tag{3.2}$$

The equation of motion for the density matrix is the *master equation*. In a closed system, this is the von Neumann equation

$$\frac{d\hat{\rho}}{dt} = -\frac{i}{\hbar}\left[\hat{H}_S, \hat{\rho}\right], \tag{3.3}$$

where $\hat{H}_S$ is the closed system Hamiltonian. Note that $\hat{\rho}$ is a matrix of states $|\psi_a\rangle$, so we are implicitly working in the Schrödinger picture.

Equation (3.3) can be used to find the full dynamics of the system, or the evolution of the average of a particular operator $\langle\hat{A}\rangle$. To achieve the latter, we first derive from equation (3.2)that[1]

$$\left\langle \hat{A} \right\rangle = \mathrm{Tr}\left\{\hat{A}\hat{\rho}\right\} = \sum_a P_a \left\langle \psi_a \left| \hat{A} \right| \psi_a \right\rangle. \tag{3.4}$$

[1]The proof follows from inserting the identity $\hat{1} = \sum_k |k\rangle\langle k|$ into the right-hand side of equation (3.4), where $\{|k\rangle\}$ is some orthonormal basis.

We then take the time derivative of equation (3.4) and substitute equation (3.3) to obtain

$$\begin{aligned}\frac{d\left\langle \hat{A}\right\rangle}{dt} &= \mathrm{Tr}\left\{\hat{A}\frac{d\hat{\rho}}{dt}\right\} \\ &= -\frac{i}{\hbar}\mathrm{Tr}\left\{\hat{A}\left(\hat{H}_S\hat{\rho}-\hat{\rho}\hat{H}_S\right)\right\} \\ &= -\frac{i}{\hbar}\left\langle\left[\hat{A},\hat{H}_S\right]\right\rangle,\end{aligned} \tag{3.5}$$

where in the final step we used the cyclic nature of the trace.

3.1.2 System-reservoir coupling

The evolution of two interacting quantum systems A and B can be studied via the density operator $\hat{\rho}_{AB}$, which evolves under equation (3.3) for a joint Hamiltonian $\hat{H}_{AB}$. The evolution of A can be found by tracing over the possible states of B; that is, $d\hat{\rho}_A = \mathrm{Tr}_B\{d\hat{\rho}_{AB}\}$. However, the full evolution of $\hat{\rho}_{AB}$ under equation (3.3) is typically intractable.

In order to proceed further, we consider a particular case: a quantum system with Hilbert space $\hat{\mathcal{H}}_S$ coupled to some reservoir with Hilbert space $\hat{\mathcal{H}}_R$. We describe more rigorously the approximations made upon the reservoir in a moment, but physically we are treating the reservoir as a large quantum object which is unaffected by its interaction with $\mathcal{H}_S$. We do this because we will be considering the measurement of a system with light, of which is there is practically an infinite supply, or "reservoir".

For a system coupled to a reservoir, it is possible to derive a tractable master equation for the evolution of the system $d\hat{\rho}_S$. The details of the derivation are beyond the scope of this thesis (see Ref. [153] for a pedagogical introduction), but we make note of the key assumptions:

1. The system and reservoir are always separable; that is, $\hat{\rho}_{SR}(t) = \hat{\rho}_S(t)\otimes\hat{\rho}_R(t)$. This is the *Born Approximation*.
2. The system S is *Markovian*; the dynamics are wholly determined by its present state, and unaffected by its past history.
3. The reservoir is so large that it is statistically unaffected by the interaction with the system; the most simple mathematical consequence of this is that $\hat{\rho}_R(t) = \hat{\rho}_R(0)$.[2]

Using these approximations, the master equation for the system has the *Linbladian* form

$$\frac{d\hat{\rho}_S}{dt} = \underbrace{-\frac{i}{\hbar}\left[\hat{H}_S,\hat{\rho}_S\right]}_{\text{Hamiltonian Evolution}} + \underbrace{\sum_a \mathcal{D}\left[\hat{c}_a\right]\hat{\rho}_S}_{\text{Decoherence}}, \tag{3.6}$$

where $\mathcal{D}$ is the *decoherence superoperator* defined as

$$\mathcal{D}\left[\hat{c}\right]\hat{\rho} = \hat{c}\hat{\rho}\hat{c}^\dagger - \frac{1}{2}\hat{c}^\dagger\hat{c}\hat{\rho} - \frac{1}{2}\hat{\rho}\hat{c}^\dagger\hat{c}. \tag{3.7}$$

[2]This is a rather broad conceptual summary of a number of mathematical approximations made. In particular, see equations 5.1.14, 5.1.15, 5.1.16 and 5.1.18 of Ref. [152].

Physically, the decoherence term models the change in order of the system due to the interaction with the reservoir, and the $\hat{c}_a$ are any operators in the combined Hilbert space which contribute to this decoherence. With equation (3.6), we therefore have a tool for modelling the average evolution of a system coupled to a large reservoir, without having to model the evolution of that reservoir itself.

However, this thesis is not solely concerned with the interaction between a system and a reservoir of light; we want to model the measurement of that light, to estimate density of the system. As each measured photon is entangled with individual atoms in our gas, measuring a photon induces wavefunction collapse of the entangled atom into a random state.[3] In order to model the random process of wavefunction collapse, we will need the tools of *stochastic calculus*, which we introduce in the next section.

3.2 An introduction to stochastic calculus

The rules of regular calculus break down for processes which include random "kicks" in the evolution of a variable. The techniques needed to successfully model these effects, the tools of stochastic calculus, are briefly introduced in this section. For a pedagogical introduction to the subject, the interested reader should consult Ref. [154]. Otherwise, a succinct summary of useful results can be found in Refs. [155] or [156].

So far in this thesis, we have considered equations of motion which are deterministic. That is, we have considered variables x which change with respect to a dynamic variable t as

$$dx = f(x(t), t)dt, \tag{3.8}$$

where $f(x(t), t)$ is a continuous, differentiable function. We will now consider *stochastic differential equations* (SDE) of the form

$$dx = f(x(t), t)dt + g(x(t), t)dW(t), \tag{3.9}$$

where $dW(t)$ is a *Wiener increment* representing our noise, and $g(x(t), t)$ is the magnitude of that noise. In particular, a Wiener increment models *white noise* — noise which acts completely independently of the past. Several examples of such noise are included in Figure 3.1. By the Central Limit Theorem, the sum of many random variables from an arbitrary distribution obeys a Gaussian distribution, so are defined by their mean and variance. Therefore, we formally define Wiener increments by

$$\begin{aligned} \mathbb{E}\left\{dW(t)\right\} &= 0, \\ \mathbb{E}\left\{dW(t)^2\right\} &= dt, \\ \mathbb{E}\left\{dW(t)dW(t')\right\} &= dtdt'\delta\left(t - t'\right), \end{aligned} \tag{3.10}$$

where $\mathbb{E}\left\{\cdot\right\}$ is a *stochastic average* - an average over a large number of possible values for a stochastic quantity[4]. Now that we have the form of $dW(t)$, we may naïvely try and solve

[3] Note that we are therefore not completely ignoring the reservoir; we instead study an evolution conditional upon a particular measurement record.

[4] Formally, $\mathbb{E}\left\{A(t)\right\} = \lim_{N\to\infty} \sum_{n=1}^{N} A(t)/N$, for some stochastic process $A(t)$.

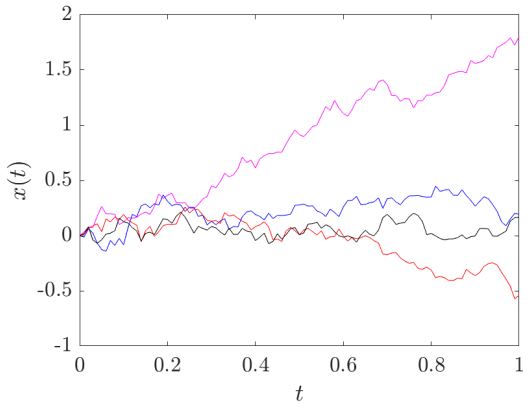

Figure 3.1: Four solutions to the differential equation $dx = dW(t)$. The solutions are completely uncorrelated and random. Any infinitely small region of each signal obeys those same properties.

equation (3.9) by integrating

$$x(t) = x(t_0) + \int_{t_0}^{t} f(x(t'), t')dt' + \int_{t_0}^{t} g(x(t'), t')dW(t'), \tag{3.11}$$

where t_0 is some initial time. The problem with equation (3.11) is that there are many ways to define the integral $\int dW(t')$. We can see this by defining the *stochastic integral* as

$$\int_{t_0}^{t} g\left(x(t'), t'\right) dW\left(t'\right) = \lim_{n\to\infty} S_n. \tag{3.12}$$

where S_n is the sum

$$S_n = \sum_{i=1}^{n} g\left(t_i^*\right)\left(dW(t_i) - dW(t_{i-1})\right), \tag{3.13}$$

and $t_{i-1} \leq t_i^* \leq t_i$. That is, we have broken $[t_0, t]$ into n small regions $\{[t_0, t_1] \ldots [t_{n-1}, t_n]\}$, and then summed over the function at some point within each region.[5] Now suppose that the point t_i^* is always chosen as $t_i^* = (1-\alpha)t_{i-1} + \alpha t_i$ for some real α which obeys $0 \leq \alpha \leq 1$. If $g(t) = dW(t)$, it is straightforward to show that

$$\mathbb{E}\left\{S_n\right\} = \sum_{i=1}^{n} \alpha\left(t_i - t_{i-1}\right) = \alpha\left(t - t_0\right). \tag{3.14}$$

Thus, the value of the stochastic integral depends upon which point in each small interval we choose. This ultimately means that different rules, such as the chain rule or product rule, are determined by which value of α is chosen. Note crucially that in deterministic calculus, the integral is independent of α [157]. Conversely, in stochastic calculus, α is chosen depending on which properties of differential equations are desired.

Choosing $\alpha = 0$ corresponds to picking the lower bound on each interval, and is referred to as *Itô integration*. Integrating in the Itô picture has the convenient property

[5] Note that equation (3.13) has the form of a Riemann sum.

that

$$\mathbb{E}\left\{\int_{t_0}^{t} g\left(x(t'),t'\right) dW\left(t'\right)\right\} = 0. \tag{3.15}$$

Equation (3.15) means that noisy terms disappear when taking the average of equations of motion. This makes it possible to analytically compute the moments of the distribution of a quantity. The downside is that the chain and product rules of regular calculus break; instead we have for some functions $h(x)$ and $j(x)$[6]

$$dh(x) = \left(\frac{\partial h(x)}{\partial x} f(x(t),t) + \frac{1}{2}\frac{\partial^2 h(x)}{\partial x^2} g(x(t),t)^2\right) dt + \frac{\partial h(x)}{\partial x} g(x(t),t) dW(t), \tag{3.16a}$$

$$d(h(x)j(x)) = dh(x)j(x) + h(x)dj(x) + dh(x)dj(x), \tag{3.16b}$$

the *Itô chain rule* and *Itô product rule* respectively. In this thesis, we derive and numerically integrate our finite temperature model in the Itô formalism.

An alternative formalism for the stochastic integral is *Stratonovich integration*, which corresponds to a choice of $\alpha = 1/2$. Using the same procedure to derive equation (3.16), it can be shown that the Stratonovich formalism follows the chain rule and product rule of deterministic calculus. It is possible to recast Itô equations of the form of equation (3.9) into the Stratonovich form by introducing the *Stratonovich correction*. Specifically, the equation of motion becomes

$$dx = \underbrace{f(x(t),t)dt}_{\text{Deterministic}} - \underbrace{\frac{1}{2} g(x(t),t)\cdot\nabla g(x(t),t)}_{\text{Stratonovich Correction}} + \underbrace{g(x(t),t)\eta(t)}_{\text{Noise (Stratonovich)}}, \tag{3.17}$$

where we use the notation $\eta(t)$ to refer to noise in the Stratonovich formalism. In this thesis, we derive and numerically solve Itô equations of motion. However, the merits and detriments of the Stratonovich formalism will be discussed in detail as an alternative method for more efficient numeric simulation in Chapter 6.

The Itô differential equations considered in this thesis have multiple noise sources, which have the form

$$dx_j = A_j dt + \sum_k^N B_{jk} dW_k(t), \tag{3.18}$$

where the index j is over the number of equations and N the number of noise sources. The model of Szigeti *et al.*, to be discussed in Section 3.5, will consider a sufficiently large number of noise sources where we can instead consider an integral over possible noises

$$\sum_k^N dW_k \to \int dx dW(x,t),$$

[6] In order to derive these results, estimate the change in a function $h(x)$ as $dh(x_i^*) = h(x_i) - h(x_{i-1})$ at a point x_i^* in the interval $x_{i-1} \le x_i^* \le x_i$. A similar process to deriving the chain rule in regular calculus is followed, except one must recognise that $dW(t)$ is of the order of $\sqrt{dt}$. For more details and different approaches, the interested reader should see Refs. [152] or [154].

and equation (3.18) becomes

$$dx_j = A_j dt + \int dx B_j(x) dW(x,t). \tag{3.19}$$

We now have the tools of stochastic calculus necessary to understand conditional measurement theory and model continuous measurement.

3.3 Conditional measurement theory

In Section 3.1, we described a quantum system interacting with a reservoir, concluding with a model for the dynamics which did not require studying the dynamics of the reservoir. Ultimately, we want to use this interaction to obtain some knowledge about the system, by measuring the reservoir (for a reservoir of light, we measure some photons from it). However, the interaction between the reservoir and part of the system entangles them. By measuring an element of the reservoir — say, a photon — we collapse the wavefunction of that photon, but also the wavefunction of the entangled part of the system. This measurement backaction is a stochastic process, so the evolution of the system is uniquely determined by that measurement. That is, each experimental realisation (trajectory) of a quantum system undergoing measurement is unique.

The goal of *conditional measurement theory* is to describe each of these single trajectories of a quantum system. The idea that a quantum system can take a single trajectory differs from traditional quantum mechanics, which says that you can only describe ensemble averages of observables. We only consider the key elements of conditional measurement theory here; a reader interested in a thorough introduction should see Ref. [158].

In conditional measurement theory, the density operator $\hat{\rho}$ is actually the average over all possible trajectories

$$\hat{\rho}(t) = \mathbb{E}\left\{\hat{\rho}_c(t)\right\}, \tag{3.20}$$

where $\hat{\rho}_c$ represents an individual trajectory of the system. The master equation for $\hat{\rho}_c$ depends upon the measurement considered. In this thesis, we assume *homodyne detection*, where a particular quadrature[7] (such as number or phase) of the optical field is measured [159]. For more details on homodyne detection, see Ref. [160]. Under homodyne detection, each individual trajectory evolves under the *stochastic master equation*

$$d\hat{\rho}_c = \underbrace{-\frac{i}{\hbar}\left[\hat{H},\hat{\rho}_c\right]dt}_{\text{Hamiltonian Evolution}} + \underbrace{\sum_a \mathcal{D}\left[\hat{c}_a\right]\hat{\rho}_c dt}_{\text{Decoherence}} + \underbrace{\sum_a \mathcal{H}\left[\hat{c}_a\right]\hat{\rho}_c dW_a(t)}_{\text{Innovations}}, \tag{3.21}$$

where $dW_a(t)$ is the noise associated with each $\hat{c}_a$, which obey $\mathbb{E}\left\{dW_a(t)dW_b(t)\right\} = \delta_{ab}dt$. The new term in the equation is referred to as the *innovations* term. Physically, the innovations term represents the information about a system observable $(\hat{c}_a + \hat{c}_a^\dagger)$ obtained by the continuous measurement. That information is wrapped up in the *innovations*

[7] The quadratures of an operator $\hat{c}_a$ are essentially proportional to its real and imaginary components, i.e. $(\hat{c}_a^\dagger + \hat{c}_a)$ and $i(\hat{c}_a^\dagger - \hat{c}_a)$. We will introduce quadratures in more detail, specifically for the Bogoliubov modes, in Chapter 4.2.

superoperator $\mathcal{H}$, which is defined as

$$\mathcal{H}\left[\hat{c}\right]\hat{\rho} = \hat{c}\hat{\rho} + \hat{\rho}\hat{c}^{\dagger} - \mathrm{Tr}\left\{\left(\hat{c} + \hat{c}^{\dagger}\right)\hat{\rho}\right\}\hat{\rho}. \tag{3.22}$$

For a full derivation of equation (3.21), see Chapter 4 of Ref. [158]. Note that taking the expectation value of this stochastic master equation obtains equation (3.6), the Lindblad master equation[8]. Why, then, should we be concerned with any individual trajectory $\hat{\rho}_c$?

The answer is that, in an experiment, we will only ever observe a particular trajectory. As will be discussed in the following section, a feedback control depends upon measured values of quantities in the system, so the Hamiltonian evolution is unique to each trajectory. To fully characterise a feedback control scheme, we will therefore need to study a large number of individual trajectories. In particular, we use the following procedure to characterise a continuously-measured system undergoing feedback control:

1. Generate an initial state $\hat{\rho}(t = 0)$. In this thesis, the initial state will be a thermal state of a particular temperature.

2. Make many ($\mathcal{O}(100)$) copies $\hat{\rho}_c$ of that initial state, and evolve each copy under different random noise sources. This can be achieved by using a pseudo-random number generator for the noise $dW_j(t)$.

3. Throughout the evolution, average particular observables across all trajectories. This approximates their average value to within an uncertainty estimated by computing the standard deviation across all trajectories.

In reality, when a feedback control is applied, it is done by looking at the *filter* $\hat{\pi}_c$, which is the experimenter's esimate of $\hat{\rho}_c$. The dynamics of the filter are different to the dynamics of the trajectory; the filter dynamics depend on how well the system state is approximated by the information obtained via measurement. In order to fully characterise a feedback control, it would be necessary to complete a *system-filter separation*, where $\hat{\pi}_c$ and $\hat{\rho}_c$ are modelled by two separate equations of motion. Such a separation will not be made in this thesis; we will assume our filter $\hat{\pi}_c$ perfectly estimates the trajectory $\hat{\rho}_c$. In Chapter 7, we will propose a system-filter separation based upon that in Ref. [161]. For a more detailed introduction to system-filter separation, the interested reader should consult Ref. [162].

3.4 An analytic perspective on feedback cooling

Now that we have reviewed conditional measurement theory, we are ready to introduce how we model feedback cooling. In particular, we will review how a feedback control based upon a conditional measurement is used to cool a gas, and introduce two control schemes proposed in the literature to achieve feedback cooling.

3.4.1 Basic principles

Closed-loop feedback control is used to cool a trapped atomic gas by introducing an additional time-dependent potential, $V_C(x, t)$, termed the control potential. Introducing this

[8] To obtain this result, note that $\mathbb{E}\left\{\hat{\rho}_c dW_a(t)\right\} = \mathbb{E}\left\{\hat{\rho}_c\right\}\mathbb{E}\left\{dW_a(t)\right\} = 0$. This is because the trajectory $\hat{\rho}_c$ is completely independent of any future value of $dW(t)$, so the two are uncorrelated. A more rigorous justification of this can be found in Chapter 4 of Ref. [155].

potential is equivalent to making the transformation $V_{\text{ext}}(x,t) \to V_0(x) + V_C(x,t)$, where $V_0(x)$ refers to the time-independent potential used to trap the gas. Our 1D Hamiltonian becomes

$$\hat{H} = \hat{H}_0 + \int dx \hat{\psi}^\dagger(x) V_C(x,t) \hat{\psi}(x), \tag{3.23}$$

where $\hat{H}_0$ now denotes the cold-atom Hamiltonian introduced in equation (2.22) with a trapping potential $V_0(x)$. The second term in equation (3.23) will be referred to as $\hat{H}_C$, or the *feedback Hamiltonian*.

In reality, what constraints are there on our control potential? Experimentally, attractive (repulsive) dipole interactions between red (blue) detuned light and atoms are used to prepare a broad range of trapping potentials [55]. Via the implementation of digital micromirror devices [163], this detuned light can be varied on a time-scale faster than the atom dynamics, and to a resolution finer than the size of density fluctuations in the gas. Therefore, we will assume arbitrary spatial and temporal control over $V_C(x,t)$.

Although we are ultimately concerned with increasing the condensate fraction of the gas, feedback cooling achieves this by damping out energy excitations. Feedback cooling should therefore decrease the total energy in an atomic gas. In particular, we are concerned with the energy in the absence of feedback: this will be the energy left in the gas once feedback cooling is completed. That is, we are concerned with $E_0 = \langle \hat{H}_0 \rangle$. Using the Heisenberg equation of motion (equation (2.17)), we obtain[9]

$$\begin{aligned} \frac{dE_0}{dt} &= -\frac{i}{\hbar} \left\langle \left[\hat{H}_0, \hat{H} \right] \right\rangle \\ &= -\frac{i}{\hbar} \left\langle \left[\hat{H}_0 + \hat{H}_C - \hat{H}_C, \hat{H}_0 + \hat{H}_C \right] \right\rangle \\ &= \frac{i}{\hbar} \left\langle \left[\int dx \hat{\psi}^\dagger(x) V_C(x,t) \hat{\psi}(x), \hat{H} \right] \right\rangle_C . \end{aligned} \tag{3.24}$$

Note that we have introduced the subscript C to indicate that we are taking the *conditional* expectation value, because $V_C(x,t)$ is computed in real time, depending upon the unique trajectory of the quantum system. To continually decrease the energy of the gas, we are concerned with picking a form for $V_C(x,t)$ such that this expression is negative. We now review some control schemes which have been used to theoretically demonstrate feedback cooling.

3.4.2 Picking a control

Feedback control was first used to model cooling by Haine *et al.* in Ref. [89]. The authors simulated a mean-field model of a BEC using the GPE (equation (2.25)) and demonstrated that energy could be removed from the condensate using *moment control*. Moment control refers to a potential of the form

$$V_C(x,t) = \sum_n c_n f_n(x) \frac{d \langle f_n(x) \rangle_C}{dt}, \tag{3.25}$$

[9] To go from the second line to the third, we use the fact that $\hat{H}$ (as does any operator) commutes with itself.

where the $f_n(x)$ are arbitrary functions of x, and c_n are positive constants. Again, the subscript C is used to indicate that the expectation value is computed uniquely for each trajectory. The functions $f_n(x)$ are typically chosen as a single polynomial term, such as $f_n(x) = x^n$, so that each term in the control corresponds to a particular moment of the BEC density (hence the name). Substituting the moment control potential into equation, (3.24)

$$\begin{aligned}\frac{dE_0}{dt} &= \frac{i}{\hbar}\sum_n c_n \frac{d\left\langle f_n(x)\right\rangle_C}{dt}\left\langle\left[\int dx\hat{\psi}^\dagger(x)f_n(x)\hat{\psi}(x),\hat{H}\right]\right\rangle_C \\ &= -\sum_n c_n\left(\frac{d\left\langle f_n(x)\right\rangle_C}{dt}\right)^2.\end{aligned} \tag{3.26}$$

As $c_n > 0$, energy is driven out of the gas when the fluctuations $d\left\langle f_n(x)\right\rangle_C/dt$ are non-zero. The fluctuations $d\left\langle f_n(x)\right\rangle_C/dt$ are the *error signals* of the feedback control. Much of the early work in feedback cooling was done using moment control [164, 1, 2]. However, if there are no fluctuations in the moment being controlled (if $d\left\langle f_n(x)\right\rangle_C/dt = 0$) the feedback no longer cools the gas, and the system is in a *dark state*. For a collection of interacting atoms, the non-linear interaction term couples density moments of equal parity[10], which allows fluctuations in higher-order moments to be slowly damped as atoms move between moments. However, this process takes place over timescales an order of magnitude larger than to cool the lower-order density moments — so is not particularly efficient [89].

Two recent theses by Goh [64] and Taylor [95] have shown that an alternative, the *energy damping control*, can cool an atomic gas from any state that is not an eigenstate of the Hamiltonian. Furthermore, the energy damping control can cool both Bose and Fermi gases more effectively than the moment control. The energy damping control has the form[11]

$$V_C(x,t) = -k_{\mathrm{ED}}\nabla_x\cdot\left\langle\hat{j}(x)\right\rangle_C, \tag{3.27}$$

where k_{ED} is a positive real constant and $\hat{j}(x)$ is the particle current defined as

$$\hat{j}(x) = \frac{\hbar}{2mi}\left[\hat{\psi}^\dagger(x)\left(\nabla_x\hat{\psi}(x)\right) - \left(\nabla_x\hat{\psi}^\dagger(x)\right)\hat{\psi}(x)\right]. \tag{3.28}$$

We can understand what the energy damping control physically does by recalling the continuity equation [167]

$$-\nabla_x\cdot\hat{j}(x) = -\frac{\partial\left(\hat{\psi}^\dagger(x)\hat{\psi}(x)\right)}{\partial t}, \tag{3.29}$$

where $\hat{\psi}^\dagger(x)\hat{\psi}(x)$ is the density of the wavefunction. Thus, changes in the average density of the gas are the error signals of the energy damping control. Substituting this control

[10] That is, odd density moments couple to odd density moments, and even density moments couple to even density moments.

[11] The form of the energy damping control - being proportional to the spatial derivative of the particle current - is inspired by a similar term which damps energy fluctuations in the stochastic-projected Gross-Pitaevskii equation (SPGPE) [165]. The SPGPE is a finite temperature classical field model for the dynamics of a Bose gas first presented in Ref. [166].

into equation (3.24), we observe

$$\begin{aligned}\frac{dE_0}{dt} &= \frac{i}{\hbar}\left\langle\left[\int dx\hat{\psi}^\dagger(x)\left(k_{\mathrm{ED}}\frac{d\left\langle\hat{\rho}(x)\right\rangle}{dt}\right)\hat{\psi}(x), \hat{H}\right]\right\rangle_C \\ &= k_{\mathrm{ED}}\int dx\frac{d\left\langle\hat{\psi}^\dagger(x)\hat{\psi}(x)\right\rangle_C}{dt}\frac{i}{\hbar}\left\langle\left[\hat{\psi}^\dagger(x)\hat{\psi}(x), \hat{H}\right]\right\rangle_C \\ &= -k_{\mathrm{ED}}\int dx\left(\frac{d\left\langle\hat{\psi}^\dagger(x)\hat{\psi}(x)\right\rangle_C}{dt}\right)^2.\end{aligned} \tag{3.30}$$

That is, as $k_{\mathrm{ED}} > 0$, the energy damping control will always decrease the energy of the gas if there are density fluctuations. This control does not rely upon fluctuations in any particular moment of the density, which is why it is more effective than moment control.

Of course, moment control and energy damping control are not our only choices for $V_C(x,t)$; for a thorough introduction to the different possibilities for the control of an atomic gas, see Chapters 5 and 6 of Ref. [158]. Indeed, other controls have been implemented to feedback cool a system. However, these have either been not physically feasible [100], or designed for other physical systems such as a mechanical resonator [168] or individual particles [169, 170] (as opposed to an ensemble of gaseous atoms).

We now have developed an understanding of how feedback cooling is achieved via a control potential $V_C(x,t)$. With the conditional measurement theory introduced in the preceding sections, we are now ready to introduce the stochastic master equation that will be used in this thesis to build a model for a continuously-monitored BEC at finite temperature.

3.5 Stochastic master equation for a BEC undergoing phase-contrast imaging

In this thesis, we use the master equation first proposed by Szigeti *et al.* in Ref. [1] and used in subsequent works [2, 94, 95]. We consider a Bose gas harmonically confined at frequencies $\omega_x \ll \omega_y = \omega_z$, so that it has sufficiently thin width $R_\perp$ in the y and z directions to be considered effectively 1D (as discussed in Section 2.3.1).

The model of Szigeti *et al.* assumes measurement via phase-contrast imaging, an experimentally successful scheme for performing continuous density measurements of BECs [101, 5]. In a phase-contrast imaging scheme, coherent light highly detuned from atomic resonance is shone upon a gas. As photons scatter off the gas, they pick up a phase shift. Encoded in this phase shift is information about the density of the BEC, which is extracted via homodyne detection of the number quadrature. This information is used to update the filter $\hat{\pi}_c$ and update the control potential $V_C(x,t)$. Phase-contrast imaging is considered to be a *non-destructive* process, because the light is highly detuned from resonance; so excitations are not induced. However, measurement backaction still causes decoherence that heats the system, which must be accounted for in the model. A diagram of this measurement-feedback process is included in Figure 3.2.

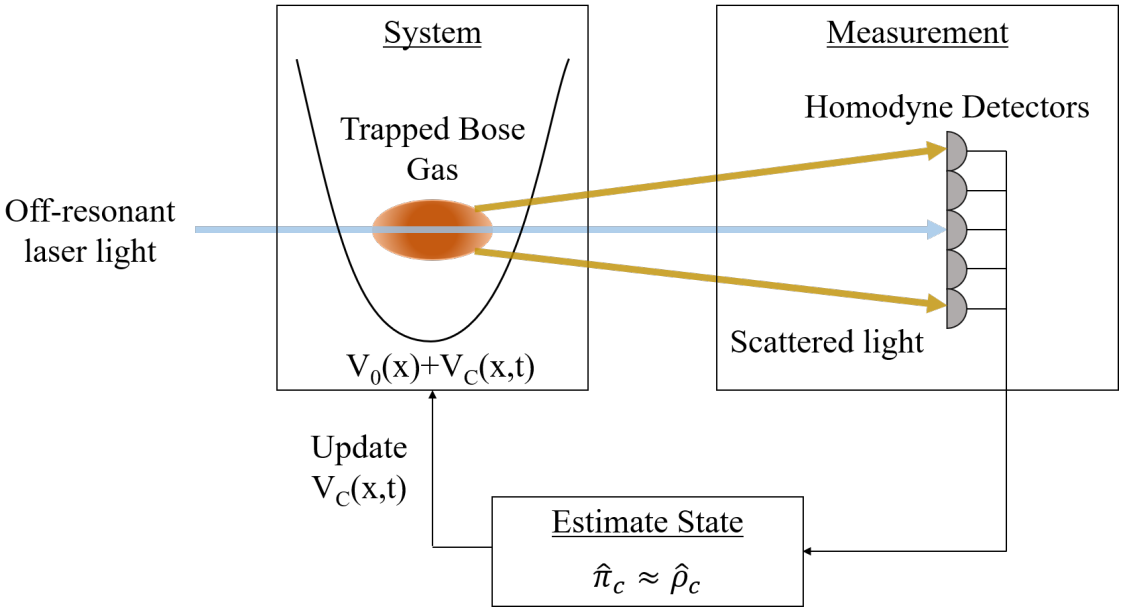

Figure 3.2: Measurement-feedback scheme introduced in Ref. [1] and modelled in this thesis. Off-resonant laser light shines on a Bose gas in a time-independent trapping potential $V_0(x)$ and time-dependent control potential $V_C(x,t)$. Some light scatters off atoms in the gas, picking up a phase shift. This phase shift is then measured by homodyne detection, and the gas density at a particular spatial resolution r is extracted from the phase measurement. That number quadrature is used to make an estimate of the system density and update the filter $\hat{\pi}_c$. In this thesis, we assume that $\hat{\pi}_c = \hat{\rho}_c$ (the filter exactly approximates the state). This state estimation is used to instantaneously update the control potential $V_C(x,t)$.

We assume that the filter $\hat{\pi}_c$ exactly approximates the system trajectory $\hat{\rho}_c$ so that we can model the former with the latter. The full derivation of the filter equation that leads to the stochastic master equation is beyond the scope of this thesis (the interested reader should see the Appendix of Ref. [1]) and leads to the stochastic master equation

$$d\hat{\rho}_c = \underbrace{-\frac{i}{\hbar}\left[\hat{H},\hat{\rho}_c\right]dt}_{\text{Unitary}} + \underbrace{\alpha\int dx\mathcal{D}\left[\hat{M}(x)\right]\hat{\rho}_c dt}_{\text{Decoherence}} + \underbrace{\sqrt{\alpha}\int dx\mathcal{H}\left[\hat{M}(x)\right]\hat{\rho}_c dW(x,t)}_{\text{Innovations}}. \quad (3.31)$$

The unitary term describes how the trajectory evolves under the cold atom Hamiltonian and the damping from an arbitrary feedback control. The decoherence term models how the laser light heats the system. The innovations term models the random information obtained from the homodyne detection, and is used to update the filter $\hat{\pi}_c$. Before unpacking the meaning of each term in equation (3.31), note that we use the notation introduced in Refs. [64, 95] instead of that in Ref. [1, 2, 94], because the former separates the contributions of the measurement strength and measurement resolution (to be introduced shortly).

In equation (3.31), the parameter α denotes the *measurement strength* and is defined as

$$\alpha = \frac{3\Gamma(5/4)}{16\sqrt{2}\pi^4}\left(\frac{\lambda}{R_\perp}\right)^{3/2}\frac{\Gamma_{\text{sp}}}{\omega_x}\frac{\Omega^2}{\Delta^2}. \quad (3.32)$$

Here, $\Gamma(x)$ is the Gamma function, λ is the wavelength of the measurement light, Γ_{sp} is the rate of spontaneous photon emission[12], Ω is the Rabi frequency, and Δ is the detuning of the laser from resonance. The Rabi frequency Ω characterises the coupling between the initial and final state of an atom in the case of spontaneous emission [160]. Increasing α increases the information obtained from the innovations terms but also the heating from the decoherence terms, so α is a parameter which should be optimised. Fortunately, as the Rabi frquency can be easily controlled by varying laser intensity [171], the measurement strength can effectively be treated as a free parameter.

The *measurement operator* $\hat{M}(x)$ is defined

$$\hat{M}(x) = \int dy K_r(x-y)\hat{\psi}^\dagger(y)\hat{\psi}(y), \quad (3.33)$$

and represents a measurement of the gas density $\hat{\rho}(x)$. Note that the integral over the measurement operator is the Linblad operator for this system; it arises in the limit of many operators

$$\sum_a \mathcal{D}\left[\hat{c}_a\right]\hat{\rho}_c \to \int dx\mathcal{D}\left[\hat{M}(x)\right]\hat{\rho}_c,\ \sum_a \mathcal{H}\left[\hat{c}_a\right]\hat{\rho}_c \to \int dx\mathcal{H}\left[\hat{M}(x)\right]\hat{\rho}_c.$$

[12]Specifically, the rate at which photons are randomly emitted from atoms as the laser passes through them (not resonant excitations), which changes the phase of the outgoing probe beam. The effects of spontaneous emission will not be otherwise rigorously considered in this thesis, because whilst they are unavoidable, they have been shown to have a negligible effect upon dispersive imaging techniques like phase contrast imaging upon the typcial experimental-time scales relevant to applications of feedback cooling [60]. For a more detailed discussion on spontaneous emission, see chapter 18 of Ref. [160].

Specifically, $\hat{M}(x)$ models a measurement of the convolution of the density with the *measurement kernel* $K_r(x)$

$$K_r(x) = \frac{1}{\sqrt{2\pi}} \int dk \left(\sqrt{\frac{r}{2\Gamma\left(5/4\right)}} e^{-(rk)^4/2} \right) e^{ikx}, \tag{3.34}$$

and is normalised as $\int dx \left|K_r(x)\right|^2 = 1$ by Plancherel's theorem [172]. This definition enforces that the measurement operator $\hat{M}(x)$ is Hermitian, symmetric and real. The measurement kernel blurs the density measurement, modelling the physical limitation to how accurately density can be measured. This limit is precisely modelled by the *measurement resolution* r

$$r = \frac{1}{2L} \sqrt{\frac{R_\perp \lambda}{\pi}}, \tag{3.35}$$

which is the diffraction limit of an optical measurement. Note that by changing the length of the trap and frequency of the laser, r can be varied (above the diffraction limit), in order to optimise the feedback control.[13]

The full dynamics of equation (3.31) are intractable analytically or numerically. It has been so far studied through mean-field approximations and the NPW method: in the original paper [1], Szigeti *et al.* numerically integrated a mean-field model for a coherent state of a single particle. However, as the measurement operator $\hat{M}(x)$ is defined in terms of a number density measurement (equation (3.33)), the feedback actually drives the gas towards a Fock state. In a subsequent work, Szigeti *et al.* successfully integrated equation (3.31) with a Hartree-Fock mean-field approximation upon the trajectory $\hat{\rho}_c$. Similarly, a Hartree-Fock mean-field model was used to integrate a similar master equation for an ultra-cold Fermi gas [64]. The NPW method was used to study equation (3.31) at finite temperature in Ref. [95].

In this thesis, we will derive and perform preliminary characterisation of a model for solving equation (3.31) at low, finite temperatures. This aim will be achieved by implementing the Bogoliubov perturbation theory introduced in Chapter 2.

[13] Note that the model of Szigeti *et al.* requires a non-zero r; at $r = 0$ (perfect measurement resolution), the kernel $K_r(x)$ becomes a delta function. This would then project the quantum state to a perfectly localised state in position space, which corresponds to an infinite uncertainty in momentum. Setting $r = 0$ is therefore unphysical: the measurement backaction would become infinite, leading to an infinite energy state.

Chapter 4

Deriving a finite temperature model for feedback cooling

Having introduced in Chapter 3 the closed-loop feedback scheme we will study in this thesis, we are now ready to model it at low temperatures by implementing the Bogoliubov theory introduced in Chapter 2. In this chapter, we derive our full perturbative model for an arbitrary $V_0(x)$ and $V_C(x,t)$. In Chapter 5, we will derive the model for a particular $V_0(x)$ and $V_C(x,t)$.

The first portion of this chapter will be justifying the analytic tools used to build our model. In particular, in Section 4.1 we motivate using a number-conserving Bogoliubov theory, and in Section 4.2, we rigorously introduce the quadrature representation for the Bogoliubov modes used throughout the derivation.

In deriving the full model, we break down the unitary evolution in equation (3.31) as

$$-\underbrace{\frac{i}{\hbar}\left[\hat{H},\hat{\rho}_c\right]dt}_{\text{Unitary}} = -\underbrace{\frac{i}{\hbar}\left[\hat{H}_0,\hat{\rho}_c\right]dt}_{\text{Cold atom dynamics}} - \underbrace{\frac{i}{\hbar}\left[\hat{H}_C,\hat{\rho}_c\right]dt}_{\text{Feedback dynamics}}, \tag{4.1}$$

where we have separated out the dynamics due to the cold atom Hamiltonian and the feedback potential. This is because the feedback is real-time, so it is not physically defined in absence of the measurement. Thus, we will first derive the cold atom dynamics in Section 4.3, then the measurement dynamics in Section 4.4, and finally the feedback dynamics in Section 4.5.

4.1 Choice of Bogoliubov theory

In developing a model of feedback cooling with Bogoliubov theory, one could either use the symmetry-breaking or number-conserving approach. This thesis will use the latter, and in this section we present a simple calculation to justify why. In particular, we will show that in a symmetry-breaking approach, the feedback control cannot change the average number of excitations in the gas.

In a symmetry-breaking Bogoliubov approach, the condensate is treated as a classical reservoir, which obeys $N_C \approx N_C + 1$. The temperature of the gas is therefore quantified by the average number of excitations $\langle \hat{N}_T \rangle$. If the number of excitations is the

number of non-condensate atoms, then

$$\begin{aligned}\left\langle \hat{N}_T \right\rangle &= \left\langle \hat{N} \right\rangle - N_C \\ &= \int dx \left\langle \left[\left(\chi_0^*(x)\hat{\delta}(x) + \text{h.c.} \right) + \hat{\delta}^\dagger(x)\hat{\delta}(x) \right] \right\rangle \\ &= \int dx \left\langle \hat{\delta}^\dagger(x)\hat{\delta}(x) \right\rangle ,\end{aligned} \tag{4.2}$$

where we take advantage of the fact that $\langle \hat{\delta}(x) \rangle = 0$. Let us now consider the evolution of the number of excitations under the feedback Hamiltonian. From the Heisenberg equation of motion (equation (2.17)), we have

$$\frac{\left\langle d\hat{N}_T \right\rangle}{dt}_{\text{Feedback}} = -\frac{i}{\hbar} \left\langle \left[\hat{N}_T, \hat{H}_C \right] \right\rangle , \tag{4.3}$$

where we are only considering the effect of feedback on the number of excitations. We expand the feedback Hamiltonian as

$$\hat{H}_C = \int dx V_C(x,t) \left(|\chi_0(x)|^2 + \chi_0^*(x)\hat{\delta}(x) + \chi_0(x)\hat{\delta}^\dagger(x) + \hat{\delta}^\dagger(x)\hat{\delta}(x) \right) , \tag{4.4}$$

and so can calculate the relevant commutator

$$\begin{aligned}\left\langle \left[\hat{N}_T, \hat{H}_C \right] \right\rangle &= \int dx \int dy V_C(y,t) \left\langle \left[\hat{\delta}^\dagger(x)\hat{\delta}(x), |\chi_0(y)|^2 + \left(\chi_0^*(y)\hat{\delta}(y) + \text{h.c.} \right) + \hat{\delta}^\dagger(y)\hat{\delta}(y) \right] \right\rangle \\ &= \int dx \int dy V_C(y,t)\delta(x-y) \left\langle \left[\left(\chi_0(y)\hat{\delta}^\dagger(x) - \text{h.c.} \right) + \hat{\delta}^\dagger(x)\hat{\delta}(y) - \hat{\delta}^\dagger(y)\hat{\delta}(x) \right] \right\rangle \\ &= \int dx V_C(x,t) \left[\chi_0(x) \left\langle \hat{\delta}^\dagger(x) \right\rangle - \chi_0^*(x) \left\langle \hat{\delta}(x) \right\rangle \right] \\ &= 0.\end{aligned} \tag{4.5}$$

Here, we have gone from the penultimate line to the final line by again using that the average of the fluctuation parameter $\langle \hat{\delta}(x) \rangle = 0$ in a symmetry-breaking approach. It follows immediately from substituting equation (4.5) into equation (4.3) that $\langle d\hat{N}_T \rangle / dt_{\text{Feedback}} = 0$. Therefore, any arbitrary feedback potential cannot change the average number of excitations. Note that in deriving this result, we did not use the Bogoliubov transformation; it arises solely as a consequence of the symmetry-breaking approximation (equation (2.30)).

The physical meaning of this result is that, in order to have particle exchange between the excitations and the condensate, the condensate cannot be treated as a classical reservoir. Therefore, to model feedback *cooling* rather than control[1], we must treat the condensate as a quantum degree of freedom. We will therefore proceed with a number-conserving approach.

[1] It is worth noting that Hurst *et al.* claim in Ref. [99] to have modelled feedback cooling with a symmetry-breaking model. However, their use of the phrase "feedback cooling" has a different meaning to that of this thesis - they use feedback control to damp out excitations induced by measurement of their system. In fact, the average number of excitations does not change in their model, agreeing with the above result.

4.2 Introducing Bogoliubov mode quadratures

It is standard, in Bogoliubov theory, to introduce the Bogoliubov transformation in terms of the creation and annihilation operators $\hat{\beta}_j^\dagger$ and $\hat{\beta}_j$, as in Chapter 2.4. This is because these operators natrually motivate the idea of quasiparticles as collective excitations of the Bose gas. However, it is sometimes more useful to instead use the equivalent transformation

$$\hat{\delta}(x) = \sum_{j>0} \left[f_j^-(x)\hat{X}_j + i f_j^+ \hat{P}_j \right], \tag{4.6}$$

where $\{\hat{X}_j, \hat{P}_j\}$ are the dimensionless quadrature operators defined as[2]

$$\hat{X}_j = \frac{1}{\sqrt{2}}\left(\hat{\beta}_j^\dagger + \hat{\beta}_j\right), \text{ and } \hat{P}_j = \frac{i}{\sqrt{2}}\left(\hat{\beta}_j^\dagger - \hat{\beta}_j\right), \tag{4.7}$$

where $j > 0$. These are, respectively, the *position* and *momentum quadratures* of the Bogolibuov operators. They are called so because these definitions are analogous to the relationship between the position/momentum and creation/annihilation operators for the quantum harmonic oscillator; their actual physical meaning depends upon the form of the Bogoliubov modes. As a consequence of their definition, the quadrature operators are Hermitian and obey

$$\left[\hat{X}_j, \hat{P}_k\right] = i\delta_{jk}, \text{ and } \left[\hat{X}_j, \hat{X}_k\right] = \left[\hat{P}_j, \hat{P}_k\right] = 0, \tag{4.8}$$

and the coefficients $f_j^\pm(x)$ are defined as

$$f_j^\pm(x) = \frac{1}{\sqrt{2}}\left(u_j(x) \mp v_j^*(x)\right). \tag{4.9}$$

These quadrature coefficients obey a modified set of Bogoliubov-de Gennes equations

$$\hat{\mathcal{L}}(x) f_j^-(x) + C(x) f_j^{-*}(x) = \epsilon_j f_j^+(x), \tag{4.10a}$$
$$\hat{\mathcal{L}}(x) f_j^+(x) - C(x) f_j^{+*}(x) = \epsilon_j f_j^-(x), \tag{4.10b}$$

and it is straightforward to show that this is the same ϵ_j as in equation (2.42).

We are motivated to introduce a quadrature representation for the Bogoliubov excitations for two reasons. Firstly, symmetrised pairs of these operators (i.e. $(\hat{X}_j\hat{P}_k + \hat{P}_k\hat{X}_j)/2$) are real. Secondly, the quadrature representation is the most common notation for the analytic solutions of a particular class of quantum systems. Specifically, we are referring to systems described by *linear quadratic gaussian* control theory [158], which we discuss in Chapter 7. The feedback and measurement terms in the model derived in this thesis do not satisfy the properties of LQG control, however in Chapter 7 we will present a possible approximation scheme in which they do. In order to set up future work under that approximation scheme, we use the quadrature representation in this thesis.

[2] Technically, for a one-dimensional system, it is actually standard to use phase and number quadratures. For a more detailed discussion of why, the interested reader should see Ref. [107]. However, in this thesis we deal with an *effective* one-dimensional system, so the position and momentum quadratures in equation (4.7) are suitable.

4.2.1 Quadrature representation of the condensate mode

In a number-conserving Bogoliubov approach, the condensate is a quantum degree of freedom described by the operator $\hat{a}_0$. That is, our field operator is defined as

$$\hat{\psi}(x) = \chi_0(x)\hat{a}_0 + \hat{\delta}(x), \tag{4.11}$$

where $\chi_0(x)$ is the condensate wavefunction solved by the GPE. It is straightforward to include a pair of additional, $j = 0$, quadratures

$$\hat{X}_0 = \frac{1}{\sqrt{2}}\left(\hat{a}_0^\dagger + \hat{a}_0\right), \text{ and } \hat{P}_0 = \frac{i}{\sqrt{2}}\left(\hat{a}_0^\dagger - \hat{a}_0\right), \tag{4.12}$$

which obey the commutation relations in equation (4.8) for $j = 0$ and commute with the $j \neq 0$ quadratures. Rather than separating out the condensate mode from the Bogoliubov excitations, we can then include the condensate as the 0th Bogoliubov mode. That is, our wavefunction becomes

$$\hat{\psi}(x) = \sum_{j=0}\left[f_j^-(x)\hat{X}_j + if_j^+\hat{P}_j\right], \tag{4.13}$$

where

$$f_{j=0}^{\pm}(x) = \frac{\chi_0(x)}{\sqrt{2}}. \tag{4.14}$$

Note that the sum in equation (4.13) now starts at $j = 0$, rather than $j > 0$. Equation (4.13) is equivalent to equation (4.11); it is simply a more efficient notation. Representing the condensate and excitations with the quadratures for each mode, the diagonal cold atom Hamiltonian (equation (2.58)) becomes

$$\hat{H}_0 = \frac{1}{2}\sum_{j=0}\epsilon_j\left(\hat{X}_j^2 + \hat{P}_j^2\right), \tag{4.15}$$

where ϵ_0 is the condensate energy and all non-operator terms have been discarded as a constant energy offset. It is also useful to write the wavefunction density $\hat{\psi}^\dagger(x)\hat{\psi}(x)$ in the quadrature representation

$$\hat{\psi}^\dagger(x)\hat{\psi}(x) = \sum_{j,k=0}\left[f_j^{-*}(x)f_k^-(x)\hat{X}_j\hat{X}_k + f_j^{+*}(x)f_k^+(x)\hat{P}_j\hat{P}_k + \left(if_j^{-*}(x)f_k^+(x)\hat{X}_j\hat{P}_k + \text{h.c.}\right)\right], \tag{4.16}$$

because both the feedback Hamiltonian $\hat{H}_C$ and measurement operator $\hat{M}(x)$ are defined in terms of this quantity.

4.2.2 Expectation values of interest

Our goal is to study how an atomic gas evolves under feedback by modelling the evolution of the condensate fraction. At any time, the occupation of the condensate $\langle\hat{N}_C\rangle$ is given by

$$\left\langle\hat{N}_C\right\rangle = \left\langle\hat{a}_0^\dagger\hat{a}_0\right\rangle = \frac{1}{2}\left[\left\langle\hat{X}_0\hat{X}_0\right\rangle + \left\langle\hat{P}_0\hat{P}_0\right\rangle - 1\right]. \tag{4.17}$$

Therefore, to study the evolution of physical observables such as condensate fraction, we will model the dynamics of symmetrised pairs of operators

- $\left\langle\hat{X}_j\hat{X}_k + \hat{X}_k\hat{X}_j\right\rangle/2 = \left\langle\hat{X}_j\hat{X}_k\right\rangle$,

- $\left\langle \hat{P}_j\hat{P}_k + \hat{P}_k\hat{P}_j \right\rangle /2 = \left\langle \hat{P}_j\hat{P}_k \right\rangle$,
- $\left\langle \hat{X}_j\hat{P}_k + \hat{P}_k\hat{X}_j \right\rangle /2$.

We do not model the averages $\{\langle\hat{X}_j\rangle, \langle\hat{P}_j\rangle\}$, as it follows from the perturbation $\hat{\delta}$ having zero average that $\langle\hat{X}_j\rangle = \langle\hat{P}_j\rangle = 0$ (see Appendix A.2 for a proof). For that reason, we will write

$$\frac{1}{2}\left\langle \hat{X}_j\hat{P}_k + \hat{P}_k\hat{X}_j \right\rangle = \frac{1}{2}\left\langle \hat{X}_j\hat{P}_k + \hat{P}_k\hat{X}_j \right\rangle - \left\langle \hat{X}_j \right\rangle \left\langle \hat{P}_k \right\rangle = \mathrm{cov}\left(\hat{X}_j\hat{P}_k\right), \tag{4.18}$$

where $\mathrm{cov}(\hat{S}\hat{T})$ is the symmetrised co-variance of two operators $\hat{S}$ and $\hat{T}$, defined as above. Because the averages of the quadrature modes are zero, note that implicitly $\langle\hat{X}_j\hat{X}_k\rangle = \mathrm{cov}(\hat{X}_j\hat{X}_k)$ and $\langle\hat{P}_j\hat{P}_k\rangle = \mathrm{cov}(\hat{P}_j\hat{P}_k)$. These symmetrised operators are matrices, where physically:

1. The diagonal ($j = k$) elements of $\langle\hat{X}_j\hat{X}_k\rangle$ and $\langle\hat{P}_j\hat{P}_k\rangle$ correspond to the occupation of each Bogoliubov mode;
2. The off-diagonal ($j \neq k$) elements of $\langle\hat{X}_j\hat{X}_k\rangle$ and $\langle\hat{P}_j\hat{P}_k\rangle$ correspond to the *real* quantum correlations *between* Bogoliubov modes;
3. The off-diagonal elements of $\mathrm{cov}(\hat{X}_j\hat{P}_k)$ correspond to the *imaginary* quantum correlations *between* Bogoliubov modes;
4. The diagonal elements of $\mathrm{cov}(\hat{X}_j\hat{P}_k)$ correspond to the quantum correlations *within* each Bogoliubov mode.

We calculate the expectation value of a symmetrised operator $\langle\hat{A}\rangle = \langle\hat{S}\hat{T} + \hat{T}\hat{S}\rangle/2$ from the stochastic master equation by taking the trace of $d\hat{A}\hat{\rho}_c$

$$\begin{aligned} d\left\langle \hat{A} \right\rangle_C = &\underbrace{-\frac{i}{\hbar}\mathrm{Tr}\left\{\hat{A}\left[\hat{H}, \hat{\rho}_c\right]\right\} dt}_{\text{Unitary}} + \underbrace{\alpha \int dx \mathrm{Tr}\left\{\hat{A}\mathcal{D}\left[\hat{M}(x)\right]\hat{\rho}_c\right\} dt}_{\text{Decoherence}} \\ &\underbrace{+\sqrt{\alpha}\int dx \mathrm{Tr}\left\{\hat{A}\mathcal{H}\left[\hat{M}(x)\right]\hat{\rho}_c\right\} dW(x,t),}_{\text{Innovations}} \end{aligned} \tag{4.19}$$

and using equation (3.4). We calculate the unitary terms using equation (3.5); that is

$$-\frac{i}{\hbar}\mathrm{Tr}\left\{\hat{A}\left[\hat{H}, \hat{\rho}_c\right]\right\} dt = \underbrace{-\frac{i}{\hbar}\left\langle\left[\hat{A}, \hat{H}_0\right]\right\rangle dt}_{\text{Cold atom dynamics}} \underbrace{-\frac{i}{\hbar}\left\langle\left[\hat{A}, \hat{H}_C\right]\right\rangle_C dt}_{\text{Feedback dynamics}}, \tag{4.20}$$

where we separate out the cold atom and feedback dynamics, because the latter is conditioned upon a particular measurement record. We now are equipped with the formalism to derive our full model. In Section 4.3 we derive the cold atom dynamics; in Section 4.4 the measurement dynamics; and in Section 4.5 the feedback dynamics.

4.3 Cold atom dynamics

The cold atom dynamics of an operator $\hat{A}$ are found by computing

$$d\left\langle \hat{A}\right\rangle_{\hat{H}_0} = -\frac{i}{\hbar}\left\langle \left[\hat{A},\hat{H}_0\right]\right\rangle dt, \tag{4.21}$$

where we use the subscript $\hat{H}_0$ to indicate the cold atom dynamics. For a symmetrised operator, $\hat{A} = (\hat{S}\hat{T} + \hat{T}\hat{S})/2$, we apply the commutator identity $[\hat{A}\hat{B},\hat{C}] = \hat{A}[\hat{B},\hat{C}] + [\hat{A},\hat{C}]\hat{B}$ to obtain

$$\left\langle \left[\hat{A},\hat{H}_i\right]\right\rangle = \frac{1}{2}\left\langle \left(\hat{S}\left[\hat{T},\hat{H}_i\right] + \left[\hat{S},\hat{H}_i\right]\hat{T}\right) - \text{h.c.}\right\rangle, \tag{4.22}$$

for a Hamiltonian $\hat{H}_i$, where we have used the fact that Hamiltonians and quadrature operators are Hermitian. To compute the cold atom dynamics, we simply need to find the commutator of the position and momentum quadrature operators with the cold atom Hamiltonian. From the diagonal Hamiltonian (equation (4.15)) we obtain

$$\left[\hat{X}_j,\hat{H}_0\right] = \frac{1}{2}\sum_a \epsilon_a\left[\hat{X}_j,\hat{X}_a\hat{X}_a + \hat{P}_a\hat{P}_a\right] = i\epsilon_j\hat{P}_j, \tag{4.23a}$$

$$\left[\hat{P}_j,\hat{H}_0\right] = \frac{1}{2}\sum_a \epsilon_a\left[\hat{P}_j,\hat{X}_a\hat{X}_a + \hat{P}_a\hat{P}_a\right] = -i\epsilon_j\hat{X}_j. \tag{4.23b}$$

Substituting equation (4.23) into equation (4.22), we obtain the cold atom dynamics for each symmetrised operator pair

$$d\left\langle \hat{X}_j\hat{X}_k\right\rangle_{\hat{H}_0} = \left[\frac{\epsilon_k}{\hbar}\text{cov}\left(\hat{X}_j\hat{P}_k\right) + \frac{\epsilon_j}{\hbar}\text{cov}\left(\hat{X}_k\hat{P}_j\right)\right]dt, \tag{4.24a}$$

$$d\left\langle \hat{P}_j\hat{P}_k\right\rangle_{\hat{H}_0} = -\left[\frac{\epsilon_k}{\hbar}\text{cov}\left(\hat{X}_k\hat{P}_j\right) + \frac{\epsilon_j}{\hbar}\text{cov}\left(\hat{X}_j\hat{P}_k\right)\right]dt, \tag{4.24b}$$

$$d\text{cov}\left(\hat{X}_j\hat{P}_k\right)_{\hat{H}_0} = \left[\frac{\epsilon_j}{\hbar}\left\langle \hat{P}_j\hat{P}_k\right\rangle - \frac{\epsilon_k}{\hbar}\left\langle \hat{X}_j\hat{X}_k\right\rangle\right]dt. \tag{4.24c}$$

For m Bogoliubov modes, the cold atom dynamics in equation (4.24) describe a set of $m+1$ uncoupled harmonic oscillators.

4.4 Measurement dynamics

Observe from equation (4.19) that, in order to compute that decoherence and innovations terms, we must first compute the measurement operator $\hat{M}(x)$, defined as

$$\hat{M}(x) = \int dy K_r(x-y)\hat{\psi}^\dagger(y)\hat{\psi}(y). \tag{4.25}$$

Using the wavefunction density equation (4.16), we obtain

$$\hat{M}(x) = \sum_{a,b=0}\left[M^-_{ab}(x)\hat{X}_a\hat{X}_b + M^+_{ab}(x)\hat{P}_a\hat{P}_b + \left(N_{ab}(x)\hat{X}_a\hat{P}_b + \text{h.c.}\right)\right], \tag{4.26}$$

where we have defined the *measurement matrices*

$$M_{ab}^{\pm}(x) = \int dy K_r(x-y) f_a^{\pm *}(y) f_b^{\pm}(y), \tag{4.27a}$$

$$N_{ab}(x) = i \int dy K_r(x-y) f_a^{-*}(y) f_b^{+}(y). \tag{4.27b}$$

Note that we have not written the $\hat{X}_a \hat{P}_b$ terms or their Hermitian conjugate in terms of the symmetrised covariance. This is in order to make the derivation of the decoherence and innovations terms clearer.

4.4.1 Decoherence terms

We now are able to derive the decoherence terms. Expanding the decoherence superoperator, recognising that the measurement operator is Hermitian, and using the cyclic nature of the trace, we obtain

$$\begin{aligned} \mathrm{Tr}\left\{\hat{A}\mathcal{D}\left[\hat{M}(x)\right]\hat{\rho}_c\right\} &= \mathrm{Tr}\left\{\hat{A}\hat{M}(x)\hat{\rho}_c\hat{M}^\dagger(x)\right\} - \frac{1}{2}\mathrm{Tr}\left\{\hat{A}\hat{M}^\dagger(x)\hat{M}(x)\hat{\rho}_c\right\} \\ &\quad - \frac{1}{2}\mathrm{Tr}\left\{\hat{A}\hat{\rho}_c\hat{M}(x)\hat{M}(x)\right\} \\ &= \left\langle \hat{M}(x)\hat{A}\hat{M}(x) - \frac{1}{2}\hat{A}\hat{M}(x)\hat{M}(x) - \frac{1}{2}\hat{M}(x)\hat{M}(x)\hat{A}\right\rangle. \end{aligned} \tag{4.28}$$

where we have obtained expectation values using equation (3.4). We then rewrite the expression using commutators

$$\mathrm{Tr}\left\{\hat{A}\mathcal{D}\left[\hat{M}(x)\right]\hat{\rho}_c\right\} = \frac{1}{2}\left\langle\left[\hat{M}(x),\left[\hat{A},\hat{M}(x)\right]\right]\right\rangle. \tag{4.29}$$

For a symmetrised operator pair $\hat{A} = (\hat{S}\hat{T} + \hat{T}\hat{S})/2$, we use the commutator identity $[\hat{A}\hat{B},\hat{C}] = \hat{A}[\hat{B},\hat{C}] + [\hat{A},\hat{C}]\hat{B}$ to obtain

$$\begin{aligned} \mathrm{Tr}\left\{\hat{A}\mathcal{D}\left[\hat{M}(x)\right]\hat{\rho}_c\right\} =& \frac{1}{4}\left\langle\hat{S}\left[\hat{M}(x),\left[\hat{T},\hat{M}(x)\right]\right] + \mathrm{h.c.}\right\rangle + \frac{1}{4}\left\langle\left[\hat{M}(x),\left[\hat{S},\hat{M}(x)\right]\right]\hat{T} + \mathrm{h.c.}\right\rangle \\ & - \frac{1}{2}\left\langle\left[\hat{S},\hat{M}(x)\right]\left[\hat{T},\hat{M}(x)\right] + \mathrm{h.c.}\right\rangle, \end{aligned} \tag{4.30}$$

where we have again used that the measurement and quadrature operators are Hermitian. Therefore, by obtaining the commutator of each $\hat{X}_j$ and $\hat{P}_j$ with the measurement operator $\hat{M}(x)$, we can compute the decoherence terms for each of our symmetrised operator pairs. Computing each of these commutators, we obtain

$$\left[\hat{X}_j,\hat{M}(x)\right] = 2i\sum_a\left[M_{aj}^{+}(x)\hat{P}_a + \mathrm{Re}\left[N_{aj}(x)\right]\hat{X}_a\right], \tag{4.31a}$$

$$\left[\hat{P}_j,\hat{M}(x)\right] = -2i\sum_a\left[M_{aj}^{-}(x)\hat{X}_a + \mathrm{Re}\left[N_{aj}(x)\right]\hat{P}_a\right]. \tag{4.31b}$$

From equation (4.31), we then compute the second-order commutators $[\hat{M}(x),[\hat{X}_j,\hat{M}(x)]]$ and $[\hat{M}(x),[\hat{P}_j,\hat{M}(x)]]$. Substituting these commutators and those in equation (4.31) into equation (4.30) for each symmetrised operator pair yields the full decoherence term for each

symmetrised operator pair. The expressions are unwieldy, and so all three are included in Appendix B.1.1. As an example, we include here the decoherence term for $\mathrm{cov}(\hat{X}_j\hat{P}_k)$:

$$\begin{aligned}
d\left\langle \mathrm{cov}\left(\hat{X}_j\hat{P}_k\right)\right\rangle_{\mathcal{D}} = {} & 2\alpha dt\sum_{ab}\int dx\left[M^-_{ba}(x)\mathrm{Re}\left[N_{aj}(x)\right]-M^-_{ak}(x)\mathrm{Re}\left[N_{ba}(x)\right]\right]\left\langle \hat{X}_j\hat{X}_b\right\rangle \\
& + 2\alpha dt\sum_{ab}\int dx\left[M^+_{ba}(x)\mathrm{Re}\left[N_{aj}(x)\right]-M^+_{aj}(x)\mathrm{Re}\left[N_{ba}(x)\right]\right]\left\langle \hat{P}_b\hat{P}_k\right\rangle \\
& - 4\alpha dt\sum_{ab}\int dx\mathrm{Re}\left[N_{aj}(x)\right]M^-_{bk}(x)\left\langle \hat{X}_a\hat{X}_b\right\rangle \\
& - 4\alpha dt\sum_{ab}\int dx M^+_{aj}(x)\mathrm{Re}\left[N_{bk}(x)\right]\left\langle \hat{P}_a\hat{P}_b\right\rangle \\
& + 2\alpha dt\sum_{ab}\int dx\left[\mathrm{Re}\left[N_{ak}(x)\right]\mathrm{Re}\left[N_{ba}(x)\right]-M^-_{ak}(x)M^+_{ba}(x)\right]\mathrm{cov}\left(\hat{X}_j\hat{P}_b\right) \\
& + 2\alpha dt\sum_{ab}\int dx\left[\mathrm{Re}\left[N_{aj}(x)\right]\mathrm{Re}\left[N_{ba}(x)\right]-M^+_{aj}(x)M^-_{ba}(x)\right]\mathrm{cov}\left(\hat{X}_b\hat{P}_k\right) \\
& - 4\alpha dt\sum_{ab}\int dx\left[M^+_{aj}(x)M^-_{bk}(x)+\mathrm{Re}\left[N_{bj}(x)\right]\mathrm{Re}\left[N_{ak}(x)\right]\right]\mathrm{cov}\left(\hat{X}_b\hat{P}_a\right).
\end{aligned} \tag{4.32}$$

Here, the subscript $\mathcal{D}$ indicates the decoherence term. Whilst this full term seems intractable, we will see in Chapter 5 that specifying a trapping potential $V_0(x)$ introduces symmetries to the Bogoliubov modes which simplifies the measurement matrices, and in turns simplifies each of the decoherence terms.

4.4.2 Innovations terms

We will now compute the innovations term for a symmetrised operator pair $\hat{A} = (\hat{S}\hat{T}+\hat{T}\hat{S})/2$. Expanding the innovations superoperator and using the definition of the measurement operator:

$$\begin{aligned}
\mathrm{Tr}\left\{\hat{A}\mathcal{H}\left[\hat{M}(x)\right]\hat{\rho}_c\right\} = {} & \frac{1}{2}\left[\left(\left\langle \hat{S}\hat{T}\hat{M}(x)+\hat{M}(x)\hat{S}\hat{T}\right\rangle-\left\langle \hat{M}(x)\right\rangle\left\langle \hat{S}\hat{T}\right\rangle\right)+\mathrm{h.c.}\right] \\
= {} & \frac{1}{2}\sum_{ab}M^-_{ab}(x)\left[\left(\left\langle \hat{S}\hat{T}\hat{X}_a\hat{X}_b+\hat{X}_a\hat{X}_b\hat{S}\hat{T}\right\rangle-2\left\langle \hat{X}_a\hat{X}_b\right\rangle\left\langle \hat{S}\hat{T}\right\rangle\right)+\mathrm{h.c.}\right] \\
& + \frac{1}{2}\sum_{ab}M^+_{ab}(x)\left[\left(\left\langle \hat{S}\hat{T}\hat{P}_a\hat{P}_b+\hat{P}_a\hat{P}_b\hat{S}\hat{T}\right\rangle-2\left\langle \hat{P}_a\hat{P}_b\right\rangle\left\langle \hat{S}\hat{T}\right\rangle\right)+\mathrm{h.c.}\right] \\
& + \frac{1}{2}\sum_{ab}N_{ab}(x)\left[\left(\left\langle \hat{S}\hat{T}\hat{X}_a\hat{P}_b+\hat{X}_a\hat{P}_b\hat{S}\hat{T}\right\rangle-2\left\langle \hat{X}_a\hat{P}_b\right\rangle\left\langle \hat{S}\hat{T}\right\rangle\right)+\mathrm{h.c.}\right] \\
& + \frac{1}{2}\sum_{ab}N^*_{ab}(x)\left[\left(\left\langle \hat{S}\hat{T}\hat{P}_b\hat{X}_a+\hat{P}_b\hat{X}_a\hat{S}\hat{T}\right\rangle-2\left\langle \hat{P}_b\hat{X}_a\right\rangle\left\langle \hat{S}\hat{T}\right\rangle\right)+\mathrm{h.c.}\right].
\end{aligned} \tag{4.33}$$

Once again, we obtain expectation values from the trace by using equation (3.4). From equation (4.33), it follows that our innovations term therefore depends upon the expectation value of products of four operators. We could compute the dynamics of these fourth order operators, but they would depend upon an innovations term in sixth order

operators. So as to not require an infinite cascade of equations of motion, we need to make an approximation upon our state to express these fourth order operators in terms of second order operators.

Recall that Bogoliubov excitations, under the cold atom Hamiltonian, evolve under a diagonal Hamiltonian as harmonic oscillator states. Eigenstates of the harmonic oscillator obey *Gaussian distributions* [173]. For a reader unfamiliar with Gaussian distributions we provide a short introduction in Appendix A.3, but it is sufficient here to quote the result that they are defined solely in terms of their average and variance. In particular, average products of four operators $\hat{\mathcal{O}}_i$ in a Gaussian state obey

$$\left\langle \hat{\mathcal{O}}_1\hat{\mathcal{O}}_2\hat{\mathcal{O}}_3\hat{\mathcal{O}}_4 \right\rangle = \left\langle \hat{\mathcal{O}}_1\hat{\mathcal{O}}_2 \right\rangle \left\langle \hat{\mathcal{O}}_3\hat{\mathcal{O}}_4 \right\rangle + \left\langle \hat{\mathcal{O}}_1\hat{\mathcal{O}}_3 \right\rangle \left\langle \hat{\mathcal{O}}_2\hat{\mathcal{O}}_4 \right\rangle + \left\langle \hat{\mathcal{O}}_1\hat{\mathcal{O}}_4 \right\rangle \left\langle \hat{\mathcal{O}}_2\hat{\mathcal{O}}_3 \right\rangle, \tag{4.34}$$

if each operator has zero average, i.e. $\langle \hat{\mathcal{O}}_i \rangle = 0$. In Appendix A.2, we prove that this is initially the case for our Bogoliubov quadratures.[3] Our states are initially Gaussian, and we will assume that they remain Gaussian under the evolution of the master equation[4]. We also assume that the average of each Bogoliubov quadrature remains zero for the evolution of the master equation, so that at all times we can express the fourth order products of operators using equation (4.34)[5]. Under the Gaussian approximation, equation (4.33) becomes:

$$\begin{aligned} \mathrm{Tr}\left\{ \hat{A}\mathcal{H}\left[\hat{M}(x)\right]\hat{\rho}_a \right\} = {} & 2\sum_{ab} \mathrm{Re}\left[N_{ab}(x)\right]\left[\left\langle \hat{S}\hat{X}_a \right\rangle \left\langle \hat{T}\hat{P}_b \right\rangle + \left\langle \hat{S}\hat{P}_b \right\rangle \left\langle \hat{T}\hat{X}_a \right\rangle + \text{h.c.}\right] \\ & + 2\sum_{ab} \mathrm{Re}\left[M^{-}_{ab}(x)\right]\left[\left\langle \hat{S}\hat{X}_a \right\rangle \left\langle \hat{T}\hat{X}_b \right\rangle + \text{h.c.}\right] \\ & + 2\sum_{ab} \mathrm{Re}\left[M^{+}_{ab}(x)\right]\left[\left\langle \hat{S}\hat{P}_a \right\rangle \left\langle \hat{T}\hat{P}_b \right\rangle + \text{h.c.}\right]. \end{aligned} \tag{4.35}$$

We then obtain the innovations term for each operator by substituting in particular $\hat{S}$ and $\hat{T}$. Once again, the full innovations terms are unwieldy; we include all three matrix equations in Appendix B.1.2. We include as an example here the innovations term for

[3] The proof follows from the definition that $\langle \hat{\delta}(x) \rangle = 0$. Note that this *does not* mean we can make a Gaussian approximation upon the perturbation operator $\hat{\delta}(x)$ as well. The cold atom Hamiltonian is not diagonal in $\hat{\delta}(x)$, but only in our Bogoliubov modes.

[4] This is an exact claim for systems undergoing linear quadratic gaussian control, which will be introduced in Chapter 7 and are discussed in more detail in Ref. [158].

[5] The validity of this approximation is discussed in Appendix A.2.

$\mathrm{cov}(\hat{X}_j\hat{P}_k)$

$$\begin{aligned} d\left\langle \mathrm{cov}\left(\hat{X}_j\hat{P}_k\right)\right\rangle_{\mathcal{H}} &= 4\sqrt{\alpha}\sum_{ab}\int dxdW(x,t)\mathrm{Re}\left[M^{-}_{ab}(x)\right]\left\langle \hat{X}_j\hat{X}_a\right\rangle\left\langle \mathrm{cov}\left(\hat{X}_b\hat{P}_k\right)\right\rangle \\ &+ 4\sqrt{\alpha}\sum_{ab}\int dxdW(x,t)\mathrm{Re}\left[M^{+}_{ab}(x)\right]\left\langle \hat{P}_k\hat{P}_b\right\rangle\left\langle \mathrm{cov}\left(\hat{X}_j\hat{P}_a\right)\right\rangle \\ &+ 4\sqrt{\alpha}\sum_{ab}\int dxdW(x,t)\mathrm{Re}\left[N_{ab}(x)\right]\left\langle \hat{X}_j\hat{X}_c\right\rangle\left\langle \hat{P}_k\hat{P}_d\right\rangle \\ &+ 4\sqrt{\alpha}\sum_{ab}\int dxdW(x,t)\mathrm{Re}\left[N_{ab}(x)\right]\mathrm{cov}\left(\hat{X}_j\hat{P}_d\right)\mathrm{cov}\left(\hat{X}_c\hat{P}_k\right) \\ &+ \sqrt{a}\int dxdW(x,t)\mathrm{Re}\left[N_{kj}(x)\right]. \end{aligned} \tag{4.36}$$

Here, the subscript $\mathcal{H}$ indicates the innovations term. The decoherence and innovations terms derived in this section complete the measurement dynamics of our model.

4.5 Feedback dynamics

The feedback dynamics of an operator $\hat{A}$ are found by computing

$$d\left\langle \hat{A}\right\rangle_C = -\frac{i}{\hbar}\left\langle \left[\hat{A},\hat{H}_C\right]\right\rangle_C dt, \tag{4.37}$$

where we use the subscript C to denotes that these expectations are conditioned on the individual trajectory, as the feedback Hamiltonian evolves under conditional expectation values. We compute the commutator in equation (4.37) for a symmetrised operator $\hat{A} = (\hat{S}\hat{T} + \hat{T}\hat{S})/2$ using equation (4.22), similar to the cold atom dynamics. Assuming a non-operator valued control potential, observe that

$$\left[\hat{S},\hat{H}_C\right] = \left[\hat{S},\int dxV_C(x,t)\hat{\psi}^\dagger(x)\hat{\psi}(x)\right] \tag{4.38}$$

$$= \int dxV_C(x,t)\left[\hat{S},\hat{\psi}^\dagger(x)\hat{\psi}(x)\right], \tag{4.39}$$

where $\hat{\psi}^\dagger(x)\hat{\psi}(x)$ is the wavefunction density. Therefore, we can compute the feedback dynamics by finding the commutator of the position and momentum quadratures with the wavefunction density. Specifically, we find

$$\left[\hat{X}_j,\hat{\psi}^\dagger\hat{\psi}(x)\right] = \sum_a\left[\left(f_j^{+*}(x)f_a^-(x) - \mathrm{h.c.}\right)\hat{X}_a + i\left(f_a^{+*}(x)f_j^+(x) + \mathrm{h.c.}\right)\hat{P}_a\right], \tag{4.40a}$$

$$\left[\hat{P}_j,\hat{\psi}^\dagger\hat{\psi}(x)\right] = \sum_a\left[\left(f_j^{-*}(x)f_a^+(x) - \mathrm{h.c.}\right)\hat{P}_a + i\left(f_a^{-*}(x)f_j^-(x) + \mathrm{h.c.}\right)\hat{X}_a\right]. \tag{4.40b}$$

Defining the *conditional feedback matrices*

$$R_{ab}(t)^{(C)} = \frac{1}{\hbar}\int dxV_C(x,t)\left[f_a^{+*}(x)f_b^-(x) - f_b^{-*}(x)f_a^+(x)\right], \tag{4.41a}$$

$$Q^{\pm}_{ab}(t)^{(C)} = \frac{1}{\hbar}\int dxV_C(x,t)\left[f_b^{\pm*}(x)f_a^{\pm}(x) + f_a^{\pm*}(x)f_b^{\pm}(x)\right], \tag{4.41b}$$

we then obtain

$$\left[\hat{X}_j, \hat{H}_C\right] = \hbar \sum_a R_{ja}(t)^{(C)} \hat{X}_a + i\hbar \sum_a Q^+_{aj}(t)^{(C)} \hat{P}_a, \tag{4.42a}$$

$$\left[\hat{P}_j, \hat{H}_C\right] = -\hbar \sum_a R_{aj}(t)^{(C)} \hat{P}_a - i\hbar \sum_a Q^-_{aj}(t)^{(C)} \hat{X}_a. \tag{4.42b}$$

The superscript (C) on the conditional feedback matrices is to indicate that we are modelling real-time feedback, and these terms depend upon the trajectory of the system. Substituting equation (4.42) into equation (4.22), and subsequently into equation (4.37), we obtain the conditional feedback dynamics for each symmetrised operator pair

$$\begin{aligned} d\left\langle \hat{X}_j\hat{X}_k \right\rangle_C =& dt \sum_{a=0} \left[Q^+_{ak}(t)^{(C)} \mathrm{cov}\left(\hat{X}_j\hat{P}_a\right) + Q^+_{aj}(t)^{(C)} \mathrm{cov}\left(\hat{X}_k\hat{P}_a\right)\right] \\ & -idt \sum_{a=0} \left[R_{ka}(t)^{(C)} \left\langle \hat{X}_j\hat{X}_a \right\rangle + R_{ja}(t)^{(C)} \left\langle \hat{X}_a\hat{X}_k \right\rangle\right], \end{aligned} \tag{4.43a}$$

$$\begin{aligned} d\left\langle \hat{P}_j\hat{P}_k \right\rangle_C =& - dt \sum_{a=0} \left[Q^-_{ak}(t)^{(C)} \mathrm{cov}\left(\hat{X}_a\hat{P}_j\right) + Q^-_{aj}(t)^{(C)} \mathrm{cov}\left(\hat{X}_a\hat{P}_k\right)\right] \\ & +idt \sum_{a=0} \left[R_{ak}(t)^{(C)} \left\langle \hat{P}_j\hat{P}_a \right\rangle + R_{aj}(t)^{(C)} \left\langle \hat{P}_a\hat{P}_k \right\rangle\right], \end{aligned} \tag{4.43b}$$

$$\begin{aligned} d\mathrm{cov}\left(\hat{X}_j\hat{P}_k\right)_C =& dt \sum_{a=0} \left[Q^+_{aj}(t)^{(C)} \left\langle \hat{P}_a\hat{P}_k \right\rangle - Q^-_{ak}(t)^{(C)} \left\langle \hat{X}_j\hat{X}_a \right\rangle\right] \\ & -idt \sum_{a=0} \left[R_{ja}(t)^{(C)} \mathrm{cov}\left(\hat{X}_a\hat{P}_k\right) - R_{ak}(t)^{(C)} \mathrm{cov}\left(\hat{X}_j\hat{P}_a\right)\right]. \end{aligned} \tag{4.43c}$$

The exact form of the feedback matrices is calculated using the Bogoliubov modes $f^{\pm}_a(x)$, which are determined by the trapping potential $V_0(x)$, and then integrating over a particular control potential $V_C(x,t)$. We now have a complete description of the feedback dynamics of our model.

4.6 Chapter summary

In this chapter, we have derived a finite temperature model for the feedback cooling of a Bose gas. In particular, we can model the dynamics of the Bose by integrating the coupled matrix equations

$$\begin{aligned} d\left\langle \hat{X}_j\hat{X}_k \right\rangle =& dt \left[\frac{\epsilon_k}{\hbar} \mathrm{cov}\left(\hat{X}_j\hat{P}_k\right) + \frac{\epsilon_j}{\hbar} \mathrm{cov}\left(\hat{X}_k\hat{P}_j\right)\right] \\ & + dt \sum_{a=0} \left[Q^+_{ak}(t)^{(C)} \mathrm{cov}\left(\hat{X}_j\hat{P}_a\right) + Q^+_{aj}(t)^{(C)} \mathrm{cov}\left(\hat{X}_k\hat{P}_a\right)\right] \\ & - idt \sum_{a=0} \left[R_{ka}(t)^{(C)} \left\langle \hat{X}_j\hat{X}_a \right\rangle + R_{ja}(t)^{(C)} \left\langle \hat{X}_a\hat{X}_k \right\rangle\right] \\ & + d\left\langle \hat{X}_j\hat{X}_k \right\rangle_{\mathcal{D}} + d\left\langle \hat{X}_j\hat{X}_k \right\rangle_{\mathcal{H}}, \end{aligned} \tag{4.44a}$$

$$
\begin{aligned}
d\left\langle \hat{P}_j\hat{P}_k\right\rangle &= -dt\left[\frac{\epsilon_k}{\hbar}\mathrm{cov}\left(\hat{X}_k\hat{P}_j\right)-\frac{\epsilon_j}{\hbar}\mathrm{cov}\left(\hat{X}_j\hat{P}_k\right)\right]\\
&\quad - dt\sum_{a=0}\left[Q^{-}_{ak}(t)^{(C)}\mathrm{cov}\left(\hat{X}_a\hat{P}_j\right)+Q^{-}_{aj}(t)^{(C)}\mathrm{cov}\left(\hat{X}_a\hat{P}_k\right)\right],\\
&\quad + idt\sum_{a=0}\left[R_{ak}(t)^{(C)}\left\langle \hat{P}_j\hat{P}_a\right\rangle + R_{aj}(t)^{(C)}\left\langle \hat{P}_a\hat{P}_k\right\rangle\right]\\
&\quad + d\left\langle \hat{P}_j\hat{P}_k\right\rangle_{\mathcal{D}} + d\left\langle \hat{P}_j\hat{P}_k\right\rangle_{\mathcal{H}},
\end{aligned}
\tag{4.44b}
$$

$$
\begin{aligned}
d\mathrm{cov}\left(\hat{X}_j\hat{P}_k\right) &= dt\left[\frac{\epsilon_j}{\hbar}\left\langle \hat{P}_j\hat{P}_k\right\rangle-\frac{\epsilon_k}{\hbar}\left\langle \hat{X}_j\hat{X}_k\right\rangle\right]\\
&\quad + dt\sum_{a=0}\left[Q^{+}_{aj}(t)^{(C)}\left\langle \hat{P}_a\hat{P}_k\right\rangle - Q^{-}_{ak}(t)^{(C)}\left\langle \hat{X}_j\hat{X}_a\right\rangle\right],\\
&\quad - idt\sum_{a=0}\left[R_{ja}(t)^{(C)}\mathrm{cov}\left(\hat{X}_a\hat{P}_k\right) - R_{ak}(t)^{(C)}\mathrm{cov}\left(\hat{X}_j\hat{P}_a\right)\right]\\
&\quad + d\mathrm{cov}\left(\hat{X}_j\hat{P}_k\right)_{\mathcal{D}} + d\mathrm{cov}\left(\hat{X}_j\hat{P}_k\right)_{\mathcal{H}},
\end{aligned}
\tag{4.44c}
$$

where the full decoherence and innovations for each symmetrised operator pair are found in Appendix B.1. This general model, for an arbitrary trapping $V_0(x)$ and control $V_C(x,t)$ potential, is the first key result of this thesis.

In the following chapters, we complete a preliminary examination of how well this model can characterise a specific control potential $V_C(x,t)$ in a given trapping potential $V_0(x)$. In Chapter 5, we consider a hard box trap and energy damping control, and simplify the conditional feedback matrices and measurement dynamics for those potentials. In Chapter 6 we perform preliminary simulations of the model for those potentials, and discuss the limitations of solving the model via numeric integration.

Chapter 5

Finite temperature model of energy damping control in a hard box trap

In the previous chapter, we derived a model for the feedback cooling of a Bose gas under continuous measurement in an arbitrary trap with any control potential $V_C(x,t)$. In this chapter, we will apply that result to construct a model for feedback cooling with the energy-damping control introduced in Chapter 3.4 in a hard box trap.

This chapter will achieve two aims. First, it will demonstrate how the general model in Chapter 4 can be used to model specific trapping and control potentials. Second, choosing these potentials will allow us to perform preliminary simulations of our finite temperature model in Chapter 6. This will serve as the first step towards validating the model derived in this thesis.

5.1 Trapping potential choice: the hard box trap

In Chapter 2.4.3, we introduced the plane-wave solutions to the Bogoliubov-de Gennes equations for a box potential (equation (2.44)). Those solutions were in the coefficients $\{u_i(x), v_i(x)\}$; the equivalent quadrature coefficients ${f_j^{(R)}}^{\pm}(x)$ are

$$ {f_j^{(R)}}^{\pm}(x) = \frac{1}{\sqrt{2L}} \left[e^{\mp r_j} \cos\left(\frac{2\pi}{L} jx\right) + i e^{\pm r_j} \sin\left(\frac{2\pi}{L} jx\right) \right]. \tag{5.1} $$

The solution in equation (5.1) has continuous (Neumann) boundary conditions: ${f_j^{(R)}}^{\pm}(L/2+\delta) = {f_j^{(R)}}^{\pm}(-L/2+\delta)$, and the solutions are non-zero at the boundaries $x = \pm L/2$. Therefore, these plane-wave solutions physically correspond to a Bose gas in a 1D *ring* of circumference L (that is why we have introduced the superscript (R) in equation (5.1)). The subtle difference between the solutions for a ring and 1D box trap embedded in 3D space[1] does not significantly effect equilibrium properties, which is why it is the standard solution considered in the literature for studying a Bose gas at equilibrium.

However, if we consider a *dynamic* system, continuous boundary conditions mean that excitations can move from $-L/2$ to $L/2$. This property is not physically sensible for an effective 1D trapped gas under feedback control. In this thesis, we therefore introduce

[1] The reader may recognise this potential (equation (2.44)) as an infinite square well.

a "hard box" solution, which is a linear superposition of ring trap modes for $j > 0$,

$$f_j^{\pm}(x) = \begin{cases} \frac{1}{\sqrt{L}} e^{\mp r_j} \sin\left(\frac{2\pi}{L} j x\right) & \text{if } -L/2 \leq x \leq L/2, \\ 0 & \text{elsewhere,} \end{cases} \tag{5.2}$$

where the condensate wavefunction is defined as uniform and discontinuous at the boundaries (as before, in equation (2.46)). Observe that at $x = \pm L/2$, the solutions in equation (5.2) go to zero, so $f_j^{\pm}(x)$ (the hard box modes) describe a 1D box which is contained in a smaller part of 1D space.

Whilst it is experimentally possible to make BECs in either a ring [174] or a box [175], it is typically easiest to prepare them in harmonic traps[2]. Whilst we will not model a Bose gas in a harmonic trap in this thesis, we summarise the solutions of the Bogoliubov-de Gennes equations for that potential for two reasons: a) to demonstrate that the hard box trap has more analytically tractable solutions and b) justify why the box trap should obtain qualitatively similar results. These reasons will motivate using the box trap, rather than the harmonic trap, to derive analytically tractable equations of motion in this thesis.[3]

For a harmonic trap $V_0(x) = m\omega^2 x^2/2$, the Thomas-Fermi approximation (equation (2.45)) can be used to estimate the condensate wavefunction as

$$\chi_0^{(h)}(x) = \sqrt{\frac{\mu}{g}\left(1 - \left(\frac{x}{R_{TF}}\right)^2\right)}, \tag{5.3}$$

where $R_{TF} = \sqrt{2\mu/m\omega^2}$ is the *Thomas-Fermi radius*. Integration of equation (5.3) and the normalisation of $\chi_0(x)$ to the number of particles can be used to obtain the relationship between the chemical potential μ and the 1D interaction strength g

$$\mu = \frac{3}{4}\frac{gN}{R_{TF}}. \tag{5.4}$$

With the harmonic potential and corresponding condensate wavefunction, in 1D the Bogoliubov-de Gennes equations become linear superpositions of Legendre's differential equation[4] [177]. These are solved by

$$f_j^{(h)\pm}(x) = P_j(x/R_{TF}) \sqrt{\frac{j+\frac{1}{2}}{R_{TF}}} \left[\frac{2\mu}{\epsilon_j^{(h)}}\left(1 - \left(\frac{x}{R_{TF}}\right)^2\right)\right]^{\mp 1/2}, \tag{5.5}$$

where $P_j(x/R_{TF})$ is the jth Legendre polynomial. Note that, like the hard box trap, the harmonic trap has real Bogoliubov modes. The Bogoliubov spectrum for the harmonic trap $\epsilon_j^{(h)}$ is given by

$$\epsilon_j^{(h)} = \frac{\hbar}{2}\sqrt{j\,(j+1)}\sqrt{\frac{3N}{m{R_{TF}}^3}g}, \tag{5.6}$$

[2] Indeed, the first observation of a BEC by the Cornell group [3] was in a harmonic trap.

[3] We suggest working in the harmonic trap as a possible option for future work in Chapter 7.

[4] For a useful reference on the Legendre's differential equation and the associated Legendre polynomials, see Appendix C of Ref. [176].

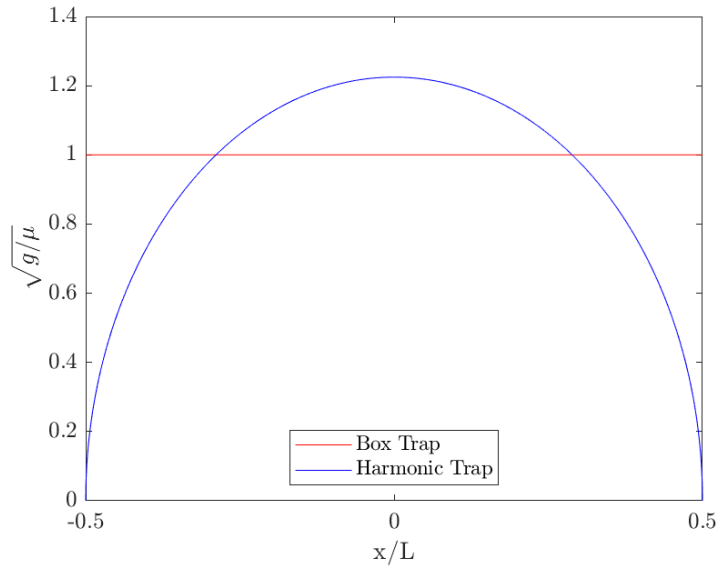

Figure 5.1: Condensate wavefunction $\chi_0(x)$ in the Thomas-Fermi approximation for a box trap (red) and harmonic trap (blue) with $L = 2R_{TF}$. The wavefunctions are similar towards the center of the trap ($|x| \ll L$), but differ at the edges of the trap $|x| \to L$. The difference has little qualitative effect on the equilibrium properties of the gas [178], because the particle density is small towards the boundaries of the trap [179].

where we have chosen this form to illustrate the dependence on $\sqrt{g}$. Note that this is the same dependency as the box trap solution in the low-energy regime. Indeed, in Figure 5.1 we plot $\chi_0(x)$ in the Thomas-Fermi regime for both a box and harmonic trap for $L = 2R_{TF}$. The condensate wavefunctions are similar close to the centre of the trap, but differ significantly at the boundaries (where the box trap solution is discontinuous because of the Thomas-Fermi approximation). However, at thermal equilibrium the particle density is negligible near the edges of the trap for both traps (see Ref. [179] for more details)[5], so the equilibrium properties of a Bose gas are qualitatively similar in both a box and harmonic trap. In fact, in Ref. [178] it is found that the difference only becomes non-negligible at temperatures within 0.01% of T_C for the experimental values of Refs. [3] and [4]. This is significantly hotter than the regime $T \ll T_C$, so these differences in the condensate wavefunction should not make a significant different to a Bogoliubov theory. As plane-wave/sinusoidal solutions are more analytically tractable than equation (5.5), Bogoliubov theory is often completed in ring/box traps with the expectation that it will be qualitatively similar to harmonic traps.

In this thesis, we will study feedback cooling of a thermal gas in a hard box, with the Bogoliubov modes given by equation (5.2). As we are modelling an effective 1D system with a trap of finite length, the hard box solution is a more appropriate description of the system than the ring trap solution.

Note that both $f_j^{\pm}(x)$ and $f_j^{(h)^{\pm}}(x)$ are real. When finding the conditional feedback and measurement matrices in the box trap, we will note where a result holds true

[5]We plot the wavefunction density for a thermal state in a box trap in Section 5.3, demonstrating this result.

for any real solutions to the Bogoliubov-de Gennes equations, to indicate where it also applies to the harmonic trap. This allows for extending the results of this thesis to the harmonic trap, a possible avenue for future work discussed in Chapter 7.

5.1.1 Important quantities in the hard box trap

Having chosen a trapping potential, we can now approximate the ground state energy per particle ϵ_0 by substituting $\chi_0(x)$ into the cold atom Hamiltonian (equation (2.22)) and calculating $\langle \hat{H}_0 \rangle / N$. For the box potential, this obtains

$$\epsilon_0 = \frac{gN}{2L}. \tag{5.7}$$

Quantum depletion of the condensate (introduced in Chapter 2.4.4) actually shifts this result by changing the effective interaction strength [81]. The corrected energy, to first order, was first calculated in Ref. [138] to be $\epsilon_0 = \frac{gN}{2L}\left[1 + \frac{128}{15\sqrt{\pi}}\sqrt{na^3}\right]$. However, as the correction term is negligible, we will use the approximation in equation (5.7) for the ground state energy.

We will also include the condensate mode as the $j = 0$ Bogoliubov mode, by defining for $j \geq 0$

$$f_j^{\pm}(x) = \frac{1}{\sqrt{L}} e^{\mp r_j} \left[\sin\left(\frac{2\pi}{L} j x\right) + \frac{\delta_{j,0}}{\sqrt{2}} \right], \tag{5.8}$$

where we now define r_j piecewise as

$$r_j = \begin{cases} \frac{1}{2} \ln \frac{\epsilon_j}{\epsilon_j^{(0)}} & \text{if } j > 0, \\ 0 & \text{if } j = 0. \end{cases} \tag{5.9}$$

A piecewise definition is necessary as $\epsilon_{j=0}^{(0)} = 0$. Note that in equation (5.2) we have normalised the condensate wavefunction $\chi_0(x)$ by a factor of $1/\sqrt{N}$, so that all Bogoliubov modes have the same normalisation. Hence, all dimensionless parameters used in this thesis will be defined in terms of this energy scale. Finally, the wavefunction density in the hard box trap simplifies to

$$\hat{\psi}^\dagger(x)\hat{\psi}(x) = \sum_{a,b=0} \left[f_a^-(x) f_b^-(x) \hat{X}_a \hat{X}_b + f_a^+(x) f_b^+(x) \hat{P}_a \hat{P}_b \right] - \sum_{a=0} f_a^-(x) f_a^+(x). \tag{5.10}$$

Note that this wavefunction density depends only upon the occupation of each mode and the real correlations between each mode.

5.1.2 Measurement dynamics in the hard box trap

For real Bogoliubov modes, the measurement matrices become

$$M_{ab}^{\pm}(x) = \int dy K_r(x-y) f_a^{\pm}(y) f_b^{\pm}(y) = M_{ba}^{\pm}(x), \tag{5.11a}$$

$$N_{ab}(x) = i \int dy K_r(x-y) f_a^-(y) f_b^+(y), \tag{5.11b}$$

where have noted that $M^{\pm}_{ab}(x)$ is now symmetric. The form of the kernel means that (even in the hard box approximation) analytically integrating these integrals is intractable, except in the limit $L \to \infty$. We will later compute them numerically when completing simulations in Chapter 6. However, note that because the kernel is real, $M^{\pm}_{ab}(x)$ is real and $N_{ab}(x)$ is imaginary. Applying these properties, the measurement dynamics become significantly more tractable. Specifically, the decoherence terms become:

$$\begin{aligned} d\left\langle \hat{X}_j\hat{X}_k\right\rangle_{\mathcal{D}} &= 4\alpha dt\sum_{ab}\int dx M^{+}_{aj}(x)M^{+}_{bk}(x)\left\langle \hat{P}_a\hat{P}_b\right\rangle \\ &\quad - 2\alpha dt\sum_{ab}\int dx\left[M^{+}_{ak}(x)M^{-}_{ab}(x)\left\langle \hat{X}_j\hat{X}_b\right\rangle + M^{+}_{aj}(x)M^{-}_{ab}(x)\left\langle \hat{X}_b\hat{X}_k\right\rangle\right], \end{aligned} \tag{5.12a}$$

$$\begin{aligned} d\left\langle \hat{P}_j\hat{P}_k\right\rangle_{\mathcal{D}} &= 4\alpha dt\sum_{ab}\int dx M^{-}_{aj}(x)M^{-}_{bk}(x)\left\langle \hat{X}_a\hat{X}_b\right\rangle \\ &\quad - 2\alpha dt\sum_{ab}\int dx\left[M^{-}_{ak}(x)M^{+}_{ab}(x)\left\langle \hat{P}_j\hat{P}_b\right\rangle + M^{-}_{aj}(x)M^{+}_{ab}(x)\left\langle \hat{P}_b\hat{P}_k\right\rangle\right], \end{aligned} \tag{5.12b}$$

$$\begin{aligned} d\left\langle \mathrm{cov}\left(\hat{X}_j\hat{P}_k\right)\right\rangle_{\mathcal{D}} &= -4\alpha dt\sum_{ab}\int dx M^{+}_{aj}(x)M^{-}_{bk}(x)\left\langle \mathrm{cov}\left(\hat{X}_b\hat{P}_a\right)\right\rangle \\ &\quad - 2\alpha dt\sum_{ab}\int dx M^{-}_{ak}(x)M^{+}_{ab}(x)\left\langle \mathrm{cov}\left(\hat{X}_j\hat{P}_b\right)\right\rangle \\ &\quad - 2\alpha dt\sum_{ab}\int dx M^{+}_{aj}(x)M^{-}_{ab}(x)\left\langle \mathrm{cov}\left(\hat{X}_b\hat{P}_k\right)\right\rangle. \end{aligned} \tag{5.12c}$$

The innovations terms become:

$$\begin{aligned} d\left\langle \hat{X}_j\hat{X}_k\right\rangle_{\mathcal{H}} &= 4\sqrt{\alpha}\sum_{ab}\int dx dW(x,t)M^{-}_{ab}(x)\left\langle \hat{X}_j\hat{X}_a\right\rangle\left\langle \hat{X}_k\hat{X}_b\right\rangle \\ &\quad + 4\sqrt{\alpha}\sum_{ab}\int dx dW(x,t)M^{+}_{ab}(x)\left\langle \mathrm{cov}\left(\hat{X}_j\hat{P}_a\right)\right\rangle\left\langle \mathrm{cov}\left(\hat{X}_k\hat{P}_b\right)\right\rangle \\ &\quad - \sqrt{\alpha}\int dx dW(x,t)M^{+}_{jk}(x), \end{aligned} \tag{5.13a}$$

$$\begin{aligned} d\left\langle \hat{P}_j\hat{P}_k\right\rangle_{\mathcal{H}} &= 4\sqrt{\alpha}\sum_{ab}\int dx dW(x,t)M^{+}_{ab}(x)\left\langle \hat{P}_j\hat{P}_a\right\rangle\left\langle \hat{P}_k\hat{P}_b\right\rangle \\ &\quad + 4\sqrt{\alpha}\sum_{ab}\int dx dW(x,t)M^{-}_{ab}(x)\left\langle \mathrm{cov}\left(\hat{X}_a\hat{P}_j\right)\right\rangle\left\langle \mathrm{cov}\left(\hat{X}_b\hat{P}_k\right)\right\rangle \\ &\quad - \sqrt{\alpha}\int dx dW(x,t)M^{-}_{jk}(x), \end{aligned} \tag{5.13b}$$

$$\begin{aligned} d\left\langle \mathrm{cov}\left(\hat{X}_j\hat{P}_k\right)\right\rangle_{\mathcal{H}} &= 4\sqrt{\alpha}\sum_{ab}\int dx dW(x,t)M^{-}_{ab}(x)\left\langle \hat{X}_j\hat{X}_a\right\rangle\left\langle \mathrm{cov}\left(\hat{X}_b\hat{P}_k\right)\right\rangle \\ &\quad + 4\sqrt{\alpha}\sum_{ab}\int dx dW(x,t)M^{+}_{ab}(x)\left\langle \hat{P}_k\hat{P}_b\right\rangle\left\langle \mathrm{cov}\left(\hat{X}_j\hat{P}_a\right)\right\rangle. \end{aligned} \tag{5.13c}$$

We therefore have the measurement dynamics of our model for any potential with real Bogoliubov modes, such as the box trap.

5.2 Control potential choice: the energy damping control

In Chapter 3.4, we reviewed two particular control choices; the moment control and the energy damping control. Taylor demonstrated with the NPW method [95] that the energy damping control is more effective than the moment control for cooling thermal states; so in this thesis we model the energy damping control. In one-dimension, the energy damping control is

$$\begin{aligned} V_C(x,t) &= -k_{\mathrm{ED}}\partial_x \left\langle \frac{\hbar}{2mi}\left[\hat{\psi}^\dagger(x)\left(\partial_x\hat{\psi}(x)\right) - \left(\partial_x\hat{\psi}^\dagger(x)\right)\hat{\psi}(x)\right]\right\rangle_C, \\ &= -\frac{\hbar}{2mi}k_{\mathrm{ED}}\left\langle \hat{\psi}^\dagger(x)\partial_x^2\left(\hat{\psi}(x)\right) - \partial_x^2\left(\hat{\psi}^\dagger(x)\right)\hat{\psi}(x)\right\rangle_C, \end{aligned} \tag{5.14}$$

where the subscript C indicates a conditional expectation value. This conditional expectation value is the error signal of our energy damping control in Bogoliubov theory. Substituting our condensate wavefunction (equation (4.13)) into the error signal yields

$$\begin{aligned} &\left\langle \hat{\psi}^\dagger(x)\partial_x^2\left(\hat{\psi}(x)\right) - \partial_x^2\left(\hat{\psi}^\dagger(x)\right)\hat{\psi}(x)\right\rangle_C \\ &= i\sum_{jk}\left(\left[f_j^{-*}(x)\partial_x^2 f_k^+(x) - f_k^+(x)\partial_x^2 f_j^{-*}(x)\right]\left\langle \hat{X}_j\hat{P}_k\right\rangle_C + \text{h.c.}\right) \\ &+ \sum_{jk}\left[f_j^{-*}(x)\partial_x^2 f_k^-(x) - f_j^-(x)\partial_x^2 f_k^{-*}(x)\right]\left\langle \hat{X}_j\hat{X}_k\right\rangle_C \\ &+ \sum_{jk}\left[f_j^{+*}(x)\partial_x^2 f_k^+(x) - f_j^+(x)\partial_x^2 f_k^{+*}(x)\right]\left\langle \hat{P}_j\hat{P}_k\right\rangle_C. \end{aligned} \tag{5.15}$$

We don't yet define our error signal using the symmetrised covariance, because that expression is (at this stage) less compact. In order to proceed further, we need the form of the Bogoliubov modes, and thus must consider the trapping potential introduced in Section 5.2.

5.2.1 Energy damping in the hard box trap

For a trap with real Bogoliubov modes, the error signal of the energy damping control immediately simplifies to

$$\begin{aligned} &\left\langle \hat{\psi}^\dagger(x)\partial_x^2\left(\hat{\psi}(x)\right) - \partial_x^2\left(\hat{\psi}^\dagger(x)\right)\hat{\psi}(x)\right\rangle \\ &= 2i\sum_{jk}\left[f_j^-(x)\partial_x^2 f_k^+(x) - f_k^+(x)\partial_x^2 f_j^-(x)\right]\mathrm{cov}\left(\hat{X}_j\hat{P}_k\right)_C, \end{aligned} \tag{5.16}$$

and the control potential becomes

$$V_C(x,t) = \frac{\hbar k_{\mathrm{ED}}}{m}\sum_{jk}\left[f_k^+(x)\partial_x^2 f_j^-(x) - f_j^-(x)\partial_x^2 f_k^+(x)\right]\mathrm{cov}\left(\hat{X}_j\hat{P}_k\right)_C. \tag{5.17}$$

Note that the conditional feedback matrix $R_{ab}(t)^{(C)} = 0$ for real Bogoliubov modes, and the other feedback matrix becomes

$$Q_{ab}^{\pm}(t)^{(C)} = \frac{2}{\hbar}\int dx V_C(x,t) f_a^{\pm}(x) f_b^{\pm}(x). \tag{5.18}$$

In the box potential, the Bogoliubov modes obey $\partial_x^2 f_a^{\pm}(x) = -(2\pi a/L)^2 f_a^{\pm}(x)$, so

$$V_C(x,t) = \frac{4\pi^2\hbar k_{\mathrm{ED}}}{mL^2}\sum_{j,k=0}\left(k^2-j^2\right) f_j^-(x) f_k^+(x)\mathrm{cov}\left(\hat{X}_j\hat{P}_k\right)_C. \tag{5.19}$$

Take a moment to note that, in the box trap, the error signal is proportional to the off-diagonal element of the symmetrised covariance for the Bogoliubov quadratures. That is, the energy damping responds to imaginary correlations between the different modes. Integrating over products of four Bogoliubov modes, we obtain the feedback matrix

$$Q_{ab}^{\pm}(t)^{(C)} = \frac{2\pi^2 k_{\mathrm{ED}}}{mL^3}\left(b^2-a^2\right)e^{\mp(r_a+r_b)}\left[e^{r_a-r_b}\mathrm{cov}\left(\hat{X}_b\hat{P}_a\right)_C - e^{r_b-r_a}\mathrm{cov}\left(\hat{X}_a\hat{P}_b\right)_C\right]. \tag{5.20}$$

It is also instructive to write the feedback Hamiltonian for the energy damping control in the box trap

$$\begin{aligned}\hat{H}_C = &\sum_{a,b=0}\frac{\pi^2\hbar k_{\mathrm{ED}}}{mL^3}\left(b^2-a^2\right)\left[e^{2r_a}\mathrm{cov}\left(\hat{X}_a\hat{P}_b\right)_C - e^{2r_b}\mathrm{cov}\left(\hat{X}_b\hat{P}_a\right)_C\right]\hat{X}_a\hat{X}_b \\ &+\sum_{a,b=0}\frac{\pi^2\hbar k_{\mathrm{ED}}}{mL^3}\left(b^2-a^2\right)\left[e^{-2r_b}\mathrm{cov}\left(\hat{X}_a\hat{P}_b\right)_C - e^{-2r_a}\mathrm{cov}\left(\hat{X}_b\hat{P}_a\right)_C\right]\hat{P}_a\hat{P}_b.\end{aligned} \tag{5.21}$$

We are therefore now fully equipped to model the dynamics of the energy damping control in the box potential. In Chapter 6, we will complete preliminary numeric simulations of this model. Firstly, we will review the particular kind of states we are ultimately interested in cooling: thermal states.

5.3 Thermal states and the energy damping control

In this thesis, we have constructed a model for the feedback cooling of low temperature Bose gases. States with a well-defined temperature are *thermal states*. For a rigorous introduction to the quantum statistics of thermal states, see Chapter 2 of Ref. [152]; it is sufficient for this thesis to understand that thermal states have a well-defined occupancy of each possible energy level determined by the temperature T. Specifically, a set of thermally occupied Bogoliubov modes obey (using the Bogoliubov mode representation) [180]

$$\left\langle\beta_j^\dagger\hat{\beta}_k\right\rangle = \delta_{j,k}\bar{n}_j, \tag{5.22}$$

where

$$\bar{n}_j = \begin{cases}\frac{1}{\exp(\epsilon_j/k_BT)-1} & \text{if } j>0,\\ N_C & \text{if } j=0.\end{cases} \tag{5.23}$$

Note that for $j>0$, $\bar{n}_j$ is the Bose-Einstein distribution with $(\epsilon_j-\mu)\to\epsilon_j$. Crucially, as the occupation of each mode is exactly defined by the temperature, there can be no correlations between the modes; that is,

$$\left\langle\hat{\beta}_j\hat{\beta}_k\right\rangle = \left\langle\hat{\beta}_j^\dagger\hat{\beta}_k^\dagger\right\rangle = 0. \tag{5.24}$$

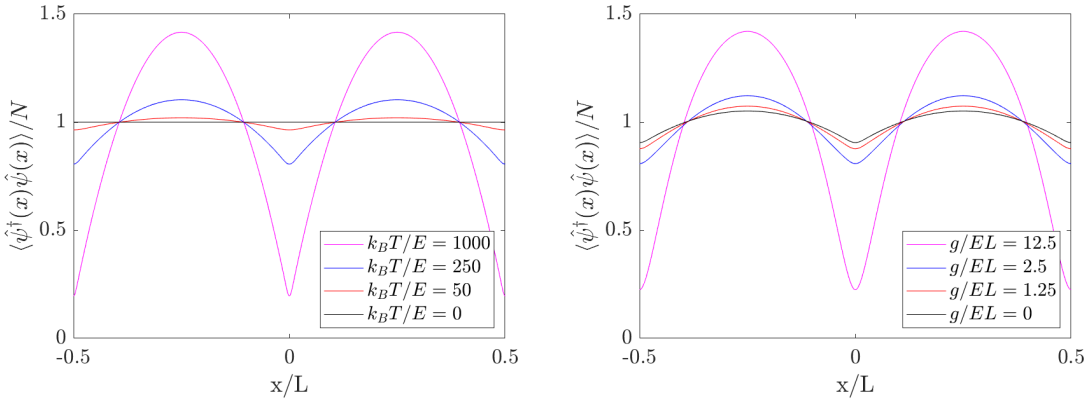

(a) Thermal states with varying T

(b) Thermal states with varying g

Figure 5.2: Thermal state density wavefunctions for varying temperature and interaction strength. In Figure 5.2a), temperature is varied at a fixed interaction strength $g = 0$. At $T = 0$, the density is uniform. As T increases, the density symmetrically decreases towards the centre and boundaries of the trap, whilst increasing away from those regions. In Figure 5.2b), interaction strength is varied at a fixed temperature $k_BT/E = 125$. Increasing interaction strength has an almost identical effect to increasing temperature.

In terms of our quadrature operators, a thermal state is defined by

$$\left\langle \hat{X}_j\hat{X}_k \right\rangle = \left\langle \hat{P}_j\hat{P}_k \right\rangle = \delta_{jk}\left[\bar{n}_j + \frac{1}{2}\right], \text{ and } \operatorname{cov}\left(\hat{X}_j\hat{P}_k\right) = 0. \tag{5.25}$$

In a thermal state, in a hard box potential the average wavefunction density (equation (5.10)) becomes

$$\left\langle \hat{\psi}^\dagger(x)\hat{\psi}(x) \right\rangle = \frac{1}{L}\sum_{a=0}\left(\sin\left(\frac{2\pi}{L}ax\right) + \frac{\delta_{a0}}{\sqrt{2}}\right)^2\left[\left(\bar{n}_j + \frac{1}{2}\right)\left(e^{2r_j} + e^{-2r_j}\right) - 1\right]. \tag{5.26}$$

We plot in Figure 5.2a) the density function over a range of temperatures for fixed $g = 0$, and in Figure 5.2b) the density function over a range of interaction strengths for fixed $k_BT/E = 125$, both for 100 modes.[6] Observe that for a non-interacting gas, at zero temperature the density is constant. In Figure 5.2a), as temperature increases, the density symmetrically decreases near the boundaries and centre of the box, but increases significantly between these two regions. From Figure 5.2b), it is apparent that increasing the interaction strength has a similar effect to increasing the temperature, although the curvature of the density is less sharp. This is because an increase in interaction strength causes a greater occupation of higher order modes — this is the physical reason behind quantum depletion at $T = 0$.

Crucially, it follows immediately from equation (5.25) that (in a trap with real Bogoliubov modes) thermal states are dark states of the energy damping control (i.e. $V_C(x,t) = 0$), as there is no coupling between modes. This result actually also holds for the ring trap modes $f_j^{(R)^\pm}(x)$, as the contributions from the integrals of four modes cancel out.

[6] Although it is not obvious from Figure 5.2, the wavefunction densities are in fact zero at $x = \pm L/2$ because the condensate wavefunction is discontinuous at $x = \pm L/2$. The wavefunction densities therefore still satisfy the Dirichlet boundary conditions.

If thermal states are dark states, how does energy damping cool them as demonstrated in Ref. [95]? The measurement dynamics terms for the covariance (see equations (5.12) and (5.13)) are initially zero in a thermal state. However, measurement backaction can drive the evolution of off-diagonal terms in $\langle \hat{X}_j \hat{X}_k \rangle$ and $\langle \hat{P}_j \hat{P}_k \rangle$, which then drives the evolution of $\mathrm{cov}(\hat{X}_j \hat{P}_k)$ and leads to a non-zero error signal. Physically, the measurement backaction stirs up density fluctuations in the thermal state, which creates a spatially dependent particle current (imaginary correlations) and the energy damping control switches on. Therefore, measurement backaction is needed for feedback cooling to occur. This is consistent with our understanding of conditional measurement; our feedback cannot be defined unless we have made a measurement of the state.

5.4 Chapter summary

In this chapter, we have demonstrated how to use the results of Chapter 4 to derive a model for a particular trapping and control potential. In particular, our Itô model for the energy damping control of a Bose gas in a hard box trap is

$$\begin{aligned} d\left\langle \hat{X}_j \hat{X}_k \right\rangle =& \frac{1}{\hbar} dt \left(\epsilon_k \mathrm{cov}\left(\hat{X}_j \hat{P}_k \right) + \epsilon_j \mathrm{cov}\left(\hat{X}_k \hat{P}_j \right) \right) \\ &+ dt \sum_{a=0} \left(Q^+_{ak}(t)^{(C)} \mathrm{cov}\left(\hat{X}_j \hat{P}_a \right) + Q^+_{aj}(t)^{(C)} \mathrm{cov}\left(\hat{X}_k \hat{P}_a \right) \right) \\ &+ 4\alpha dt \sum_{a,b=0} \int dx M^+_{aj}(x) M^+_{bk}(x) \left\langle \hat{P}_a \hat{P}_b \right\rangle \\ &- 2\alpha dt \sum_{a,b=0} \int dx \left[M^+_{ak}(x) M^-_{ab}(x) \left\langle \hat{X}_j \hat{X}_b \right\rangle + M^+_{aj}(x) M^-_{ab}(x) \left\langle \hat{X}_b \hat{X}_k \right\rangle \right] \\ &+ 4\sqrt{\alpha} \sum_{a,b=0} \int dx dW(x,t) M^-_{ab}(x) \left\langle \hat{X}_j \hat{X}_a \right\rangle \left\langle \hat{X}_k \hat{X}_b \right\rangle \\ &+ 4\sqrt{\alpha} \sum_{a,b=0} \int dx dW(x,t) M^+_{ab}(x) \left\langle \mathrm{cov}\left(\hat{X}_j \hat{P}_a \right) \right\rangle \left\langle \mathrm{cov}\left(\hat{X}_k \hat{P}_b \right) \right\rangle \\ &- \sqrt{\alpha} \int dx dW(x,t) M^+_{jk}(x), \end{aligned} \tag{5.27a}$$

$$
\begin{aligned}
d\left\langle \hat{P}_j\hat{P}_k\right\rangle =& -\frac{1}{\hbar}dt\left(\epsilon_j \mathrm{cov}\left(\hat{X}_j\hat{P}_k\right)+\epsilon_k \mathrm{cov}\left(\hat{X}_k\hat{P}_j\right)\right)\\
&-dt\sum_{a=0}\left(Q^-_{ak}(t)^{(C)}\mathrm{cov}\left(\hat{X}_a\hat{P}_j\right)+Q^-_{aj}(t)^{(C)}\mathrm{cov}\left(\hat{X}_a\hat{P}_k\right)\right)\\
&+4\alpha dt\sum_{a,b=0}\int dx M^-_{aj}(x)M^-_{bk}(x)\left\langle \hat{X}_a\hat{X}_b\right\rangle\\
&-2\alpha dt\sum_{a,b=0}\int dx\left[M^-_{ak}(x)M^+_{ab}(x)\left\langle \hat{P}_j\hat{P}_b\right\rangle+M^-_{aj}(x)M^+_{ab}(x)\left\langle \hat{P}_b\hat{P}_k\right\rangle\right]\\
&+4\sqrt{\alpha}\sum_{a,b=0}\int dx dW(x,t)M^+_{ab}(x)\left\langle \hat{P}_j\hat{P}_a\right\rangle\left\langle \hat{P}_k\hat{P}_b\right\rangle\\
&+4\sqrt{\alpha}\sum_{a,b=0}\int dx dW(x,t)M^-_{ab}(x)\left\langle \mathrm{cov}\left(\hat{X}_a\hat{P}_j\right)\right\rangle\left\langle \mathrm{cov}\left(\hat{X}_b\hat{P}_k\right)\right\rangle\\
&-\sqrt{\alpha}\int dx dW(x,t)M^-_{jk}(x).
\end{aligned}
\tag{5.27b}
$$

$$
\begin{aligned}
d\left\langle \mathrm{cov}\left(\hat{X}_j\hat{P}_k\right)\right\rangle =& \frac{1}{\hbar}dt\left(\epsilon_j\hat{P}_j\hat{P}_k-\epsilon_k\hat{X}_j\hat{X}_k\right)\\
&+dt\sum_{a=0}\left(Q^+_{aj}(t)^{(C)}\left\langle \hat{P}_k\hat{P}_a\right\rangle-Q^-_{ak}(t)^{(C)}\left\langle \hat{X}_a\hat{X}_j\right\rangle\right)\\
&-4\alpha dt\sum_{a,b=0}\int dx M^+_{aj}(x)M^-_{bk}(x)\left\langle \mathrm{cov}\left(\hat{X}_b\hat{P}_a\right)\right\rangle\\
&-2\alpha dt\sum_{a,b=0}\int dx M^-_{ak}(x)M^+_{ab}(x)\left\langle \mathrm{cov}\left(\hat{X}_j\hat{P}_b\right)\right\rangle\\
&-2\alpha dt\sum_{a,b=0}\int dx M^+_{aj}(x)M^-_{ab}(x)\left\langle \mathrm{cov}\left(\hat{X}_b\hat{P}_k\right)\right\rangle\\
&+4\sqrt{\alpha}\sum_{a,b=0}\int dx dW(x,t)M^-_{ab}(x)\left\langle \hat{X}_j\hat{X}_a\right\rangle\left\langle \mathrm{cov}\left(\hat{X}_b\hat{P}_k\right)\right\rangle\\
&+4\sqrt{\alpha}\sum_{a,b=0}\int dx dW(x,t)M^+_{ab}(x)\left\langle \hat{P}_k\hat{P}_b\right\rangle\left\langle \mathrm{cov}\left(\hat{X}_j\hat{P}_a\right)\right\rangle.
\end{aligned}
\tag{5.27c}
$$

We are now ready to complete a preliminary numeric study of this model in Chapter 6.

Chapter 6

Preliminary simulations of energy damping control

In this chapter, we complete preliminary characterisation of the energy damping control in the box potential using the model derived in Chapter 5. The simulations in this chapter are completed for a limited number of particles ($N \leq 100$) and in the no-backaction conditional measurement limit (which we define in Section 6.1). This is because of the poor scaling of the model with the number of Bogoliubov modes and measurement strength (for reasons discussed in Section 6.4). Whilst operating in the no-backaction limit, we are still able to characterise the behaviour of the energy damping control in our Bogoliubov model, and perform preliminary scans of important parameters to understand their effects.

We discuss the simulation scheme in more detail in Section 6.1. In Section 6.2, we carefully analyse a simulation with one particular set of parameters to develop a detailed characterisation of the behaviour of the energy damping control in the Bogoliubov model. We then provide a preliminary investigation into the effect of the non-measurement parameters — the number of particles, the interaction strength, and the control potential strength — upon our model in Section 6.3.

The simulations in this chapter were completed with a fixed-step Euler algorithm for Itô stochastic differential equations using the XMDS2 open-source software package [181]. These simulations were completed on the Gadi supercomputer at the National Computational Infrastructure. Unless otherwise stated, we average over 240 different trajectories.

6.1 The no-backaction conditional measurement limit

Simulating the model developed in Chapter 5 with a significant measurement strength proved difficult, for reasons that will be discussed in Section 6.4. However, feedback control is only ever defined for a single trajectory, so it is not physically sensible to study our model for $\alpha = 0$; that would be implicitly performing feedback on the average of several trajectories. Instead, we complete simulations in the *no-backaction conditional measurement* limit. In this limit, $\alpha \to 0$ and $r \to \infty$. This corresponds to a measurement so weak it has negligible effect, and a measurement resolution so poor that it cannot resolve density fluctuations within the gas. This is achieved by setting $\alpha/E = 10^{-15}$ and $r/L = 100$, where E is the natural energy scale of the system and L the length of the trap. By working in the no-backaction conditional mea-

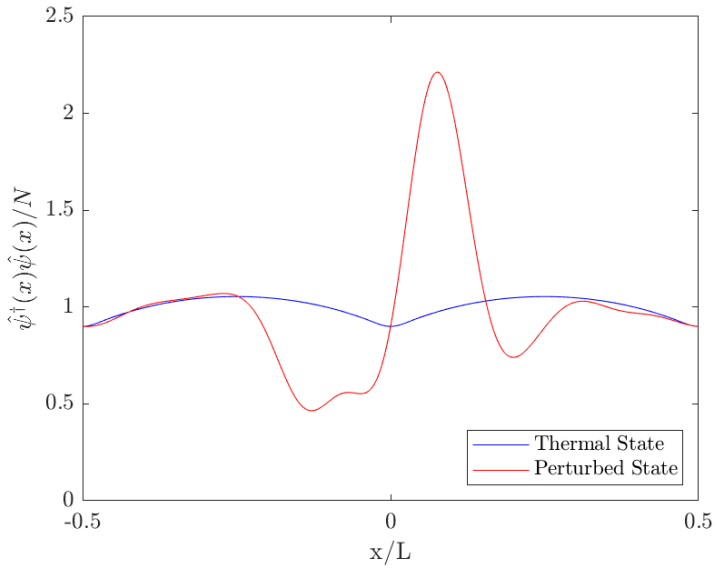

Figure 6.1: The initial state (red) used in this chapter. The state is highly perturbed from the symmetric thermal state (blue) for $gN/EL = 5.0$ and 90% condensate fraction, which is a dark state of the energy damping control. Each state is normalised to the number of particles N.

surement limit, we are effectively studying how our model behaves without measurement.[1]

Consider operating in the no-backaction conditional measurement limit with an initially thermal state. Because the backaction is so small, it takes a very long time for non-negligible fluctuations about the thermal state wavefunction density to arise. It is therefore more efficient to consider a different initial state. In particular, in this chapter we take a thermal state and add a density fluctuation, as in Figure 6.1. Mathematically, these density fluctuations add off-diagonal terms to our position and momentum quadratures. These real correlations between modes then drive imaginary coupling between the modes, and then provide a non-zero error signal for the energy-damping control.

The temperature of our gas is defined, by proxy, by the condensate fraction. As established in Chapter 2, the Bogoliubov approximation is only valid in the limit $T \ll T_C$ [107]. This corresponds to a large condensate fraction, i.e. $N_C \gg N_T$. We will therefore perform the initial characterisation of our model with a condensate fraction of $\langle \hat{N}_C \rangle / \langle \hat{N} \rangle \approx 0.9$, which satisfies this limit. This is the regime which was reached by Taylor [95] with optimal energy damping control using the NPW method, so we know that this is a feasible regime for the energy damping control.

6.1.1 Simulation Scheme

We measure the effectiveness of feedback cooling by studying the condensate fraction $\langle \hat{N}_C \rangle / \langle \hat{N} \rangle$, where $\langle \hat{N}_C \rangle$ is as defined in equation (4.17). The average of the wavefunction

[1] This is similar to how a mean-field model of feedback cooling was first studied by Haine *et al.* [89].

density (equation (5.10)) is normalised to the average number of particles $\langle \hat{N} \rangle$, so that

$$\begin{aligned}\left\langle \hat{N} \right\rangle &= \int dx \left[\sum_{a,b=0} \left[f_a^-(x) f_b^-(x) \left\langle \hat{X}_a \hat{X}_b \right\rangle + f_a^+(x) f_b^+(x) \left\langle \hat{P}_a \hat{P}_b \right\rangle \right] - \sum_{a=0} f_a^-(x) f_a^+(x) \right] \\ &= \frac{1}{2} \sum_{a=0} \left[e^{2r_a} \left\langle \hat{X}_a \hat{X}_a \right\rangle + e^{-2r_a} \left\langle \hat{P}_a \hat{P}_a \right\rangle - 1 \right].\end{aligned} \tag{6.1}$$

In theory, the sum above is defined for an infinite number of Bogoliubov modes. However, Bogoliubov theory is only valid in the $T \ll T_C$ limit, which corresponds to a low-energy limit. Therefore, the Bogoliubov basis is only appropriate for low-energy excitations (the lowest energy Bogoliubov modes), so including an infinite number of Bogoliubov modes is unphysical. Moreover, it is not practical for numeric integration. Instead, an appropriate finite number of modes must be chosen. Note that, for a finite number of modes m_t, the number of excitations N_{ex} is

$$\left\langle \hat{N}_{\text{ex}} \right\rangle (m_t) = \frac{1}{2} \sum_{a=1}^{m_t} \left[e^{2r_a} \left\langle \hat{X}_a \hat{X}_a \right\rangle + e^{-2r_a} \left\langle \hat{P}_a \hat{P}_a \right\rangle - 1 \right]. \tag{6.2}$$

In this chapter, we simulate with the smallest number of modes m such that $N_{\text{ex}}(m)/N_{\text{ex}}(100) < 0.0027$. This means that the sum in equation (6.2) has converged to within three standard deviations of what it would be for 100 modes.[2] We take this to mean that the number of modes m is sufficiently large to account for all of the non-negligible excitations. We then define the initial condensate population as

$$\left\langle \hat{N}_C \right\rangle = \left\langle \hat{N} \right\rangle - \left\langle \hat{N} \right\rangle_{\text{ex}} (m), \tag{6.3}$$

where the thermal states of the quadrature modes are defined using equation (5.25).

It is most efficient to simulate in dimensionless quantities. These are defined by the natural energy scale of the Bogoliubov mode energies ϵ_j, which is $E = \hbar^2/(mL^2)^3$, which in turn defines a time scale $t_0 = mL^2/\hbar$. We can then define a dimensionless interaction strength G and control strength K_{ED} through the parameters

$$G = \frac{g}{EL}, \text{ and } K_{\text{ED}} = \frac{k_{\text{ED}}}{\hbar L}. \tag{6.4}$$

When we want to fix the interaction strength, we will fix GN, as the effect of interactions scales linearly with both interaction strength G and number of particles N (if there are more particles, there are more particles which can interact with each other). This means we can study the effect of varying particle number independent of its effect upon the interaction strength in Section 6.3.2.

[2] Here, we have assumed that 100 modes is a sufficiently large number of modes to approximate infinity. This is because, over a wide range of parameter regimes, between 10 to 20 modes was sufficient for the sum in equation (6.2) to converge. 100 modes is an order of magnitude larger, so we do not expect to ever need more than 100 modes for equation (6.2) to converge.

[3] Note that this is a different natural energy scale to if we were working in a harmonic trap, as in Ref. [64]. We could set $L = 2R_{TF}$ and defined the energy scale in terms of an effective trapping frequency ω. However, R_{TF} is defined in terms of μ, and thus g in the Thomas-Fermi regime. This would define our energy (and therefore our time) scale in terms of g, a parameter we hope to vary.

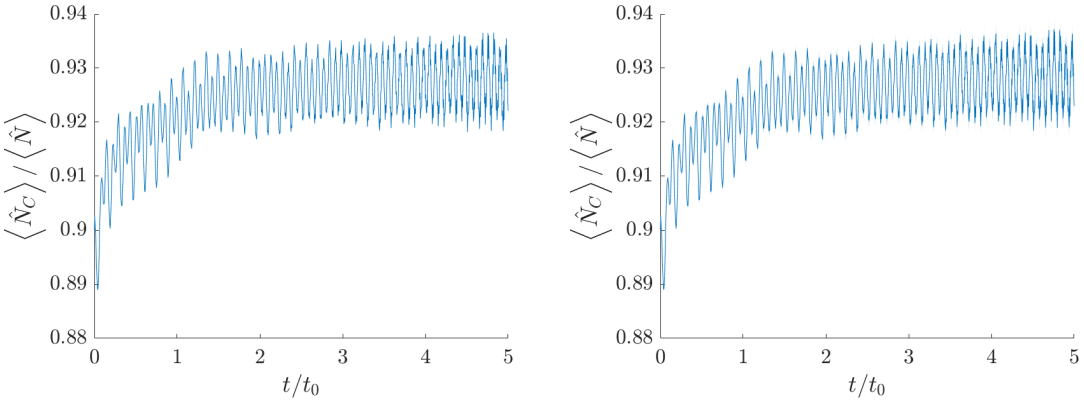

(a) Single trajectory

(b) Average of 240 trajectories

Figure 6.2: Feedback cooling with $GN = 5.0$, $K_{\mathrm{ED}} = 0.1$, $N = 100.0$, $\alpha = 10^{-15}$, $r = 100.0$ and $m = 1$, comparing one trajectory to 240. In Figure 6.2b, the solid line depicts the mean trajectory, and the shaded region around it indicates twice the standard error in the mean (95% confidence interval). This error is to small to be soon. Observe that a) there is no significant difference between one trajcetory and 240 and b) the condensate fraction oscillates from when cooling begins until the simulation has ended.

We are now ready to complete preliminary simulations of feedback cooling with the energy damping control. We first study one simulation in depth to understand the behaviour of the energy damping control at finite temperature.

6.2 Characterising feedback cooling in our Bogoliubov model

To characterise how the energy damping control behaves in our Bogoliubov model, we numerically integrate our model for $G = 5.0$, $K_{\mathrm{ED}} = 0.1$ and $N = 100.0$, which requires $m = 5$ Bogoliubov modes. We will use the condensate fraction as our metric for the effectiveness of feedback cooling, and define the end of the simulation as when the average condensate fraction has stabilised (we discuss this condition more in the following paragraphs). In Figure 6.2a we plot the evolution of the condensate fraction in a single trajectory, and in Figure 6.2b the evolution of the condensate fraction averaged over 240 trajectories. First, note that the error in the condensate fraction evolution is very small; this is because we are working in the limit of minimal backaction. Because the backaction is so small, there is no significant qualitative difference between an individual trajectory and 240.

The gas cools from 90% condensate fraction to an average final condensate fraction $93 \pm 1\%$. Here, the final average condensate fraction is computed over the final time "period" of the simulation (i.e. from $t_0 = 4.0$ to $t_0 = 5.0$)[4], and the error computed by twice the standard deviation in that interval.[5] Whilst this is not as large as the 10% to 90% increase achieved in unpublished work by Goh *et al.*, cooling is more

[4]Note that this is analogous to a "trapping period" in a harmonic trap.

[5]We use *twice* the standard deviation for a 95% confidence interval.

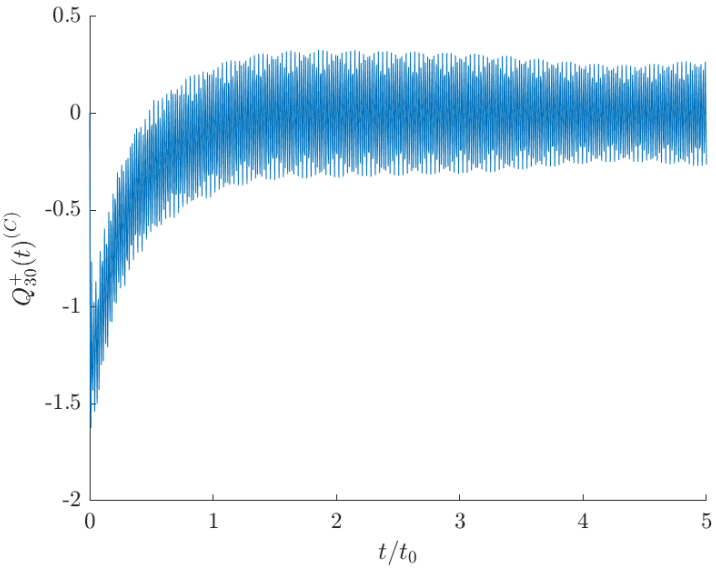

Figure 6.3: Evolution of the conditional feedback matrix $Q^{+}_{30}(t)^{(C)}$, measuring the correlations between the condensate and the third Bogoliubov mode. Solid lines depict the mean trajectory, and shaded regions around them indicate twice the standard error in the mean (95% confidence interval), however this error is negligible. Initially, the error signal is zero, then rapidly increases in magnitude due to the initial density fluctuations. As the gas cools, the error signal decreases in magnitude, before oscillating around zero.

challenging in our simulations because we are starting with a gas that is already very close to $T = 0$. It is more useful to interpret the result here (a final condensate fraction of $93 \pm 1\%$) as demonstrating that $\sim 30\%$ of the thermal excitations have been cooled.

To understand how the energy damping cools these excitations, it is instructive to study the error signal of the control. The error signal is best quantified by the conditional feedback matrices $Q^{\pm}_{ab}(t)^{(C)}$. We plot an arbitrary one of these, $Q^{+}_{30}(t)^{(C)}$ (which specifically quantifies the imaginary correlations between the third Bogoliubov excitation and the condensate) in Figure 6.3. Initially, this error signal is zero, before rapidly growing in magnitude. This indicates that the density fluctuations in the initial state (see Figure 6.1) are driving coupling between the Bogoliubov excitations and the condensate mode. The error signal then decreases in magnitude, which corresponds with an increase in the condensate fraction (see Figure 6.2). The decrease in error signal indicates that the energy damping has used the coupling to drive particles from the excited mode into the condensate. Eventually, towards the end of the simulation, the error signal begins to oscillate at constant amplitude around zero, at a time which corresponds to when the average condensate fraction has stabilised.

We can see in the evolution of both the condensate fraction (Figure 6.2) and the error signal (Figure 6.3) that the system eventually reaches a state where it is oscillating around a stable value. Indeed, this oscillation is responsible for the large error in the average final condensate fraction. Because the average condensate fraction and error signal have stabilised but the oscillations persist, we conclude that the system has reached

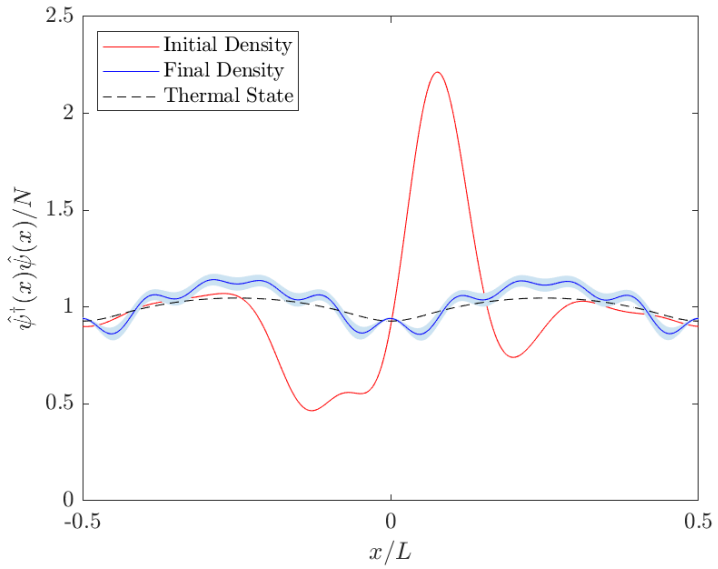

Figure 6.4: The initial wavefunction density (red), final wavefunction density (blue) and wavefunction density of a thermal state at the average final condensate fraction (93%). Shaded regions around the blue curve indicate the error in the final wavefunction density. Observe that the feedback cools the wavefunction from a highly assymetric shape to a symmetric wavefunction density. However, this final state is not a thermal state, as can be seen by comparing the black and blue lines. This indicates that there are still real correlations between the condensate and excitations in the limit cycle.

a *limit cycle*.[6]

Unpublished work by Goh *et al.*, using the NPW method, has observed similar oscillations in the condensate fraction as the gas cools. We show in Section 6.3 that these oscillations change in frequency and amplitude depending upon the dimensionless interaction strength G, so we propose that these oscillations are a consequence of coupling between the condensate and excitations at the final state of the Bose gas.

We investigate this claim further by plotting the initial and final wavefunction density in Figure 6.4. The black dotted line is the wavefunction of a thermal state with $GN = 5.0$ and 93% condensate fraction. The initial density is highly asymmetric, but upon cooling takes upon a symmetric shape (the blue curve). This wavefunction density is not the same as the wavefunction density for a thermal state at the same condensate fraction (see the black dotted curve). The small deviations between the final state and a thermal state indicate that there is coupling between the condensate and excited modes at the end of the simulation. This coupling, if there is interactions between the atoms, would lead to continued exchange of particles between the condensate and excited modes. This continued exchange is balanced out by the response of the feedback control (see Figure 6.3), which is what causes the system to reach a limit cycle, rather than a steady state. Whilst beyond the scope of this work, it would be instructive in future to complete

[6] A limit cycle is a trajectory (or average trajectory) for a system where it continues to dynamically change, but in a fixed periodic manner. For a more rigorous introduction to limit cycles, the interested reader should see Chapter 7 of Ref. [121].

a non-linear stability analysis of our system (equation (5.27)) to analytically study this behaviour.[7]

From our initial characterisation, there are two key observations. Firstly, density fluctuations (real correlations between modes) drives imaginary coupling between modes, which then drives the energy damping control. Secondly, the energy damping drives the system towards a limit cycle, where this is a small amount of coupling between the condensate and the excitations. In this limit cycle, the interactions driving particles out of the condensate is perfectly balanced by the energy-damping control.

6.3 Preliminary parameter scans

Having now characterised the energy damping control, we can study how the effectiveness of feedback cooling varies with the number of particles N, interaction strength G, and energy damping strength K_{ED} (in the no-backaction conditional measurement limit). The validity of the results presented in this section are limited by a) operating in the no-backaction limit and b) using a small number of Bogoliubov modes ($m = 5$). Validating these trends beyond these limits is an avenue for future work.

6.3.1 Varying particle number

From equation (2.51), we expect quantum depletion to decrease the condensate fraction of the system as N increases. To examine whether this is the case, we vary N between 10 and 100 for $m = 5$ Bogoliubov modes to test the dependence of our model on particle number. We fix $GN = 5.0$ (equivalent to fixing the interaction strength per particle) so that the effect of varying number is independent of varying the interaction strength. We also fixed the energy damping strength per particle to $K_{\mathrm{ED}} = 10.0/N$. We do this because the overall energy of the system scales with particle number, and thus the magnitude of the error signal. If we just fixed K_{ED} independent of the number of particles, the effect of energy damping would be much stronger for a larger particle number. We investigate K_{ED} and G in subsequent subsections; this section is concerned with whether solely N has effects upon the dynamics or steady state, such as quantum depletion.

We plot the evolution of the condensate fraction for different N in Figure 6.5. The dynamics and steady state behaviour of the gas do not (within error) change as particle number varies. This indicates that in the no-backaction limit for a limited number of particles, the system scales well with N (provided that the energy damping control and interaction strength are scaled appropriately). Such as trend is somewhat unexpected; we would predict the final condensate fraction to decrease with N due to the effects of quantum depletion. However, as the dynamics do not change within the 95% confidence interval, we conclude that (for $GN = 5.0$) we are not in a regime of significant quantum depletion.

The negligible effects of quantum depletion are due to simulations being completed for only a small number of particles N. We are restricted to this limit because a larger number of particles requires a larger number of modes. For reasons that will be discussed in Section 6.4.1, our simulation scales poorly with the number of Bogoliubov modes m,

[7] For more details on non-linear stability analysis, see Ref. [121]

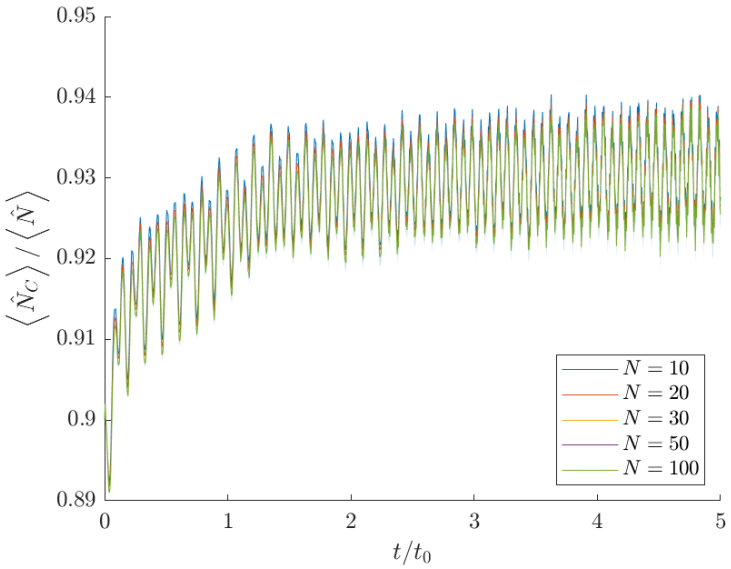

Figure 6.5: Feedback cooling with fixed $K_{\mathrm{ED}} = 10.0/N$, $GN = 5.0$, $\alpha = 10^{-15}$, $r = 100.0$, $m = 5$ and varying N. The 95% confidence interval around the average trajectory is too small to be seen. The system dynamics are qualitatively unaffected by the number of particles.

and we are restricted to the low particle number limit.

We conclude that our model (in the regimes considered in this chapter) is independent of particle number N.[8] To allow a greater variation in the interaction strength G in the following section, we then fix $N = 50.0$ for the remainder of this chapter.

6.3.2 Varying interaction strength

Previous work has found that feedback cooling is significantly affected by interactions for both bosons [2] and fermions [64]. We therefore wish to consider the effect of varying the dimensionless interaction strength scaled by the number of particles GN. This is equivalent to varying the interaction strength per particle. We fix $N = 50.0$, $K_{\mathrm{ED}} = 10.0/N$ and $m = 5$. Note that we consider $G = 0$; our Thomas-Fermi approximation on the condensate wavefunction is technically no longer valid at this interaction strength, however it is useful to indicate the dependence of the oscillations (discussed in Section 6.2) upon the interaction strength.

In Figure 6.6a we plot the evolution of the condensate fraction for different GN. In Figure 6.6b, the average final condensate fraction and its error are plotted (calculated as before), and compared to the maximum possible condensate fraction due to quantum depletion. Observe from Figure 6.6a that as the interaction strength increases, the final condensate fraction decreases. This decrease becomes particularly significant for the larger interaction strengths ($GN \sim O(10)$). Indeed, this final average condensate fraction is well below the limit imposed by quantum depletion (see Figure 6.6b). Physically, this

[8] Note that previous work in feedback cooling Bose gases at zero [2] or finite [95] temperature has not explored the dependence of their model on particle number N, so there is no relevant comparison.

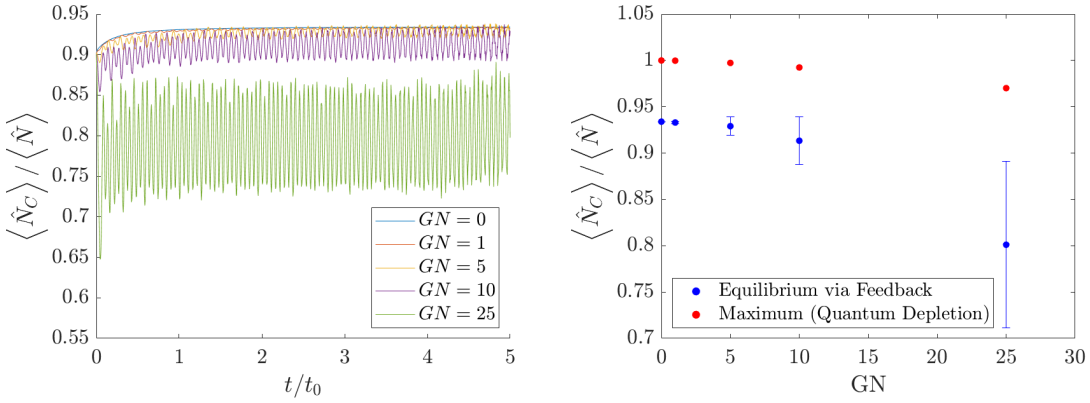

(a) Condensate fraction evolution

(b) Comparison to quantum depletion

Figure 6.6: Feedback cooling with fixed $K_{\mathrm{ED}} = 10.0/N$, $N = 50$, $\alpha = 10^{-15}$, $r = 100.0$, $m = 5$ and varying GN. In Figure 6.6a, solid lines depict the mean of 240 trajectories. The 95% confidence interval is too small to be seen. Observe that as the interaction strength increases, a) final condensate fraction decreases, and b) the magnitude and frequency of the oscillations in the condensate increase. In Figure 6.6b, the average final condensate fraction is plotted as a function of interaction strength, and compared to the maximum possible condensate fraction due to quantum depletion. The standard deviation in each average condensate fraction is shown, a measure of the amplitude of the oscillations. The final condensate fraction is well below the maximum possible value for all interaction strengths, indicating (in the no-backaction regime) that quantum depletion does not significantly affect the efficiency of feedback cooling.

trend is due to repulsive interactions forcing the atoms apart into different energy modes.

The standard deviation of the final condensate fraction, Figure 6.6b, is a measure of the amplitude of the oscillations in the condensate fraction when the limit cycle is reached. As the interaction strength increases, the magnitude of the oscillations increases. Indeed at $G = 0$ there are no oscillations (although this is a tenuous part of the trend as the Thomas-Fermi approximation breaks down in this regime). The frequency of the oscillations also increases as G increases (see Figure 6.6a). Recall that the energy of the condensate is proportional to G, and there appears to be a correlation between the frequency of the oscillations and the energy of the condensate mode.

These results indicate that the oscillations are an interaction dependent effect, verifying the claim in Section 6.2. Recall we noted that, from the final wavefunction density plotted in Figure 6.4, that there is some coupling between the condensate and excitations at the end of the simulation. At a higher interaction strength, greater quantum depletion leads to a greater of Bogoliubov modes, so this coupling can enable an even greater amount of particle exchange between the excitations and the condensate. This is why the magnitude of the oscillations (and thus, the radius of the limit cycle) increases. It is a question for future research whether these oscillations are present in other regimes (e.g. larger number of particles, or with non-negligible backaction).

For $GN = 25.0$, the final condensate fraction is below the initial condensate fraction of 90%. This indicates that interactions can limit the ability of feedback to cool a

Bose gas, even beyond that predicted by quantum depletion. Simulations at $G \geq 50.0$ failed to converge, which may be due to either a physical reason or a numeric reason. As the oscillation amplitude increases non-linearly with G, the oscillations may have become too large for the condensate to be stable at $G \geq 50.0$. Alternatively, a much larger number of Bogoliubov modes may be needed to model these higher interaction strengths, and so $m = 5$ modes was insufficient to model these higher interaction strengths. Due to the poor scaling of the model with m (as will be discussed in Section 6.4), we were unable to evaluate which of these reasons was the cause.

We conclude, at least in the low particle number, no-backaction conditional measurement limit, that the dynamics of our model are significantly affected by G, and the effectiveness of feedback cooling decreases as interactions increases. Note that this trend is in contrast to that observed by Szigeti *et al.* in Ref. [2], where the authors found that increasing interaction strength *increased* the effectiveness of feedback cooling. This was because that study consider the moment control, which can only cool higher order excitations by coupling them to lower order moments (as discussed in Chapter 3.4). Therefore, interactions are necessary for the moment control to operate effectively. In contrast, for the energy damping control studied in this thesis, stronger interactions tend to push atoms further apart into different modes, hindering the cooling. Thus, the result of this section demonstrates a significant difference between the energy damping and moment controls.

6.3.3 Optimising energy damping control

Having developed an understanding of the effect of particle number and interaction strength upon our model (in the no-backaction conditional measurement limit), we can now attempt to optimise the energy damping control. Optimising control potentials was one of the initial goals of developing the model in this thesis, and will characterise how effective our feedback cooling scheme is. To minimise the effects of oscillations upon optimising K_{ED}, we set $GN = 1.0$ and $N = 50.0$.[9] Whilst the results of this section are technically limited to the low particle number and no-backaction regimes, they will hopefully provide an initial calibration of K_{ED} that can be used as comparison in future work.

We vary the control strength per particle for $m = 5$ Bogoliubov modes. In Figure 6.7a the evolution of the condensate fraction is plotted for each energy damping control strength. Qualitatively, the largest energy damping controls take the longest to reach the limit cycle; but this may be a consequence of not exploring very low K_{ED} thoroughly. The average final condensate fraction is plotted in Figure 6.7b. The largest condensate fraction achieved is $93.5 \pm 0.1\%$. The optimal value for K_{ED} lies somewhere in the range between between $0.1/N$ and $2.5/N$; we cannot distinguish further due to the oscillations in the condensate fraction. This suggests that these oscillations, if present in other parameter regimes, may pose a challenge for further optimising the energy damping control in future work.

Simulations of $\mathcal{O}(10)$ paths were also completed for $G = 5.0$, to confirm that the

[9] Note that because we are working with a weaker interaction strength, the Thomas-Fermi approximation may be less valid.

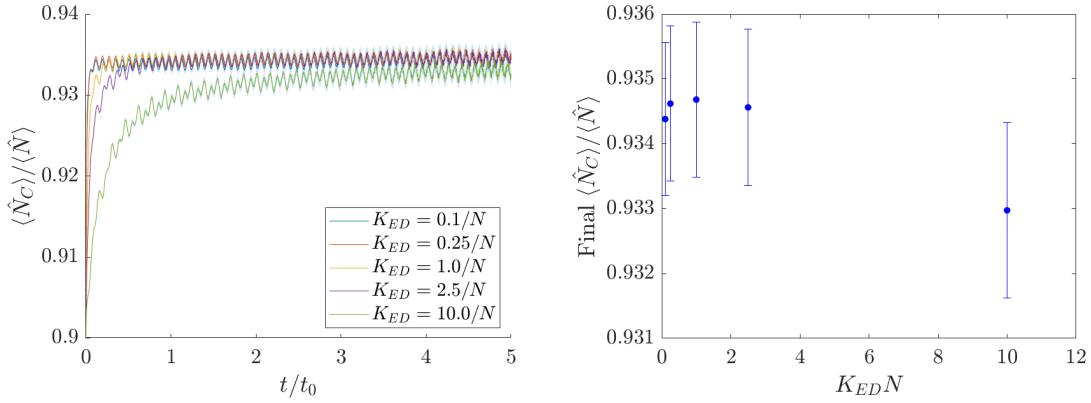

(a) Condensate fraction evolution

(b) Average final condensate fraction

Figure 6.7: Feedback cooling with fixed $N = 50$, $G = 1.0$, $m = 5$, $\alpha = 10^{-15}$, $r = 100.0$ and varying K_{ED}. In Figure 6.7a, solid lines depict the mean of 240 trajectories. The 95% confidence interval is too small to be seen. The limit cycle is reached more slowly for the stronger energy damping controls, but this is likely a consequence of mostly exploring large K_{ED} over small K_{ED}. Observe that the final condensate fraction changes negligibly for $K_{\mathrm{ED}} < 10.0/N$. The maximum condensate fraction appears to be achieved for $K_{\mathrm{ED}} = 1.0/N$, however this is not beyond the standard deviation (error) due to the oscillations in the condensate fraction.

trends observed were independent of interaction strength. The optimum energy damping parameter agreed within a 95% confidence interval, confirming that fixing G to a particular value did not affect our results. However, a detailed study of the effect of interaction strength G on the optimal K_{ED} was not completed. This is an avenue for future work.

Physically, the energy damping control measures density fluctuations, and damps in the opposite direction. Too large a K_{ED} overdamps these fluctuations, creating more fluctuations in the opposite direction. Similarly, too small a K_{ED} cannot counteract these density fluctuations. Therefore, the presence of an optimal energy damping control in our model is validation that it behaves appropriately. Additionally, the presence of an optimal energy damping control agrees qualitatively with the observations of Ref. [64].[10]

Whilst ideally, a quantitative comparison would be made between the results of this section and the NPW method, Taylor [95] did not complete a parameter scan of different energy damping strengths. A comparison between the optimal value of K_{ED} here and that found by the NPW method is therefore an open question for future work.

6.3.4 Summary

We have now completed a preliminary characterisation of low temperature feedback cooling in the no-backaction conditional measurement regime (for a limited particle number). The results of this section are therefore confined to this regime, and require verification in the presence of realistic measurement backaction. In Section 6.4, we will discuss the challenges with exploring those regimes with the model developed in this thesis. Additionally, we did

[10] Note, however, that Ref. [64] was for a Fermi gas, and worked in a harmonic trap, so the results cannot be quantitatively compared. We draw a qualitative comparison because it is the only known work where different values of the energy damping control were scanned in order to feedback cool a gas.

not study the cooling of initially thermal states. The effect of different parameters upon the cooling of states may therefore change in future work with an initially thermal state. Those caveats in mind, we found the following preliminary results in the no-backaction conditional measurement regime:

1. **Feedback cooling to $93.5 \pm 0.1\%$ condensate fraction**. Starting from a Bose gas at 90% condensate fraction (the regime achieved by Taylor [95]), we feedback cooled thermal excitations to increase the condensate fraction further. This demonstrated that our Bogoliubov model can successfully describe the feedback cooling of a Bose gas.

2. **The energy damping control drives the system towards a limit cycle.** The final state of the system is not a thermal state; there is instead coupling between the condensate and excited modes. The system oscillates about this final wavefunction density, and preliminary evidence suggests that this driven by interactions between the condensate and the excitations. However, future work is required to determine if this is a consequence of our initial state or the regime simulated in.

3. **When small, the number of particles does not qualitatively affect dynamics.** This is as long as the interaction strength and energy damping control are scaled accordingly. However, this trend likely only holds in the limit of a small number of particles: we expect quantum depletion to change this trend for simulations considering a larger number of particles.

4. **Interaction strength significantly affects the dynamics of our model.** In particular, interactions seemed to be responsible for the oscillations present in the condensate fraction. However, this may be because our model scales poorly with the number of Bogoliubov modes m (as will be explained in Section 6.4), and more Bogoliubov modes are needed to account for larger interaction strengths.

6.4 Limitations of the perturbative model for simulation

As noted throughout this chapter, our model does not integrate efficiently for a large number of Bogoliubov modes m. We discuss why this is the case in Section 6.4.1. An even more restricting limitation of model is that it does not simulate efficiently for large amounts of stochastic noise. In Section 6.4.2, we discuss the challenges associated with numerically integrating our model for a non-negligible measurement strength.

6.4.1 Scaling with number of Bogoliubov modes

Our simulations are restricted to a low number of Bogoliubov modes due to the order of the terms being integrated[11]. From our full Itô model (equation (5.27)), we can see that the least efficient terms are the decoherence and innovations terms, each of $\mathcal{O}\left(D(m+1)^4\right)$. Here, m is the number of Bogoliubov modes and D the number of x grid points numerically integrated over. By precomputing integrals over pairs of measurement matrices, the decoherence terms become of order $\mathcal{O}((m+1)^4)$. In Appendix A.4, we discuss in detail an approach using the convolution theory for Fourier transforms to

[11] This refers to the number of individual numbers the computer has to keep track of at any time. If there are m Bogoliubov modes and one condensate mode, a term with two free Bogoliubov mode indices — such as $\langle \hat{X}_j \hat{X}_k \rangle$ — is an $(m+1) \times (m+1)$ matrix, and has $\mathcal{O}((m+1)^2)$.

reduce the order of the innovations terms to $\mathcal{O}(D \log D(m+1)^2)$.

For the simulations completed in this chapter, it was found that the measurement matrices $M_{ab}^{\pm}(x)$ were negligibly changed by setting $D \geq 32$, so simulations were set with $D = 32$. For $m \leq 5$, the innovations terms were the least efficient term in the stochastic simulation. However, for more than five excited modes, the decoherence terms become the least efficient, at order $\mathcal{O}((m+1)^4)$. Even increasing the number of excited modes from five to six doubles the complexity — and thus the run time — of the simulation. Therefore, the model does not scale efficiently with the number of excited modes.

6.4.2 Inefficiency of integration algorithms

Simulations were completed in the no-backaction conditional measurement limit because the simulation performed very inefficiently for a large measurement strength α. Simulations in this chapter were completed using an Euler algorithm, which is achieved in XMDS2 with a semi-implicit fixed-step algorithm with one iteration (see Ref. [182] for more details). This means that in each time step dt, the Euler algorithm solves an Itô integral, computing the deterministic dynamics to accuracy dt^1 and the stochastic dynamics to accuracy $dt^{1/2}$ [181].

This means that an Euler algorithm has quite low accuracy for the determistic dynamics of a system of equations. In the presence of small stochastic noise (as in this chapter), only a small number of steps are needed to simulate the deterministic dynamics. However, as the stochastic noise increases, the deterministic dynamics become less stable for a small time step, and a much larger time step is needed. The effect of this upon our simulations is quantified in Figure 6.8. For a range of measurement strengths α, which quantifies the size of our noise, we plot the number of steps needed in a fixed algorithm to accurately compute a single time period t_0 with a half-step error in the wavefunction norm of 10^{-4}. By half-step error, we mean the maximum change in a quantity by re-completing the simulation with half as many steps.[12] This choice of half-step error size is arbitrary; it is to provide a fixed comparison for how many steps are needed. Observe in Figure 6.8 that as α increases, the number of steps required in the Euler algorithm increases exponentially. The Euler algorithm is therefore not very efficient for stochastic simulation beyond the no-backaction conditional measurement limit, and for measurement at the strength simulated in previous feedback cooling literature [2, 64, 94, 95].

One alternative to an Euler algorithm is a Runge-Kutta algorithm. In XMDS2, the fixed-step fourth-order Runge-Kutta (RK4) algorithm computes the deterministic dynamics to accuracy dt^4, and the stochastic dynamics to accuracy $dt^{1/2}$ [181]. Integrating with a fixed-step Runge-Kutta algorithm (or an adaptive equivalent[13]) therefore offers more accuracy than the Euler algorithm. Indeed, previous work with the model of Szigeti *et al.* has used Runge-Kutta methods [2, 64, 94, 95].

[12] For large α, the half-step error needed for safe deterministic dynamics actually decreases; so qualitatively, the estimate of the number of steps required for large α in Figure 6.8 is actually an underestimate. This means that the number of steps actually required is even higher, and in reality the trend is even more extreme.

[13] An adaptive algorithm computes the required step size at each point based upon a minimum half-step error, so is faster for periods of the simulation (such as the final limit cycle) with smaller dynamic changes. See Ref. [183] for a more detailed discussion of adaptive Runge-Kutta algorithms.

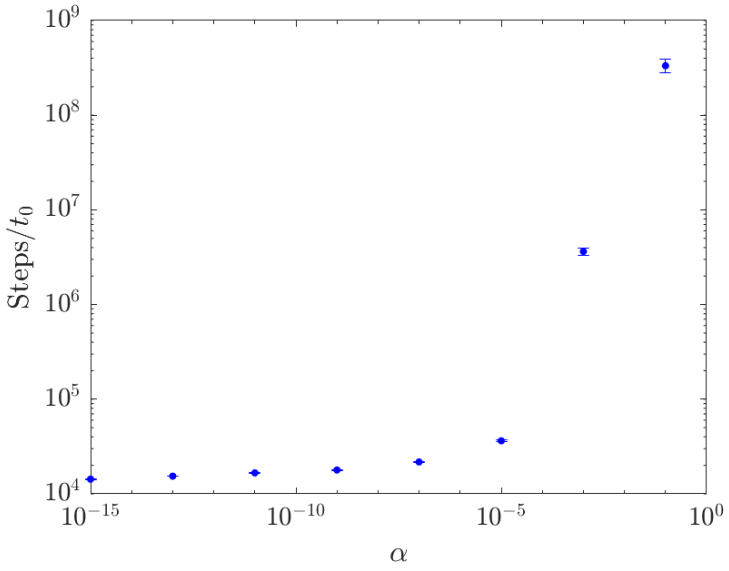

Figure 6.8: Number of steps required for different α to simulate one time interval t_0 within half-step error in the norm of 10^{-4}. The required number of steps required increases exponentially beyond very small α (the no-backaction limit). The fixed-step Euler algorithm is therefore inefficient for stochastic simulation of our model for measurement at the strength simulated in previous feedback cooling literature [2, 64, 94, 95]. We estimate the error in each value from the half-range of steps required to obtain the half-step error of 10^{-4}.

However, a Runge-Kutta algorithm requires integrating our model in the Stratonovich formalism (see Chapter 3.2), because Runge-Kutta algorithms implement the chain and product rules of deterministic calculus. We obtain the Stratonovich equation of motion for our system by implementing the Stratonovich correction, which for our model is found by computing the matrix equivalent of equation (3.17). Alternatively, the Stratonovich correction for an Itô master equation of the form of equation (3.21) is [94]

$$\sum_a \mathcal{C}\left[\hat{c}_a\right]\hat{\rho}_c,$$

where $\mathcal{C}\left[\hat{c}_a\right]\hat{\rho}_c$ is the *Stratonovich superoperator* defined as[14]

$$\mathcal{C}\left[\hat{c}_a\right]\hat{\rho}_c = \mathrm{Tr}\left\{\left(\hat{c}_a + \hat{c}_a^\dagger\right)\hat{\rho}_c\right\}\mathcal{H}\left[\hat{c}_a\right]\hat{\rho}_c - \frac{1}{2}\mathcal{H}\left[\hat{c}_a\hat{c}_a\right]\hat{\rho}_c + \mathrm{Tr}\left\{\hat{c}_a^\dagger\hat{c}_a\hat{\rho}_c\right\}\hat{\rho}_c - \hat{c}_a\hat{\rho}_c\hat{c}_a^\dagger. \quad (6.5)$$

Here, $\mathcal{H}\left[\hat{c}_a\right]\hat{\rho}_c$ is the innovations superoperator defined earlier. For the master equation of Szigeti *et al.* this Stratonovich correction contains terms of the order of the measurement operator squared, which in turn are summed over two Bogoliubov mode indices. This means the Stratonovich correction contains terms of $\mathcal{O}(D(m+1)^6)$. Precomputing integrals of measurement matrices can reduce the order of the Stratonovich correction to $\mathcal{O}((m+1)^6)$; however, this is $(m+1)^2$ times worse than the complexity of the decoherence terms.

[14]For a full derivation of equation (6.5), see the appendix of Ref. [95]. Note the sign error in front of the last term between the penultimate and final lines of equation (B.11).

Alternatively, carefully reordering sums can reduce the order of the stratonovich correction to $\mathcal{O}(D(m+1)^3)$. However, this is still not less than the complexity of the decoherence terms except for $(m+1) > D$. This would require significantly more than $\mathcal{O}(10)$ Bogoliubov modes, which likely no longer corresponds to $T \ll T_C$, so we expect the Bogoliubov approximation would break down.

Therefore, the Stratonovich correction is always significantly more complex than either of the existing terms in the equations of motion. This meant integrating in the Stratonovich formalism, even with a more efficient numeric algorithm, was not more efficient than the Itô integration approach taken.

6.4.3 Summary of limitations to simulation approach

It therefore appears that the model developed in this thesis is not efficient for numeric simulation, at least in the Itô formalism. The most obvious solution would be to find an efficient way to numerically implement the Stratonvoich correction, likely by reducing its complexity to a product of fewer Bogoliubov modes. This is a clear avenue for future research.

Whilst making it more challenging to validate its accuracy and limits, the difficulties in numeric simulation do not mean our model is useless. As will be discussed in Chapter 7, there is a possible avenue to obtain tractable analytics from this model, which will allow for rapid characterisation of different feedback controls without the need for simulation. Those analytic solutions would be able to validated via simulations with the NPW method, which is regardless a more accurate simulation scheme. However, developing a more efficient scheme to simulate the Bogoliubov model is important if we wish to use the Bogoliubov approach to model finite temperature Fermi gases.

Chapter 7

Conclusions and outlook

In this thesis, we derived a model for the feedback cooling of a finite temperature trapped Bose gas. By using the perturbation theory approach of Bogoliubov, we derived a model for an arbitrary 1D trapping and control potential, before considering specifically the energy damping control in a hard box trap. We completed preliminary characterisation of our model via numeric simulation in the no-backaction conditional measurement limit.

More specifically, in Chapter 2 we reviewed the fundamental tools of Bogoliubov theory, and in Chapter 3 introduced the full quantum model of Szigeti *et al.* for a Bose gas undergoing continuous measurement. In Chapter 4, we then used a number-conserving Bogoliubov theory to construct a perturbative model for the dynamics of a finite temperature gas. We did this by deriving the equations of motion for symmetrised pairs of quadrature operators. In particular, we broke down the derivation into the cold atom, measurement, and feedback dynamics. We derived the cold atom and decoherence dynamics through commutator relations in the Schrödinger picture. We derived the innovations terms by making a Gaussian approximation upon the excitations and the condensate. Finally, the feedback dynamics were derived in terms of a control potential, which was determined by the outcome of a conditional measurement.

In Chapter 5, we demonstrated the procedure by which our model could study a control potential of interest in a given trapping potential. Specifically, we motivated studying the hard box trap, which gave rise to sinusoidal solutions with Dirichlet boundary conditions. In this trap, we modelled the energy damping control, which is the present leading candidate for the feedback cooling of Bose gases. Our equations of motion became significantly more tractable after choosing a trapping and control potential. We found that thermal states — those with defined temperature — are dark states of the energy damping control under the Bogoliubov approximation (in both a box and harmonic trap), meaning that thermal states cannot be initially cooled by the energy damping control. Rather, a conditional measurement is needed to first couple the different excited modes, and allow the energy damping control to begin cooling the gas.

In Chapter 6, we completed preliminary numerical simulations of our Itô model in the no-backaction conditional measurement limit (which necessitates not starting in a thermal state). The scope of these simulations was limited by a) the poor scaling of the model with the number of the Bogoliubov modes, and b) the inefficiencies in both Itô and Stratonovich integrals to numerically integrate the model. However, we did demonstrate feedback cooling from 90% to $93.5 \pm 0.1\%$ condensate fraction for an optimal energy damping control (where condensate fraction was our proxy for temperature). These

simulations were completed for $N \leq 100$ particles, and in this low particle number limit the dynamics were unaffected by the number of particles. We also found that the energy damping control drives the system towards a limit cycle. This limit cycle occurs because of the interplay between the energy damping control and the coupling between Bogoliubov modes present after cooling. The amplitude of the limit cycle increased with interaction strength, which we propose is because stronger repulsive interactions increased the ability of the coupling to drive atoms out of the condensate. However, further simulations of the model in a stronger measurement regime, and with an initial thermal state, are needed to verify these results.

7.1 Limitations and future work

Let us now summarise and discuss the limitations of the model and results presented in this thesis. We provide possible solutions to these challenges, and other options for future research based upon this work.

7.1.1 Simulating beyond the no-backaction limit

In Chapter 6.4, we discussed in detail the challenges with numerically simulating our model for non-negligible measurement. As concluded there, the best alternative will be to develop an efficient scheme for calculating the Stratonovich correction, and integrating in the Stratonovich formalism. Otherwise, integrating in the Itô formalism may be possible with a different algorithm. Whilst the only algorithm for Itô integration in the XMDS2 package is a fixed-step algorithm [181], the SciML package developed by Rackauckas *et al.* [184, 185] contains an adaptive algorithm for numeric Itô integration, which may be more efficient.

It was not possible to validate the numeric results of this thesis with the NPW method, which has not been used to explore the no-backaction regime.[1] A less computationally intensive alternative for validating the results in the no-backaction limit would be via simulations with the SPGPE [165, 166]. Ultimately, a comparison between the Bogoliubov model and either of these methods will be necessary to fully characterise what condensate fraction, interaction strength, and particle number regimes the Bogoliubov model is valid in. This will indicate the validity regime for any analytic solutions (see Section 7.1.2), and provide rough predictions for the validity of a fermionic Bogoliubov model for feedback cooling.

7.1.2 Steady state analytic solutions

By diagonalising the cold-atom Hamiltonian, the Bogoliubov approach makes cold-atom dynamics tractable and lends itself towards the development of analytic solutions. Although (as seen in this thesis) the addition of feedback and measurement tend to make the system dynamics less tractable, some classes of continuously-measured

[1] It is actually quite difficult for the NPW method to study the no-backaction regime. In the NPW method, a quantum state is represented by random samples from the initial state distribution. Each of these samples is given a particular *weight*; how likely it is that the system is in that state. After each subsequent measurement of the system, these weights are accordingly evolved, and their average converges to the expected behaviour of the system. Without measurement, it is not possible to model the evolution of the weights, and thus the evolution of the system.

feedback-controlled quantum systems do have analytic solutions. One such system is those undergoing *linear quadratic Gaussian* (LQG) control. LQG control theory describes a system that is initially Gaussian, evolves under a quadratic Hamiltonian, and both the feedback Hamiltonian and measurement operators are linear. LQG control theory derives a steady-state analytic solution for such systems; the details of which are found in Chapter 6 of Ref. [158] (for an excellent introduction in the simplest case of single-mode systems, see Ref. [91]).

Observe crucially that Bogoliubov excitations obey a diagonal Hamiltonian, and it is reasonable to approximate them as Gaussian states (see Chapter 4.4.2 of this thesis). Therefore, a Bogoliubov theory for a linear feedback control and measurement scheme very naturally gives rise to an analytic steady-state solution using LQG control theory. Indeed, Wade *et al.* used LQG control theory to describe the control and entanglement of individual Bogoliubov modes in Ref. [97, 98].

Note that, in this thesis, both the energy damping control Hamiltonian and measurement operator are not linear. However, they may be linearised by making two approximations upon our state. Firstly, by making the symmetry-breaking approximation that the condensate is a classical degree of freedom, $\hat{a}_0$ would become a complex number a_0 and all terms representing the coupling between the condensate and an excitation would become linear in the excitations (i.e. $\langle \hat{X}_j \hat{X}_0 \rangle \to \sqrt{2}\mathrm{Re}\left[a_0\right] \langle \hat{X}_j \rangle$). Secondly, the terms linear in the excitations are the lowest order terms in the fluctuation parameter $\hat{\delta}$, in both the control Hamiltonian and the measurement operator. If $\hat{\delta}$ is sufficiently small, we can then discard all terms quadratic in $\hat{\delta}$; that is, terms like $\langle \hat{X}_j \hat{X}_k \rangle$ for $j, k \neq 0$. Both of these approximations would be safe in the regime that $N_T \ll N_C$.[2] Under this approximation scheme, the energy damping control Hamiltonian and measurement operator respectively become (in the hard box potential)

$$\hat{H}_C^{(L)} = k_{\mathrm{ED}} \frac{4\pi^2 \hbar}{mL^3} \sum_{j>0} j^2 \left\langle \hat{P}_a \right\rangle \hat{X}_a, \tag{7.1a}$$

$$\hat{M}^{(L)}(x) = 2\sqrt{2} \sum_{j>0} M_{j0}^{-}(x) \hat{X}_j, \tag{7.1b}$$

where we have introduced the superscript (L) to indicate that these operators are linearised, and have discarded non-operator valued terms.[3] From here, deriving the steady-state solutions is an analytically involved process relying on the details of LQG control theory, so is proposed as future work. The first goal of that work will be seeing how well the steady-state solutions agree with simulation results (either from this model or more precise ones such as NPW), and if they significantly vary between different traps. Ultimately, this linearisation procedure could be used to rapidly find steady-state analytic solutions for different control schemes, and therefore predict optimal parameter regimes. In particular, in a potential with real Bogoliubov modes (such as a hard box or harmonic

[2] Note that we argued in Chapter 4.1 that a symmetry-breaking approach cannot describe the *dynamics* of feedback cooling; but because we are proposing to use LQG control theory to study the *steady-state* behaviour, the symmetry-breaking approximation should be safe here.

[3] We have also set the phase of the complex number a_0 to 0. This is standard in the symmetry-breaking approach, as discussed in Chapter 2.4.

trap) the linearised control Hamiltonian for an arbitrary control potential $V_C(x,t)$ is

$$\hat{H}_C^{(L)} = 2\sum_a \int dx V_C^{(L)}(x,t) f_a^-(x)\chi_0(x)\hat{X}_a, \tag{7.2}$$

where $V_C^{(L)}(x,t)$ refers to only the linear terms in the control potential.

7.1.3 System-filter separation

In this thesis, we assumed that our estimate of the system state (the filter $\hat{\pi}_c$) exactly approximated the real value (the trajectory $\hat{\rho}_c$). In reality, the filter $\hat{\pi}_c$ is only the experimenter's best guess, based on the signal from the homodyne measurement. As detection is imperfect in a real experiment, the signal will not be quite the same as the trajectory $\hat{\pi}_c$. Therefore, there are actually two master equations of interest: that for the trajectory, $d\hat{\rho}_c$, and that for the filter $d\hat{\pi}_c$.

For the interested reader, we include a more detailed introduction to a system-filter separation for our system in Appendix A.5, applying the system-filter separation of Ref. [161] to the model in Ref. [1]. The key takeaway is that instead of evolving the three matrices $\langle \hat{X}_j \hat{X}_k \rangle$, $\langle \hat{P}_j \hat{P}_k \rangle$ and $\mathrm{cov}\left(\hat{X}_j \hat{P}_k\right)$, in a system-filter separation we evolve matrices for both the system and filter master equations. For example, we evolve both $\langle \hat{X}_j \hat{X}_k \rangle_{\hat{\pi}_c}$ and $\langle \hat{X}_j \hat{X}_k \rangle_{\hat{\rho}_c}$, so there are in total six coupled matrix equations. Note that crucially in both the system and filter dynamics the feedback matrices are determined by expectation values in the *filter*, as that is how the control potential is modified. Once the aim of completing simulations with non-negligible measurement is achieved, implementing a system-filter separation is an obvious avenue for future work. Given that Szigeti *et al.* [186] and Taylor [95] have demonstrated that feedback cooling is still effective even with a system-filter separation (albeit, the former for a non-interacting BEC), completing a system-filter separation is an important step in testing the validity of our Bogoliubov model.

7.1.4 Trap choice

In Chapters 5 and 6, we considered our model in a hard box trap. Future work should consider a harmonically trapped gas, as it would be a) more realistic for experimental implementation of feedback cooling and b) more easily comparable with previous work in the field. The main challenge, for the development of analytic solutions (using LQG control theory as proposed in Section 7.1.2), would be whether the control Hamiltonian is still easily linearisable.

Future work should also consider Bose gases trapped in 2D or 3D traps. Whilst presented in 1D in this thesis, both the Bogoliubov theory in Chapter 2 and the model of Szigeti *et al.* in Chapter 3 are not limited to one dimension. As the higher dimensions would be wrapped up in integrals over the measurement matrices and the number of Bogoliubov modes is independent of dimension, our model should scale quite well to higher dimensions. There are also existing numeric schemes for calculating Bogoliubov modes in higher dimensions [131, 132]. On the other hand, the number of modes in the NPW method scales as $\mathcal{O}(m^n)$, where n is the number of dimensions [92, 93]. Our

Bogoliubov model may therefore be more efficient for modelling 2D or 3D gases, which is useful because real atomic gases are 3D.

7.1.5 Bogoliubov model for feedback cooling of finite temperature fermions

A key motivation behind developing a Bogoliubov theory for the feedback cooling of finite temperature Bose gases is that there also exists a Bogoliubov approach for fermions [72]. Whilst there are possible approaches to develop a non-perturbative finite temperature model for fermions by employing time-evolving block decimation[4] [188, 189] or density matrix renormalisation techniques [190, 191], these approaches are numerically challenging. A Bogoliubov theory would be a more straightforward first study.

The basics of fermionic Bogoliubov theory are similar to the bosonic case, so much of the analytic work of this thesis applies. In particular, the fermionic cold atom Hamiltonian is diagonalised by:

1. Using a perturbation theory about the mean-field to write the interactions term as the sum of products of two operators rather than the one product of four operators (see Ref. [192] or Chapter 44 of Ref. [106] for details)

2. Transforming the fermionic creation and annihilation operators via a fermionic Bogoliubov transformation [108]. Physically, each fermionic Bogoliubov mode corresponds to creating a hole in the Fermi sea, and a particle in an excited state above it. By using this particle-hole formulation, the fermionic Bogoliubov approach inherently conserves number.

The fermionic Bogoliubov modes now obey fermionic *anti*-commutator relations, and their coefficients obey a modified set of orthonormality conditions.[5] Because the fermionic Bogoliubov transformation diagonalises the cold atom Hamiltonian, the Gaussian approximation made in Chapter 4 still applies, and the decoherence terms are simply calculated by replacing $[\hat{M}(x),[\hat{A},\hat{M}(x)]]$ with $\{\hat{M}(x),\{\hat{A},\hat{M}(x)\}\}$. The key difference is in the form for the density $\hat{\psi}^{\dagger}_{\sigma}(x)\hat{\psi}^{\dagger}_{\sigma}(x)$; in the Fermi case, it takes on a spin dependence.

Alternatively, a 1D fermionic Bogoliubov theory can be constructed through the process of *bosonisation*. The rigorous details of this approach can be found in Chapter 2 of [193]. In one dimension, particles are confined to a line so they cannot travel "around" each other exchanging coordinates; thus, the Fermi sign problem [44] does not arise. For this reason, particle-hole excitations essentially behave as density fluctuations with *bosonic* commutation relations. In that case, the bosonic theory developed in this thesis should describe the thermal excitations in the Fermi gas, except with the Bogoliubov modes (including the ground state) $f_a^+(x)$ and ϵ_a transformed to the appropriate spectra for the fermionic system. Crucial to this procedure is that the dispersion relation of excitations in the Fermi gas is approximately linear, so it only holds for a small number of excited modes. The bosonisation procedure also has no higher-dimensional equivalent, unlike the full fermionic Bogoliubov theory.

[4] This matrix method is compared to Bogoliubov approaches for bosonic systems in Ref. [187].

[5] Specifically, the orthonormality conditions for their co-efficients $\{u_j(\mathbf{x}),v_j(\mathbf{x})\}$ become $\int d\mathbf{x}\left(u_j^*(\mathbf{x})u_k(\mathbf{x})+v_j^*(\mathbf{x})v_k(\mathbf{x})\right)=\delta_{jk}$ and $\int d\mathbf{x}\left(u_j(\mathbf{x})v_k(\mathbf{x})+v_j(\mathbf{x})u_k(\mathbf{x})\right)=0$.

7.2 Outlook

In this thesis, we developed a finite temperature model for the feedback cooling of Bose gases using Bogoliubov theory. Our ability to fully characterise and validate this model was limited by its inefficiency as a model for numeric simulation.

However, LQG control theory provides a promising route to derive steady state analytic solutions to our model, with the ultimate goal of rapid analytic optimisation of different control schemes. These analytic results could be validated either with a numeric integration of the model in this thesis, or via the NPW method.

This thesis has also provided two possible directions for the derivation of a Bogoliubov model for the feedback cooling of fermions. That future work would be the first finite temperature model for the feedback cooling of fermions.

Both of these avenues forward — a pathway for achieving tractable analytic solutions for the steady state behaviour of a Bose gas, and a finite temperature model for the feedback cooling fermions — will ultimately aid in informing the first experimental implementation of feedback cooling in coming years. That experimental milestone has the potential to revolutionise the fields of atom interferometry and analogue quantum simulation.

Appendices

Appendix A

Additional theory and working

A.1 Proof of equation (2.24)

Consider a wavefunction $|\Psi\rangle$. Let us make the *Hartree approximation*, that there is always a basis where all the particles can pre written in a single particle state. In particular, in this assuming our wavefunction takes the form

$$|\Psi\rangle = |\alpha_1, \alpha_2, \dots\rangle, \tag{A.1}$$

where each $|\alpha_j\rangle$ is technically the sum of Fock states $|\alpha_j\rangle = \sum_{k_j} c_j |k_j\rangle$. In this basis, our field operator is

$$\hat{\psi}(x) = \sum_j u_j(x)\hat{a}_j, \tag{A.2}$$

where $u_j(x)$ is the spatial wavefunction for the mode annihilated by $\hat{a}_j$. We next assume that each single particle state is a *coherent* state; that is, is an eigenstate of the annihilation operator. In particular, we will write

$$\hat{a}_j|0, \dots, \alpha_j, \dots\rangle = \alpha_j|0, \dots, \alpha_j, \dots\rangle. \tag{A.3}$$

And thus, applying the field operator to the wavefunction $|\Psi\rangle$

$$\hat{\psi}(x)|\Psi\rangle = \sum_j u_j(x)\hat{a}_j|\alpha_1, \alpha_2, \dots\rangle \tag{A.4}$$

$$= \sum_j u_j(x)\alpha_j|\alpha_1, \alpha_2, \dots\rangle \tag{A.5}$$

$$= \sum_j u_j(x)\alpha_j|\Psi\rangle, \tag{A.6}$$

and so if we define the order parameter $\phi(x) = \sum_j u_j(x)\alpha_j$, we have

$$\hat{\psi}(x)|\Psi\rangle = \phi(x)|\Psi\rangle, \tag{A.7}$$

as in equation (2.24).

A.2 Bogoliubov Modes have zero average

We will first prove that the Bogoliubov modes have zero-average in the Bogoliubov basis. We will then discuss the ramifications of this for the average of the Bogoliubov modes in

our model.

From the definition of $\hat{\delta}(x)$, and using $\left\langle \hat{\delta}(x) \right\rangle = 0$, we obtain

$$\sum_a \left(u_a(x) \left\langle \hat{\beta}_a \right\rangle + v_a^*(x) \left\langle \hat{\beta}_a^\dagger \right\rangle \right) = 0. \tag{A.8}$$

Multiplying this equation by $v_b(x)$ and it's complex conjugate by $u_b(x)$ obtains

$$\sum_a u_a(x) v_b(x) \left\langle \hat{\beta}_a \right\rangle = -\sum_a v_a^*(x) v_b(x) \left\langle \hat{\beta}_a^\dagger \right\rangle, \tag{A.9a}$$

$$-\sum_a v_a(x) u_b(x) \left\langle \hat{\beta}_a \right\rangle = \sum_a u_a^*(x) u_b(x) \left\langle \hat{\beta}_a^\dagger \right\rangle. \tag{A.9b}$$

Adding equation (A.9a) to equation (A.9b) and integrating obtains

$$\sum_a \left\langle \hat{\beta}_a \right\rangle \int dx \left(u_a(x) v_b(x) - v_a(x) u_b(x) \right) = \sum_a \left\langle \hat{\beta}_a^\dagger \right\rangle \int dx \left(u_a^*(x) u_b(x) - v_a^*(x) v_b(x) \right). \tag{A.10}$$

By applying the orthonormality conditions (equation (2.40))[1], we obtain

$$\sum_a \delta_{ab} \left\langle \hat{\beta}_a^\dagger \right\rangle = 0 \Rightarrow \left\langle \hat{\beta}_b^\dagger \right\rangle = \left\langle \hat{\beta}_b \right\rangle = 0 \tag{A.11}$$

As $\hat{\beta}_b$ is an arbitrary Bogoliubov mode, it is true for all b. As the quadrature operators are a linear sum of Bogoliubov modes, it immediately follows that $\langle \hat{X}_j \rangle = \langle \hat{P}_j \rangle = 0$.

The unitary dynamics of the averages $\langle \hat{X}_j \rangle, \langle \hat{P}_j \rangle$ is proportional to each other. Similarly, it follows from equation (4.31) that

$$\begin{aligned} \left\langle \left[\hat{M}(x), \left[\hat{X}_j, \hat{M}(x) \right] \right] \right\rangle &= 4 \sum_{ab} \left[\mathrm{Re}\left[N_{aj}(x) \right] \mathrm{Re}\left[N_{ba}(x) \right] - M_{aj}^+(x) M_{ba}^-(x) \right] \left\langle \hat{X}_b \right\rangle \\ &\quad + 4 \sum_{ab} \left[M_{ba}^+(x) \mathrm{Re}\left[N_{aj}(x) \right] - M_{aj}^+(x) \mathrm{Re}\left[N_{ba}(x) \right] \right] \left\langle \hat{P}_b \right\rangle, \end{aligned} \tag{A.12a}$$

$$\begin{aligned} \left\langle \left[\hat{M}(x), \left[\hat{P}_j, \hat{M}(x) \right] \right] \right\rangle &= 4 \sum_{ab} \left[\mathrm{Re}\left[N_{aj}(x) \right] \mathrm{Re}\left[N_{ba}(x) \right] - M_{aj}^-(x) M_{ba}^+(x) \right] \left\langle \hat{P}_b \right\rangle \\ &\quad + 4 \sum_{ab} \left[M_{ba}^-(x) \mathrm{Re}\left[N_{aj}(x) \right] - M_{aj}^-(x) \mathrm{Re}\left[N_{ba}(x) \right] \right] \left\langle \hat{X}_b \right\rangle, \end{aligned} \tag{A.12b}$$

so the decoherence terms of the averages are also proportional to the averages. Finally, we know that the innovations term for each of the averages is proportional to the products $\hat{M}(x)\hat{X}_j$ and $\hat{M}(x)\hat{P}_j$ respectively. Third order Gaussian moments factorise so that each term is proportional to an average, as in equation (A.15). Thus, the innovations terms for the averages are also proportional to the averages themselves.

Thus, all the dynamics of the averages are proportional to the averages themselves, provided the Gaussian approximation is valid. In that case, the averages $\langle \hat{X}_j \rangle, \langle \hat{P}_j \rangle$

[1] Note that if we consider the condensate as the 0th Bogoliubov mode, then $u_0(x) = 1/\sqrt{L}$ and $v_0(x) = 0$, so the orthonormality conditions still hold.

remain zero under evolution of the master equation if they are initially zero. Therefore, the approximation that the averages are zero holds as long as the Gaussian approximation holds.

A.3 Gaussian Distributions

Here, we provide a short summary of the relevant details of probability theory to introduce Gaussian distributions. For a more detailed introduction to the Gaussian approximation in quantum field theory, see Ref. [194] or Chapter 2 of Ref. [155].

Consider a random variable X, which obeys some probability distribution $P(X)$. The kth moment of this probability distribution, $\left\langle X^k \right\rangle$, is the mean value of X^k. That is, if we sampled from $P(X)$ an infinitely large number of times and found X^k for each sample, averaging each of these values would obtain $\left\langle X^k \right\rangle$. Explicitly, the kth moment is defined

$$\left\langle X^k \right\rangle = \int_{-\infty}^{\infty} X^k P(X) dX. \tag{A.13}$$

It turns out that all the $\left\langle X^k \right\rangle$ fully characterise the probability distribution $P(X)$. A useful intuition for this is a series expansion of a function $f(x) = \sum_{n=0}^{\infty} a_n x^n$; if you know all the a_n, you have a complete description of $f(x)$. Now consider a Gaussian probability distribution

$$P(X) = \frac{1}{\sigma\sqrt{2\pi}} \exp\left[-\frac{(X-\mu)^2}{2\sigma^2}\right], \tag{A.14}$$

where μ and σ are the mean and variance respectively defined $\mu = \langle X \rangle$ and $\sigma = \left\langle X^2 \right\rangle - \langle X \rangle^2$. Thus, the first two moments of the Gaussian distribution ($\langle X \rangle$ and $\left\langle X^2 \right\rangle$) fully describe $P(x)$. Using equation (A.13), it is therefore possible to define every moment of a Gaussian distribution in terms of μ and σ. The general form of the higher order moments is intractable, but is simple for lower order moments. For example, for a vector of random variables $\mathbf{X}$, where X_j is the jth element, third order moments obey [195]

$$\langle X_1 X_2 X_3 \rangle = \langle X_1 \rangle \langle X_2 X_3 \rangle + \langle X_2 \rangle \langle X_1 X_3 \rangle + \langle X_3 \rangle \langle X_1 X_2 \rangle - 2 \langle X_1 \rangle \langle X_2 \rangle \langle X_3 \rangle . \tag{A.15}$$

Higher order moments become even more tractable when $\langle X_i \rangle = 0$, because moments of odd order vanish. The remaining even moments of order $2N$ obey [155]

$$\langle X_a X_b X_c \dots \rangle = \frac{(2N)!}{N! 2^N} \{ \langle X_a X_b \rangle \langle X_c X_d \rangle \dots \}_{\text{sym}} , \tag{A.16}$$

where $\{\cdot\}_{\text{sym}}$ is the symmetrised form of that product. In particular, fourth order moments obey

$$\langle X_1 X_2 X_3 X_4 \rangle = \langle X_1 X_2 \rangle \langle X_3 X_4 \rangle + \langle X_1 X_3 \rangle \langle X_2 X_4 \rangle + \langle X_1 X_4 \rangle \langle X_2 X_3 \rangle . \tag{A.17}$$

which is the result quoted in Chapter 4.4.2.

A.4 Reducing the order of decoherence and innovations terms

When simulating equation (5.27), we estimate the behaviour of the system by averaging over hundreds of individual trajectories $\hat{\rho}_c$. Each individual trajectory essentially integrates the evolution of three matrices, $\langle \hat{X}_j \hat{X}_k \rangle$, $\langle \hat{P}_j \hat{P}_k \rangle$ and $\langle \mathrm{cov}(\hat{X}_j \hat{P}_k) \rangle$. Each of these matrices has complexity $\mathcal{O}\left(m^2\right)$, where m is the number of Bogoliubov modes. The complexity of each term in each equation of motion dictates how fast it will simulate.

The harmonic and feedback terms are of complexity $\mathcal{O}\left(m^2\right)$ and $\mathcal{O}\left(m^3\right)$ respectively. The innovations and decoherence terms each involve integrals over some variable x, which are numerically integrated by summing a grid of D points. In the form presented in equation (5.27), the innovations and decoherence terms are both $\mathcal{O}\left(Dm^4\right)$, so are the highest complexity terms in our simulation. By precomputing integrals over pairs of measurement matrices (i.e. $\int dx M^+_{ab}(x) M^-_{cd}(x)$), we reduce the complexity of the decoherence terms to $\mathcal{O}\left(m^4\right)$. We compute each measurement matrix by applying the convolution theorem. Recall that a convolution $(f \circ g)(x)$ of two functions $f(x)$ and $g(x)$ is defined

$$(f \circ g)(x) = \int dy g(x-y) f(y). \tag{A.18}$$

Convolutions obey the useful property under the Fourier transform $\mathcal{F}\{\cdot\}$:

$$\mathcal{F}\{(f \circ g)(x)\}(k_x) = \sqrt{2\pi}\mathcal{F}\{f(x)\}(k_x) \cdot \mathcal{F}\{g(x)\}(k_x). \tag{A.19}$$

The convolution theorem is therefore useful for integrals which are of the form of equation (A.18), such as the measurement matrices (equation (4.27). Using the convolution theorem

$$\tilde{M^{\pm}_{ab}}(k_x) = \sqrt{2\pi}\mathcal{F}\{K_r(x)\}(k_x)\mathcal{F}\left\{f^{\pm}_a(x) f^{\pm}_b(x)\right\}(k_x) \tag{A.20}$$

where $\tilde{M^{\pm}_{ab}}(k_x)$ is the Fourier transform of the measurement matrix. Note from equation (3.34) that the measurement kernel is naturally defined in Fourier space as

$$\tilde{K_r}(k_x) = \sqrt{\frac{r}{2\Gamma(5/4)}} e^{-(rk_x)^4/2}, \tag{A.21}$$

where $\tilde{K_r}(k_x)$ is the Fourier transform of the measurement kernel. Pre-computing the measurement matrices is therefore most efficient in Fourier space. Using equation (A.20), we compute the innovations terms more efficiently by defining

$$W^{\pm}_{ab}(t) = \int dx dW(x,t) M^{\pm}_{ab}(x) = \int dk_x \mathcal{F}\{dW(x,t)\}(k_x) \tilde{M^{\pm}_{ab}}(k_x), \tag{A.22}$$

where the second equation is computed in k_x space. This is straightforward to do using the Fourier transform of a real Wiener process in k_x-space, denoted $\eta(k,t)$ [155]

$$\mathcal{F}\{dW(x,t)\}(k_x) = \frac{1}{2}(i-1)\left(\eta(k_x,t) + i\eta(-k_x,t)\right). \tag{A.23}$$

By using equation (A.22), we make each innovations term of complexity $\mathcal{O}\left(m^4\right)$. Computationally, Fourier transforms have complexity $\mathcal{O}(D \log D)$ when using the fast Fourier

transform [181], so $W^{\pm}_{ab}(t)$ has complexity $\mathcal{O}\left(D \log Dm^2\right)$. Unless we are working with an extremely large grid size or only one or two modes, $\log D \ll m^2$, this series of computations reduces the maximum complexity of the simulation by a factor of D.

A.5 System-Filter Separation

In a real experiment, the experimenter's best guess of the system state $\hat{\pi}_c$ (the filter) will not be the same as the actual trajectory $\hat{\rho}_c$. This is because any experimental measurement is imperfect. In Ref. [161], Szigeti *et al.* derive the master equation for the filter $\hat{\pi}_c$ for the case of a trajectory undergoing a homodyne measurement (the model discussed in Chapter 3.3). Here, we apply that system-filter separation to the measurement-feedback scheme used in this thesis (from Ref. [1]). Recall that a trajectory $\hat{\rho}_c$ evolves under the stochastic master equation

$$d\hat{\rho}_c = -\frac{i}{\hbar}\left[\hat{H}, \hat{\rho}_c\right] dt + \alpha \int dx \mathcal{D}\left[\hat{M}(x)\right] \hat{\rho}_c dt + \sqrt{\alpha} \int dx \mathcal{H}\left[\hat{M}(x)\right] \hat{\rho}_c dW(x,t). \quad \text{(A.24)}$$

The filter therefore evolves under the master equation

$$\begin{aligned} d\hat{\pi}_c = &-\frac{i}{\hbar}\left[\hat{H}, \hat{\pi}_c\right] dt + \alpha \int dx \mathcal{D}\left[\hat{M}(x)\right] \hat{\pi}_c dt \\ &+ \sqrt{\alpha} \int dx \mathcal{H}\left[\hat{M}(x)\right] \hat{\rho}_c \left(d\tilde{Y}(x,t) - \alpha \left\langle \hat{M}(x) + \hat{M}^\dagger(x) \right\rangle_{\hat{\pi}_c} \right), \end{aligned} \quad \text{(A.25)}$$

where $d\tilde{Y}(x,t)$ is the *corrupted measurement signal*, and the subscript $\hat{\pi}_c$ indicates that the expectation value is computed with respect to the filter $\hat{\pi}_c$. The corrupted measurement signal is the signal used by the experimenter to compute the filter $\hat{\pi}_c$, and is defined

$$d\tilde{Y}(x,t) = dY(x,t) + \sqrt{\nu} dW^{(\nu)}(x,t), \quad \text{(A.26)}$$

where $dY(x,t)$ is the *measurement signal* (uncorrupted) and $dW^{(\nu)}(x,t)$ a Wiener process with an associated strength ν. By this definition, the corrupted signal is the actual signal from the system with some associated random noise. The measurement signal is defined

$$dY(x,t) = \alpha \left\langle \hat{M}(x) + \hat{M}^\dagger(x) \right\rangle_{\hat{\rho}_c} + dW^{(Y)}(x,t), \quad \text{(A.27)}$$

where we have used the superscript Y on the Wiener process to indicate that it is associated with the measurement signal. So physically, the system-filter separation works like this: a measurement of the system is made causing some backaction; the experimenter sees that measurement corrupted by some noise; and the experiment makes an estimate of the system, in order to change the control potential. As $\nu \to 0$, $\hat{\pi}_c \to \hat{\rho}_c$; the filter converges to the system. In this thesis, we have effectively assumed $\nu = 0$. Note that as $\alpha \to 0$, the measurement signal $dY(x,t)$ depends only upon noise. That is, if effectively measurement is made, the experimenter just sees the background noise in the homodyne detector.

Appendix B

Full Itô model measurement terms

B.1 Full Itô model: decoherence and innovations terms

In this appendix, we present the full decoherence and innovations terms of the low temperature Itô model for our feedback controlled system.

B.1.1 Decoherence terms

The decoherence terms are

$$\begin{aligned}
d\left\langle \hat{X}_j\hat{X}_k\right\rangle_{\mathcal{D}} &= 4\alpha dt\sum_{ab}\int dx M^{+}_{aj}(x)M^{+}_{bk}(x)\left\langle \hat{P}_a\hat{P}_b\right\rangle \\
&+ 4\alpha dt\sum_{ab}\int dx \mathrm{Re}\left[N_{aj}(x)\right]\mathrm{Re}\left[N_{bk}(x)\right]\left\langle \hat{X}_a\hat{X}_b\right\rangle \\
&+ 2\alpha dt\sum_{ab}\int dx \left[\mathrm{Re}\left[N_{ak}(x)\right]\mathrm{Re}\left[N_{ba}(x)\right] - M^{+}_{ak}(x)M^{-}_{ba}(x)\right]\left\langle \hat{X}_b\hat{X}_j\right\rangle \\
&+ 2\alpha dt\sum_{ab}\int dx \left[\mathrm{Re}\left[N_{aj}(x)\right]\mathrm{Re}\left[N_{ba}(x)\right] - M^{+}_{aj}(x)M^{-}_{ba}(x)\right]\left\langle \hat{X}_b\hat{X}_k\right\rangle \\
&+ 2\alpha dt\sum_{ab}\int dx \left[M^{+}_{ba}(x)\mathrm{Re}\left[N_{ak}(x)\right] - M^{+}_{ak}(x)\mathrm{Re}\left[N_{ba}(x)\right]\right]\mathrm{cov}\left(\hat{X}_j\hat{P}_b\right) \\
&+ 2\alpha dt\sum_{ab}\int dx \left[M^{+}_{ba}(x)\mathrm{Re}\left[N_{aj}(x)\right] - M^{+}_{aj}(x)\mathrm{Re}\left[N_{ba}(x)\right]\right]\mathrm{cov}\left(\hat{X}_k\hat{P}_b\right) \\
&+ 4\alpha dt\sum_{ab}\int dx \left[\mathrm{Re}\left[N_{aj}(x)\right]M^{+}_{bk}(x) + M^{+}_{bj}(x)\mathrm{Re}\left[N_{ak}(x)\right]\right]\mathrm{cov}\left(\hat{X}_a\hat{P}_b\right),
\end{aligned} \tag{B.1a}$$

$$
\begin{aligned}
d\left\langle \hat{P}_j\hat{P}_k\right\rangle_{\mathcal{D}} &= 4\alpha dt\sum_{ab}\int dx M^{-}_{aj}(x)M^{-}_{bk}(x)\left\langle \hat{X}_a\hat{X}_b\right\rangle \\
&+ 4\alpha dt\sum_{ab}\int dx \mathrm{Re}\left[N_{aj}(x)\right]\mathrm{Re}\left[N_{bk}(x)\right]\left\langle \hat{P}_a\hat{P}_b\right\rangle \\
&+ 2\alpha dt\sum_{ab}\int dx \left[\mathrm{Re}\left[N_{ak}(x)\right]\mathrm{Re}\left[N_{ba}(x)\right]-M^{-}_{ak}(x)M^{+}_{ba}(x)\right]\left\langle \hat{P}_b\hat{P}_j\right\rangle \\
&+ 2\alpha dt\sum_{ab}\int dx \left[\mathrm{Re}\left[N_{aj}(x)\right]\mathrm{Re}\left[N_{ba}(x)\right]-M^{-}_{aj}(x)M^{+}_{ba}(x)\right]\left\langle \hat{P}_b\hat{P}_k\right\rangle \\
&+ 2\alpha dt\sum_{ab}\int dx \left[M^{-}_{ba}(x)\mathrm{Re}\left[N_{ak}(x)\right]-M^{-}_{ak}(x)\mathrm{Re}\left[N_{ba}(x)\right]\right]\mathrm{cov}\left(\hat{X}_b\hat{P}_j\right) \\
&+ 2\alpha dt\sum_{ab}\int dx \left[M^{-}_{ba}(x)\mathrm{Re}\left[N_{aj}(x)\right]-M^{-}_{aj}(x)\mathrm{Re}\left[N_{ba}(x)\right]\right]\mathrm{cov}\left(\hat{X}_b\hat{P}_k\right) \\
&+ 4\alpha dt\sum_{ab}\int dx \left[\mathrm{Re}\left[N_{bj}(x)\right]M^{-}_{ak}(x)+M^{-}_{aj}(x)\mathrm{Re}\left[N_{bk}(x)\right]\right]\mathrm{cov}\left(\hat{X}_a\hat{P}_b\right),
\end{aligned}
\tag{B.1b}
$$

$$
\begin{aligned}
d\left\langle \mathrm{cov}\left(\hat{X}_j\hat{P}_k\right)\right\rangle_{\mathcal{D}} &= 2\alpha dt\sum_{ab}\int dx \left[M^{-}_{ba}(x)\mathrm{Re}\left[N_{aj}(x)\right]-M^{-}_{ak}(x)\mathrm{Re}\left[N_{ba}(x)\right]\right]\left\langle \hat{X}_j\hat{X}_b\right\rangle \\
&+ 2\alpha dt\sum_{ab}\int dx \left[M^{+}_{ba}(x)\mathrm{Re}\left[N_{aj}(x)\right]-M^{+}_{aj}(x)\mathrm{Re}\left[N_{ba}(x)\right]\right]\left\langle \hat{P}_b\hat{P}_k\right\rangle \\
&- 4\alpha dt\sum_{ab}\int dx \mathrm{Re}\left[N_{aj}(x)\right]M^{-}_{bk}(x)\left\langle \hat{X}_a\hat{X}_b\right\rangle \\
&- 4\alpha dt\sum_{ab}\int dx M^{+}_{aj}(x)\mathrm{Re}\left[N_{bk}(x)\right]\left\langle \hat{P}_a\hat{P}_b\right\rangle \\
&+ 2\alpha dt\sum_{ab}\int dx \left[\mathrm{Re}\left[N_{ak}(x)\right]\mathrm{Re}\left[N_{ba}(x)\right]-M^{-}_{ak}(x)M^{+}_{ba}(x)\right]\mathrm{cov}\left(\hat{X}_j\hat{P}_b\right) \\
&+ 2\alpha dt\sum_{ab}\int dx \left[\mathrm{Re}\left[N_{aj}(x)\right]\mathrm{Re}\left[N_{ba}(x)\right]-M^{+}_{aj}(x)M^{-}_{ba}(x)\right]\mathrm{cov}\left(\hat{X}_b\hat{P}_k\right) \\
&- 4\alpha dt\sum_{ab}\int dx \left[M^{+}_{aj}(x)M^{-}_{bk}(x)+\mathrm{Re}\left[N_{bj}(x)\right]\mathrm{Re}\left[N_{ak}(x)\right]\right]\mathrm{cov}\left(\hat{X}_b\hat{P}_a\right).
\end{aligned}
\tag{B.1c}
$$

B.1.2 Innovations terms

The innovations terms are

$$
\begin{aligned}
d\left\langle \hat{X}_j\hat{X}_k\right\rangle_{\mathcal{H}} &= 4\sqrt{\alpha}\sum_{ab}\int dxdW(x,t)\mathrm{Re}\left[M^-_{ab}(x)\right]\left\langle \hat{X}_j\hat{X}_a\right\rangle\left\langle \hat{X}_k\hat{X}_b\right\rangle \\
&\quad + 4\sqrt{\alpha}\sum_{ab}\int dxdW(x,t)\mathrm{Re}\left[M^+_{ab}(x)\right]\left\langle \mathrm{cov}\left(\hat{X}_j\hat{P}_a\right)\right\rangle\left\langle \mathrm{cov}\left(\hat{X}_k\hat{P}_b\right)\right\rangle \\
&\quad + 4\sqrt{\alpha}\sum_{ab}\int dxdW(x,t)\mathrm{Re}\left[N_{ab}(x)\right]\left\langle \hat{X}_j\hat{X}_c\right\rangle\mathrm{cov}\left(\hat{X}_k\hat{P}_d\right) \\
&\quad + 4\sqrt{\alpha}\sum_{ab}\int dxdW(x,t)\mathrm{Re}\left[N_{ab}(x)\right]\mathrm{cov}\left(\hat{X}_j\hat{P}_d\right)\left\langle \hat{X}_k\hat{X}_c\right\rangle \\
&\quad - \sqrt{\alpha}\int dxdW(x,t)\mathrm{Re}\left[M^+_{jk}(x)\right],
\end{aligned}
\tag{B.2a}
$$

$$
\begin{aligned}
d\left\langle \hat{P}_j\hat{P}_k\right\rangle_{\mathcal{H}} &= 4\sqrt{\alpha}\sum_{ab}\int dxdW(x,t)\mathrm{Re}\left[M^+_{ab}(x)\right]\left\langle \hat{P}_j\hat{P}_a\right\rangle\left\langle \hat{P}_k\hat{P}_b\right\rangle \\
&\quad + 4\sqrt{\alpha}\sum_{ab}\int dxdW(x,t)\mathrm{Re}\left[M^-_{ab}(x)\right]\left\langle \mathrm{cov}\left(\hat{X}_a\hat{P}_j\right)\right\rangle\left\langle \mathrm{cov}\left(\hat{X}_b\hat{P}_k\right)\right\rangle \\
&\quad + 4\sqrt{\alpha}\sum_{ab}\int dxdW(x,t)\mathrm{Re}\left[N_{ab}(x)\right]\left\langle \hat{P}_j\hat{P}_d\right\rangle\mathrm{cov}\left(\hat{X}_c\hat{P}_k\right) \\
&\quad + 4\sqrt{\alpha}\sum_{ab}\int dxdW(x,t)\mathrm{Re}\left[N_{ab}(x)\right]\mathrm{cov}\left(\hat{X}_c\hat{P}_j\right)\left\langle \hat{P}_k\hat{P}_d\right\rangle \\
&\quad - \sqrt{\alpha}\int dxdW(x,t)\mathrm{Re}\left[M^-_{jk}(x)\right],
\end{aligned}
\tag{B.2b}
$$

$$
\begin{aligned}
d\left\langle \mathrm{cov}\left(\hat{X}_j\hat{P}_k\right)\right\rangle_{\mathcal{H}} &= 4\sqrt{\alpha}\sum_{ab}\int dxdW(x,t)\mathrm{Re}\left[M^-_{ab}(x)\right]\left\langle \hat{X}_j\hat{X}_a\right\rangle\left\langle \mathrm{cov}\left(\hat{X}_b\hat{P}_k\right)\right\rangle \\
&\quad + 4\sqrt{\alpha}\sum_{ab}\int dxdW(x,t)\mathrm{Re}\left[M^+_{ab}(x)\right]\left\langle \hat{P}_k\hat{P}_b\right\rangle\left\langle \mathrm{cov}\left(\hat{X}_j\hat{P}_a\right)\right\rangle \\
&\quad + 4\sqrt{\alpha}\sum_{ab}\int dxdW(x,t)\mathrm{Re}\left[N_{ab}(x)\right]\left\langle \hat{X}_j\hat{X}_c\right\rangle\left\langle \hat{P}_k\hat{P}_d\right\rangle \\
&\quad + 4\sqrt{\alpha}\sum_{ab}\int dxdW(x,t)\mathrm{Re}\left[N_{ab}(x)\right]\mathrm{cov}\left(\hat{X}_j\hat{P}_d\right)\mathrm{cov}\left(\hat{X}_c\hat{P}_k\right) \\
&\quad + \sqrt{a}\int dxdW(x,t)\mathrm{Re}\left[N_{kj}(x)\right].
\end{aligned}
\tag{B.2c}
$$

Bibliography

[1] S. S. Szigeti, M. R. Hush, A. R. R. Carvalho, and J. J. Hope, "Continuous measurement feedback control of a Bose-Einstein condensate using phase-contrast imaging," *Physical Review A*, vol. 80, p. 013614, July 2009. Publisher: American Physical Society.

[2] S. S. Szigeti, M. R. Hush, A. R. R. Carvalho, and J. J. Hope, "Feedback control of an interacting Bose-Einstein condensate using phase-contrast imaging," *Physical Review A*, vol. 82, p. 043632, Oct. 2010. Publisher: American Physical Society.

[3] M. H. Anderson, J. R. Ensher, M. R. Matthews, C. E. Wieman, and E. A. Cornell, "Observation of Bose-Einstein Condensation in a Dilute Atomic Vapor," *Science*, vol. 269, no. 5221, pp. 198–201, 1995. Publisher: American Association for the Advancement of Science.

[4] K. B. Davis, M. O. Mewes, M. R. Andrews, N. J. van Druten, D. S. Durfee, D. M. Kurn, and W. Ketterle, "Bose-Einstein Condensation in a Gas of Sodium Atoms," *Physical Review Letters*, vol. 75, pp. 3969–3973, Nov. 1995.

[5] C. C. Bradley, C. A. Sackett, and R. G. Hulet, "Bose-Einstein Condensation of Lithium: Observation of Limited Condensate Number," *Physical Review Letters*, vol. 78, pp. 985–989, Feb. 1997. Publisher: American Physical Society.

[6] M. Saffman, "Quantum computing with atomic qubits and Rydberg interactions: progress and challenges," *Journal of Physics B: Atomic, Molecular and Optical Physics*, vol. 49, p. 202001, Oct. 2016. Publisher: IOP Publishing.

[7] C. Barcel, S. Liberati, and M. Visser, "Analogue Gravity," *Living Reviews in Relativity*, vol. 14, p. 3, May 2011.

[8] M. Albiez, R. Gati, J. Flling, S. Hunsmann, M. Cristiani, and M. K. Oberthaler, "Direct Observation of Tunneling and Nonlinear Self-Trapping in a Single Bosonic Josephson Junction," *Physical Review Letters*, vol. 95, p. 010402, June 2005. Publisher: American Physical Society.

[9] N. P. Robins, P. A. Altin, J. E. Debs, and J. D. Close, "Atom lasers: Production, properties and prospects for precision inertial measurement," *Physics Reports*, vol. 529, pp. 265–296, Aug. 2013.

[10] D. Carney, P. C. E. Stamp, and J. M. Taylor, "Tabletop experiments for quantum gravity: a users manual," *Classical and Quantum Gravity*, vol. 36, p. 034001, Feb. 2019.

[11] C. Gross and I. Bloch, "Quantum simulations with ultracold atoms in optical lattices," *Science*, vol. 357, pp. 995–1001, Sept. 2017. Publisher: American Association for the Advancement of Science Section: Review.

[12] I. Bloch, "Quantum simulations come of age," *Nature Physics*, vol. 14, pp. 1159–1161, Dec. 2018. Number: 12 Publisher: Nature Publishing Group.

[13] D. C. McKay and B. DeMarco, "Cooling in strongly correlated optical lattices: prospects and challenges," *Reports on Progress in Physics*, vol. 74, p. 054401, May 2011.

[14] A. A. Michelson and E. W. Morley, "LVIII. On the relative motion of the earth and the luminiferous ther," *The London, Edinburgh, and Dublin Philosophical Magazine and Journal of Science*, vol. 24, pp. 449–463, Dec. 1887. Publisher: Taylor & Francis _eprint: https://doi.org/10.1080/14786448708628130.

[15] LIGO Scientific Collaboration and Virgo Collaboration, B. Abbott, R. Abbott, T. Abbott, M. Abernathy, F. Acernese, K. Ackley, C. Adams, T. Adams, P. Addesso, R. Adhikari, V. Adya, C. Affeldt, M. Agathos, K. Agatsuma, N. Aggarwal, O. Aguiar, L. Aiello, A. Ain, P. Ajith, B. Allen, A. Allocca, P. Altin, S. Anderson, W. Anderson, K. Arai, M. Arain, M. Araya, C. Arceneaux, J. Areeda, N. Arnaud, K. Arun, S. Ascenzi, G. Ashton, M. Ast, S. Aston, P. Astone, P. Aufmuth, C. Aulbert, S. Babak, P. Bacon, M. Bader, P. Baker, F. Baldaccini, G. Ballardin, S. Ballmer, J. Barayoga, S. Barclay, B. Barish, D. Barker, F. Barone, B. Barr, L. Barsotti, M. Barsuglia, D. Barta, J. Bartlett, M. Barton, I. Bartos, R. Bassiri, A. Basti, J. Batch, C. Baune, V. Bavigadda, M. Bazzan,

B. Behnke, M. Bejger, C. Belczynski, A. Bell, C. Bell, B. Berger, J. Bergman, G. Bergmann, C. Berry, D. Bersanetti, A. Bertolini, J. Betzwieser, S. Bhagwat, R. Bhandare, I. Bilenko, G. Billingsley, J. Birch, R. Birney, O. Birnholtz, S. Biscans, A. Bisht, M. Bitossi, C. Biwer, M. Bizouard, J. Blackburn, C. Blair, D. Blair, R. Blair, S. Bloemen, O. Bock, T. Bodiya, M. Boer, G. Bogaert, C. Bogan, A. Bohe, P. Bojtos, C. Bond, F. Bondu, R. Bonnand, B. Boom, R. Bork, V. Boschi, S. Bose, Y. Bouffanais, A. Bozzi, C. Bradaschia, P. Brady, V. Braginsky, M. Branchesi, J. Brau, T. Briant, A. Brillet, M. Brinkmann, V. Brisson, P. Brockill, A. Brooks, D. Brown, D. Brown, N. Brown, C. Buchanan, A. Buikema, T. Bulik, H. Bulten, A. Buonanno, D. Buskulic, C. Buy, R. Byer, M. Cabero, L. Cadonati, G. Cagnoli, C. Cahillane, J. C. Bustillo, T. Callister, E. Calloni, J. Camp, K. Cannon, J. Cao, C. Capano, E. Capocasa, F. Carbognani, S. Caride, J. C. Diaz, C. Casentini, S. Caudill, M. Cavagli, F. Cavalier, R. Cavalieri, G. Cella, C. Cepeda, L. C. Baiardi, G. Cerretani, E. Cesarini, R. Chakraborty, T. Chalermsongsak, S. Chamberlin, M. Chan, S. Chao, P. Charlton, E. Chassande-Mottin, H. Chen, Y. Chen, C. Cheng, A. Chincarini, A. Chiummo, H. Cho, M. Cho, J. Chow, N. Christensen, Q. Chu, S. Chua, S. Chung, G. Ciani, F. Clara, J. Clark, F. Cleva, E. Coccia, P.-F. Cohadon, A. Colla, C. Collette, L. Cominsky, M. Constancio, A. Conte, L. Conti, D. Cook, T. Corbitt, N. Cornish, A. Corsi, S. Cortese, C. Costa, M. Coughlin, S. Coughlin, J.-P. Coulon, S. Countryman, P. Couvares, E. Cowan, D. Coward, M. Cowart, D. Coyne, R. Coyne, K. Craig, J. Creighton, T. Creighton, J. Cripe, S. Crowder, A. Cruise, A. Cumming, L. Cunningham, E. Cuoco, T. D. Canton, S. Danilishin, S. DAntonio, K. Danzmann, N. Darman, C. Da Silva Costa, V. Dattilo, I. Dave, H. Daveloza, M. Davier, G. Davies, E. Daw, R. Day, S. De, D. DeBra, G. Debreczeni, J. Degallaix, M. De Laurentis, S. Delglise, W. Del Pozzo, T. Denker, T. Dent, H. Dereli, V. Dergachev, R. DeRosa, R. De Rosa, R. DeSalvo, S. Dhurandhar, M. Daz, L. Di Fiore, M. Di Giovanni, A. Di Lieto, S. Di Pace, I. Di Palma, A. Di Virgilio, G. Dojcinoski, V. Dolique, F. Donovan, K. Dooley, S. Doravari, R. Douglas, T. Downes, M. Drago, R. Drever, J. Driggers, Z. Du, M. Ducrot, S. Dwyer, T. Edo, M. Edwards, A. Effler, H.-B. Eggenstein, P. Ehrens, J. Eichholz, S. Eikenberry, W. Engels, R. Essick, T. Etzel, M. Evans, T. Evans, R. Everett, M. Factourovich, V. Fafone, H. Fair, S. Fairhurst, X. Fan, Q. Fang, S. Farinon, B. Farr, W. Farr, M. Favata, M. Fays, H. Fehrmann, M. Fejer, D. Feldbaum, I. Ferrante, E. Ferreira, F. Ferrini, F. Fidecaro, L. Finn, I. Fiori, D. Fiorucci, R. Fisher, R. Flaminio, M. Fletcher, H. Fong, J.-D. Fournier, S. Franco, S. Frasca, F. Frasconi, M. Frede, Z. Frei, A. Freise, R. Frey, V. Frey, T. Fricke, P. Fritschel, V. Frolov, P. Fulda, M. Fyffe, H. Gabbard, J. Gair, L. Gammaitoni, S. Gaonkar, F. Garufi, A. Gatto, G. Gaur, N. Gehrels, G. Gemme, B. Gendre, E. Genin, A. Gennai, J. George, L. Gergely, V. Germain, A. Ghosh, A. Ghosh, S. Ghosh, J. Giaime, K. Giardina, A. Giazotto, K. Gill, A. Glaefke, J. Gleason, E. Goetz, R. Goetz, L. Gondan, G. Gonzlez, J. G. Castro, A. Gopakumar, N. Gordon, M. Gorodetsky, S. Gossan, M. Gosselin, R. Gouaty, C. Graef, P. Graff, M. Granata, A. Grant, S. Gras, C. Gray, G. Greco, A. Green, R. Greenhalgh, P. Groot, H. Grote, S. Grunewald, G. Guidi, X. Guo, A. Gupta, M. Gupta, K. Gushwa, E. Gustafson, R. Gustafson, J. Hacker, B. Hall, E. Hall, G. Hammond, M. Haney, M. Hanke, J. Hanks, C. Hanna, M. Hannam, J. Hanson, T. Hardwick, J. Harms, G. Harry, I. Harry, M. Hart, M. Hartman, C.-J. Haster, K. Haughian, J. Healy, J. Heefner, A. Heidmann, M. Heintze, G. Heinzel, H. Heitmann, P. Hello, G. Hemming, M. Hendry, I. Heng, J. Hennig, A. Heptonstall, M. Heurs, S. Hild, D. Hoak, K. Hodge, D. Hofman, S. Hollitt, K. Holt, D. Holz, P. Hopkins, D. Hosken, J. Hough, E. Houston, E. Howell, Y. Hu, S. Huang, E. Huerta, D. Huet, B. Hughey, S. Husa, S. Huttner, T. Huynh-Dinh, A. Idrisy, N. Indik, D. Ingram, R. Inta, H. Isa, J.-M. Isac, M. Isi, G. Islas, T. Isogai, B. Iyer, K. Izumi, M. Jacobson, T. Jacqmin, H. Jang, K. Jani, P. Jaranow, "Observation of Gravitational Waves from a Binary Black Hole Merger," *Physical Review Letters*, vol. 116, p. 061102, Feb. 2016. Publisher: American Physical Society.

[16] L. De Broglie, "Waves and Quanta," *Nature*, vol. 112, pp. 540–540, Oct. 1923. Number: 2815 Publisher: Nature Publishing Group.

[17] R. M. Wald, *General Relativity*. Chicago: The University of Chicago Press, 1 ed., 1984.

[18] T. Byrnes and E. O. Ilo-Okeke, *Quantum Atom Optics: Theory and Applications to Quantum Technology*. Cambridge University Press, 2020. arXiv: 2007.14601.

[19] J. M. Overduin, "Solar system tests of the equivalence principle and constraints on higher-dimensional gravity," *Physical Review D*, vol. 62, p. 102001, Oct. 2000. Publisher: American Physical Society.

[20] K. Becker, M. Becker, and J. H. Schwarz, *String Theory and M-Theory: A Modern Introduction*. Cambridge: Cambridge University Press, 1 ed., 2007.

[21] T. Damour, "Testing the equivalence principle: why and how?," *Classical and Quantum Gravity*, vol. 13, pp. A33–A41, Nov. 1996. Publisher: IOP Publishing.

[22] M. Zych and a. Brukner, "Quantum formulation of the Einstein equivalence principle," *Nature Physics*, vol. 14, pp. 1027–1031, Oct. 2018. Number: 10 Publisher: Nature Publishing Group.

[23] S. Dimopoulos, P. W. Graham, J. M. Hogan, and M. A. Kasevich, "Testing General Relativity with Atom Interferometry," *Physical Review Letters*, vol. 98, p. 111102, Mar. 2007. Publisher: American Physical Society.

[24] C. Marletto and V. Vedral, "Gravitationally Induced Entanglement between Two Massive Particles is Sufficient Evidence of Quantum Effects in Gravity," *Physical Review Letters*, vol. 119, p. 240402, Dec. 2017.

[25] S. Bose, A. Mazumdar, G. W. Morley, H. Ulbricht, M. Toro, M. Paternostro, A. A. Geraci, P. F. Barker, M. Kim, and G. Milburn, "Spin Entanglement Witness for Quantum Gravity," *Physical Review Letters*, vol. 119, p. 240401, Dec. 2017. Publisher: American Physical Society.

[26] J. F. Donoghue, "Leading quantum correction to the Newtonian potential," *Physical Review Letters*, vol. 72, pp. 2996–2999, May 1994. Publisher: American Physical Society.

[27] S. Dimopoulos, P. W. Graham, J. M. Hogan, M. A. Kasevich, and S. Rajendran, "Atomic gravitational wave interferometric sensor," *Physical Review D*, vol. 78, p. 122002, Dec. 2008. Publisher: American Physical Society.

[28] G. Geneves, P. Gournay, A. Gosset, M. Lecollinet, F. Villar, P. Pinot, P. Juncar, A. Clairon, A. Landragin, D. Holleville, F. Dos Santos, J. David, M. Besbes, F. Alves, L. Chassagne, and S. Topcu, "The BNM Watt balance project," *IEEE Transactions on Instrumentation and Measurement*, vol. 54, pp. 850–853, Apr. 2005. Conference Name: IEEE Transactions on Instrumentation and Measurement.

[29] F. Sorrentino, Q. Bodart, L. Cacciapuoti, Y.-H. Lien, M. Prevedelli, G. Rosi, L. Salvi, and G. M. Tino, "Sensitivity limits of a Raman atom interferometer as a gravity gradiometer," *Physical Review A*, vol. 89, p. 023607, Feb. 2014. Publisher: American Physical Society.

[30] G. D'Amico, F. Borselli, L. Cacciapuoti, M. Prevedelli, G. Rosi, F. Sorrentino, and G. M. Tino, "Bragg interferometer for gravity gradient measurements," *Physical Review A*, vol. 93, p. 063628, June 2016. Publisher: American Physical Society.

[31] E. H. van Leeuwen, "BHP develops airborne gravity gradiometer for mineral exploration," *The Leading Edge*, vol. 19, pp. 1296–1297, Dec. 2000. Publisher: Society of Exploration Geophysicists.

[32] G. Stern, B. Battelier, R. Geiger, G. Varoquaux, A. Villing, F. Moron, O. Carraz, N. Zahzam, Y. Bidel, W. Chaibi, F. Pereira Dos Santos, A. Bresson, A. Landragin, and P. Bouyer, "Light-pulse atom interferometry in microgravity," *The European Physical Journal D*, vol. 53, pp. 353–357, June 2009.

[33] J. L. Chen, C. R. Wilson, and B. D. Tapley, "Satellite Gravity Measurements Confirm Accelerated Melting of Greenland Ice Sheet," *Science*, vol. 313, pp. 1958–1960, Sept. 2006. Publisher: American Association for the Advancement of Science Section: Report.

[34] M. Leblanc, P. Tregoning, G. Ramillien, S. Tweed, and A. Fakes, "Basin-scale, integrated observations of the early 21st century multiyear drought in southeast Australia," *Water Resources Research*, 2009. Accepted: 2015-12-08T22:14:11Z Last Modified: 2020-05-19 Publisher: American Geophysical Union.

[35] C. Jekeli, "Cold Atom Interferometer as Inertial Measurement Unit for Precision Navigation," pp. 604–613, June 2004.

[36] B. Battelier, B. Barrett, L. Fouch, L. Chichet, L. Antoni-Micollier, H. Porte, F. Napolitano, J. Lautier, A. Landragin, and P. Bouyer, "Development of compact cold-atom sensors for inertial navigation," in *Quantum Optics*, vol. 9900, p. 990004, International Society for Optics and Photonics, Apr. 2016.

[37] A. DeGregoria, *Gravity gradiometry and map matching: an aid to aircraft inertial navigation systems*. PhD, Air Force Institute of Technology, 2010.

[38] J. A. Richeson, *Gravity gradiometer aided inertial navigation within non-GNSS environments*. PhD, University of Maryland, 2008.

[39] K. Huang, *Introduction to Statistical Physics*. Boca Raton, Florida: CRC Press, 2 ed., 2010.

[40] S. S. Szigeti, S. P. Nolan, J. D. Close, and S. A. Haine, "High-Precision Quantum-Enhanced Gravimetry with a Bose-Einstein Condensate," *Physical Review Letters*, vol. 125, p. 100402, Sept. 2020.

[41] K. Bongs, M. Holynski, J. Vovrosh, P. Bouyer, G. Condon, E. Rasel, C. Schubert, W. P. Schleich, and A. Roura, "Taking atom interferometric quantum sensors from the laboratory to real-world applications," *Nature Reviews Physics*, vol. 1, pp. 731–739, Dec. 2019. Number: 12 Publisher: Nature Publishing Group.

[42] S. S. Szigeti, J. E. Debs, J. J. Hope, N. P. Robins, and J. D. Close, "Why momentum width matters for atom interferometry with Bragg pulses," *New Journal of Physics*, vol. 14, p. 023009, Feb. 2012. Publisher: IOP Publishing.

[43] A. J. Leggett, "Bose-Einstein condensation in the alkali gases: Some fundamental concepts," *Reviews of Modern Physics*, vol. 73, pp. 307–356, Apr. 2001. Publisher: American Physical Society.

[44] E. Y. Loh, J. E. Gubernatis, R. T. Scalettar, S. R. White, D. J. Scalapino, and R. L. Sugar, "Sign problem in the numerical simulation of many-electron systems," *Physical Review B*, vol. 41, pp. 9301–9307, May 1990. Publisher: American Physical Society.

[45] R. Feynman, "Simulating physics with computers," *International Journal of Theoretical Physics*, vol. 21, pp. 467–488, June 1982.

[46] S. Lloyd, "Universal Quantum Simulators," *Science*, vol. 273, no. 5278, pp. 1073–1078, 1996. Publisher: American Association for the Advancement of Science.

[47] I. Georgescu, S. Ashhab, and F. Nori, "Quantum simulation," *Reviews of Modern Physics*, vol. 86, pp. 153–185, Mar. 2014. Publisher: American Physical Society.

[48] M. Nielsen and I. Chuang, *Quantum Computation and Quantum Information*. New York: Cambridge University Press, 10th anniversary ed., 2010.

[49] F. Arute, K. Arya, R. Babbush, D. Bacon, J. C. Bardin, R. Barends, R. Biswas, S. Boixo, F. G. S. L. Brandao, D. A. Buell, B. Burkett, Y. Chen, Z. Chen, B. Chiaro, R. Collins, W. Courtney, A. Dunsworth, E. Farhi, B. Foxen, A. Fowler, C. Gidney, M. Giustina, R. Graff, K. Guerin, S. Habegger, M. P. Harrigan, M. J. Hartmann, A. Ho, M. Hoffmann, T. Huang, T. S. Humble, S. V. Isakov, E. Jeffrey, Z. Jiang, D. Kafri, K. Kechedzhi, J. Kelly, P. V. Klimov, S. Knysh, A. Korotkov, F. Kostritsa, D. Landhuis, M. Lindmark, E. Lucero, D. Lyakh, S. Mandr, J. R. McClean, M. McEwen, A. Megrant, X. Mi, K. Michielsen, M. Mohseni, J. Mutus, O. Naaman, M. Neeley, C. Neill, M. Y. Niu, E. Ostby, A. Petukhov, J. C. Platt, C. Quintana, E. G. Rieffel, P. Roushan, N. C. Rubin, D. Sank, K. J. Satzinger, V. Smelyanskiy, K. J. Sung, M. D. Trevithick, A. Vainsencher, B. Villalonga, T. White, Z. J. Yao, P. Yeh, A. Zalcman, H. Neven, and J. M. Martinis, "Quantum supremacy using a programmable superconducting processor," *Nature*, vol. 574, pp. 505–510, Oct. 2019. Number: 7779 Publisher: Nature Publishing Group.

[50] C. Rigetti, J. M. Gambetta, S. Poletto, B. L. T. Plourde, J. M. Chow, A. D. Crcoles, J. A. Smolin, S. T. Merkel, J. R. Rozen, G. A. Keefe, M. B. Rothwell, M. B. Ketchen, and M. Steffen, "Superconducting qubit in a waveguide cavity with a coherence time approaching 0.1 ms," *Physical Review B*, vol. 86, p. 100506, Sept. 2012. Publisher: American Physical Society.

[51] H. Hffner, C. F. Roos, and R. Blatt, "Quantum computing with trapped ions," *Physics Reports*, vol. 469, pp. 155–203, Dec. 2008.

[52] P. Hauke, F. M. Cucchietti, L. Tagliacozzo, I. Deutsch, and M. Lewenstein, "Can one trust quantum simulators?," *Reports on Progress in Physics*, vol. 75, p. 082401, July 2012. Publisher: IOP Publishing.

[53] I. Bloch, J. Dalibard, and S. Nascimbne, "Quantum simulations with ultracold quantum gases," *Nature Physics*, vol. 8, pp. 267–276, Apr. 2012. Number: 4 Publisher: Nature Publishing Group.

[54] B. Zimmermann, T. Mller, J. Meineke, T. Esslinger, and H. Moritz, "High-resolution imaging of ultracold fermions in microscopically tailored optical potentials," *New Journal of Physics*, vol. 13, p. 043007, Apr. 2011. Publisher: IOP Publishing.

[55] T. A. Bell, J. A. P. Glidden, L. Humbert, M. W. J. Bromley, S. A. Haine, M. J. Davis, T. W. Neely, M. A. Baker, and H. Rubinsztein-Dunlop, "BoseEinstein condensation in large time-averaged optical ring potentials," *New Journal of Physics*, vol. 18, p. 035003, Mar. 2016. Publisher: IOP Publishing.

[56] R. Grimm, M. Weidemller, and Y. B. Ovchinnikov, "Optical Dipole Traps for Neutral Atoms," in *Advances In Atomic, Molecular, and Optical Physics* (B. Bederson and H. Walther, eds.), vol. 42, pp. 95–170, Academic Press, Jan. 2000.

[57] P. A. Altin, N. P. Robins, D. Dring, J. E. Debs, R. Poldy, C. Figl, and J. D. Close, "R85b tunable-interaction BoseEinstein condensate machine," *Review of Scientific Instruments*, vol. 81, p. 063103, June 2010. Publisher: American Institute of Physics.

[58] J. Stenger, S. Inouye, M. R. Andrews, H.-J. Miesner, D. M. Stamper-Kurn, and W. Ketterle, "Strongly Enhanced Inelastic Collisions in a Bose-Einstein Condensate near Feshbach Resonances," *Physical Review Letters*, vol. 82, pp. 2422–2425, Mar. 1999. Publisher: American Physical Society.

[59] W. Ketterle and M. W. Zwierlein, "Making, probing and understanding ultracold Fermi gases," *La Rivista del Nuovo Cimento*, vol. 31, pp. 247–422, July 2008. arXiv: 0801.2500.

[60] P. B. Wigley, P. J. Everitt, K. S. Hardman, M. R. Hush, C. H. Wei, M. A. Sooriyabandara, P. Manju, J. D. Close, N. P. Robins, and C. C. N. Kuhn, "Non-destructive shadowgraph imaging of ultra-cold atoms," *Optics Letters*, vol. 41, pp. 4795–4798, Oct. 2016. Publisher: Optical Society of America.

[61] G. K. Campbell, M. M. Boyd, J. W. Thomsen, M. J. Martin, S. Blatt, M. D. Swallows, T. L. Nicholson, T. Fortier, C. W. Oates, S. A. Diddams, N. D. Lemke, P. Naidon, P. Julienne, J. Ye, and A. D. Ludlow, "Probing Interactions Between Ultracold Fermions," *Science*, vol. 324, pp. 360–363, Apr. 2009. Publisher: American Association for the Advancement of Science Section: Report.

[62] E. Haller, J. Hudson, A. Kelly, D. A. Cotta, B. Peaudecerf, G. D. Bruce, and S. Kuhr, "Single-atom imaging of fermions in a quantum-gas microscope," *Nature Physics*, vol. 11, pp. 738–742, Sept. 2015. Number: 9 Publisher: Nature Publishing Group.

[63] D. Jaksch, C. Bruder, J. I. Cirac, C. W. Gardiner, and P. Zoller, "Cold Bosonic Atoms in Optical Lattices," *Physical Review Letters*, vol. 81, pp. 3108–3111, Oct. 1998. Publisher: American Physical Society.

[64] M. L. Goh, *Feedback control of atomic Fermi gases*. Honours Thesis, The Australian National University, Canberra, 2019.

[65] J. Hubbard and B. H. Flowers, "Electron correlations in narrow energy bands," *Proceedings of the Royal Society of London. Series A. Mathematical and Physical Sciences*, vol. 276, pp. 238–257, Nov. 1963. Publisher: Royal Society.

[66] M. C. Gutzwiller, "Effect of Correlation on the Ferromagnetism of Transition Metals," *Physical Review Letters*, vol. 10, pp. 159–162, Mar. 1963. Publisher: American Physical Society.

[67] J. Kanamori, "Electron Correlation and Ferromagnetism of Transition Metals," *Progress of Theoretical Physics*, vol. 30, pp. 275–289, Sept. 1963. Publisher: Oxford Academic.

[68] H. A. Gersch and G. C. Knollman, "Quantum Cell Model for Bosons," *Physical Review*, vol. 129, pp. 959–967, Jan. 1963. Publisher: American Physical Society.

[69] P. W. Anderson, P. A. Lee, M. Randeria, T. M. Rice, N. Trivedi, and F. C. Zhang, "The physics behind high-temperature superconducting cuprates: the plain vanilla version of RVB," *Journal of Physics: Condensed Matter*, vol. 16, pp. R755–R769, June 2004. Publisher: IOP Publishing.

[70] K. Okazaki, Y. Ito, Y. Ota, Y. Kotani, T. Shimojima, T. Kiss, S. Watanabe, C.-T. Chen, S. Niitaka, T. Hanaguri, H. Takagi, A. Chainani, and S. Shin, "Superconductivity in an electron band just above the Fermi level: possible route to BCS-BEC superconductivity," *Scientific Reports*, vol. 4, p. 4109, Feb. 2014. Number: 1 Publisher: Nature Publishing Group.

[71] J. Bardeen, L. N. Cooper, and J. R. Schrieffer, "Theory of Superconductivity," *Physical Review*, vol. 108, pp. 1175–1204, Dec. 1957. Publisher: American Physical Society.

[72] N. N. Bogoljubov, V. V. Tolmachov, and D. V. irkov, "A New Method in the Theory of Superconductivity," *Fortschritte der Physik*, vol. 6, no. 11-12, pp. 605–682, 1958. _eprint: https://onlinelibrary.wiley.com/doi/pdf/10.1002/prop.19580061102.

[73] E. Snider, N. Dasenbrock-Gammon, R. McBride, M. Debessai, H. Vindana, K. Vencatasamy, K. V. Lawler, A. Salamat, and R. P. Dias, "Room-temperature superconductivity in a carbonaceous sulfur hydride," *Nature*, vol. 586, pp. 373–377, Oct. 2020. Number: 7829 Publisher: Nature Publishing Group.

[74] M. Ono, S. Koga, and H. Ohtsuki, "Japan's superconducting Maglev train," *IEEE Instrumentation Measurement Magazine*, vol. 5, pp. 9–15, Mar. 2002. Conference Name: IEEE Instrumentation Measurement Magazine.

[75] W. Hofstetter, J. I. Cirac, P. Zoller, E. Demler, and M. D. Lukin, "High-Temperature Superfluidity of Fermionic Atoms in Optical Lattices," *Physical Review Letters*, vol. 89, p. 220407, Nov. 2002. Publisher: American Physical Society.

[76] R. Onofrio, "Physics of our Days: Cooling and thermometry of atomic Fermi gases," *Physics-Uspekhi*, vol. 59, p. 1129, Nov. 2016. Publisher: IOP Publishing.

[77] K. M. O'Hara, S. L. Hemmer, M. E. Gehm, S. R. Granade, and J. E. Thomas, "Observation of a Strongly Interacting Degenerate Fermi Gas of Atoms," *Science*, vol. 298, pp. 2179–2182, Dec. 2002. Publisher: American Association for the Advancement of Science Section: Report.

[78] T. Fukuhara, Y. Takasu, M. Kumakura, and Y. Takahashi, "Degenerate Fermi Gases of Ytterbium," *Physical Review Letters*, vol. 98, p. 030401, Jan. 2007. Publisher: American Physical Society.

[79] H. J. Metcalf and P. v. d. Straten, "Laser Cooling and Trapping of Neutral Atoms," in *The Optics Encyclopedia*, American Cancer Society, July 2007.

[80] W. Ketterle and N. J. V. Druten, "Evaporative Cooling of Trapped Atoms," in *Advances In Atomic, Molecular, and Optical Physics* (B. Bederson and H. Walther, eds.), vol. 37, pp. 181–236, Academic Press, Jan. 1996.

[81] C. J. Pethick and H. Smith, *BoseEinstein Condensation in Dilute Gases*. Cambridge University Press, Sept. 2008. Google-Books-ID: G8kgAwAAQBAJ.

[82] B. Desruelle, V. Boyer, S. G. Murdoch, G. Delannoy, P. Bouyer, A. Aspect, and M. Lcrivain, "Interrupted evaporative cooling of 87 Rb atoms trapped in a high magnetic field," *Physical Review A*, vol. 60, pp. R1759–R1762, Sept. 1999.

[83] A. G. Truscott, K. E. Strecker, W. I. McAlexander, G. B. Partridge, and R. G. Hulet, "Observation of Fermi Pressure in a Gas of Trapped Atoms," *Science*, vol. 291, pp. 2570–2572, Mar. 2001. Publisher: American Association for the Advancement of Science Section: Report.

[84] F. Schreck, G. Ferrari, K. L. Corwin, J. Cubizolles, L. Khaykovich, M.-O. Mewes, and C. Salomon, "Sympathetic cooling of bosonic and fermionic lithium gases towards quantum degeneracy," *Physical Review A*, vol. 64, p. 011402, June 2001. Publisher: American Physical Society.

[85] L. D. Carr, T. Bourdel, and Y. Castin, "Limits of sympathetic cooling of fermions by zero-temperature bosons due to particle losses," *Physical Review A*, vol. 69, p. 033603, Mar. 2004. Publisher: American Physical Society.

[86] J. Zhang, Y.-x. Liu, R.-B. Wu, K. Jacobs, and F. Nori, "Quantum feedback: Theory, experiments, and applications," *Physics Reports*, vol. 679, pp. 1–60, Mar. 2017.

[87] H. M. Wiseman and L. K. Thomsen, "Reducing the Linewidth of an Atom Laser by Feedback," *Physical Review Letters*, vol. 86, pp. 1143–1147, Feb. 2001. Publisher: American Physical Society.

[88] L. K. Thomsen and H. M. Wiseman, "Atom-laser coherence and its control via feedback," *Physical Review A*, vol. 65, p. 063607, June 2002. Publisher: American Physical Society.

[89] S. A. Haine, A. J. Ferris, J. D. Close, and J. J. Hope, "Control of an atom laser using feedback," *Physical Review A*, vol. 69, p. 013605, Jan. 2004. Publisher: American Physical Society.

[90] M. Johnsson, S. Haine, and J. J. Hope, "Stabilizing an atom laser using spatially selective pumping and feedback," *Physical Review A*, vol. 72, p. 053603, Nov. 2005. Publisher: American Physical Society.

[91] A. C. Doherty and K. Jacobs, "Feedback control of quantum systems using continuous state estimation," *Physical Review A*, vol. 60, pp. 2700–2711, Oct. 1999.

[92] M. R. Hush, A. R. R. Carvalho, and J. J. Hope, "Number-phase Wigner representation for efficient stochastic simulations," *Physical Review A*, vol. 81, p. 033852, Mar. 2010. Publisher: American Physical Society.

[93] M. R. Hush, A. R. R. Carvalho, and J. J. Hope, "Number-phase Wigner representation for scalable stochastic simulations of controlled quantum systems," *Physical Review A*, vol. 85, p. 023607, Feb. 2012. Publisher: American Physical Society.

[94] M. R. Hush, S. S. Szigeti, A. R. R. Carvalho, and J. J. Hope, "Controlling spontaneous-emission noise in measurement-based feedback cooling of a BoseEinstein condensate," *New Journal of Physics*, vol. 15, p. 113060, Nov. 2013.

[95] R. L. Taylor, *Applications of quantum control: scaling of quantum computers and BEC-based quantum sensors*. PhD Thesis, The Australian National University, Canberra, 2020.

[96] N. Bogoliubov, "On the theory of superfluidity," *J. Phys (USSR)*, vol. 11, no. 1, pp. 23–32, 1947.

[97] A. C. Wade, J. F. Sherson, and K. Mlmer, "Squeezing and Entanglement of Density Oscillations in a Bose-Einstein Condensate," *Physical Review Letters*, vol. 115, p. 060401, Aug. 2015. Publisher: American Physical Society.

[98] A. C. J. Wade, J. F. Sherson, and K. Mlmer, "Manipulation of collective quantum states in Bose-Einstein condensates by continuous imaging," *Physical Review A*, vol. 93, p. 023610, Feb. 2016. Publisher: American Physical Society.

[99] H. M. Hurst, S. Guo, and I. B. Spielman, "Feedback Induced Magnetic Phases in Binary Bose-Einstein Condensates," *arXiv:2007.07266 [cond-mat, physics:quant-ph]*, July 2020. arXiv: 2007.07266.

[100] M. Schemmer, A. Johnson, R. Photopoulos, and I. Bouchoule, "Monte Carlo wave-function description of losses in a one-dimensional Bose gas and cooling to the ground state by quantum feedback," *Physical Review A*, vol. 95, p. 043641, Apr. 2017. Publisher: American Physical Society.

[101] M. R. Andrews, M.-O. Mewes, N. J. van Druten, D. S. Durfee, D. M. Kurn, and W. Ketterle, "Direct, Nondestructive Observation of a Bose Condensate," *Science*, vol. 273, p. 84, July 1996.

[102] S. Weinberg, *The Quantum Theory of Fields*. Austin: Cambridge University Press, 1 ed., 2013.

[103] A. Einstein, "Quantentheorie des einatomigen idealen Gases," *Sitzungsberichte der Preussischen Akademie der Wissenschaften*, vol. 1, no. 3, 1925.

[104] Bose, "Plancks Gesetz und Lichtquantenhypothese," *Zeitschrift fr Physik*, vol. 26, pp. 178–181, Dec. 1924.

[105] A. Zee, *Quantum Field Theory in a Nutshell*. Princeton, New Jersey: Princeton University Press, 2 ed., 2010.

[106] T. Lancaster and S. J. Blundell, *Quantum Field Theory for the Gifted Amateur*. New York: Oxford University Press, 1 ed., 2014.

[107] N. P. Proukakis and B. Jackson, "Finite Temperature Models of Bose-Einstein Condensation," *Journal of Physics B: Atomic, Molecular and Optical Physics*, vol. 41, p. 203002, Oct. 2008. arXiv: 0810.0210.

[108] H. Bruus and K. Flensberg, *Many-body quantum theory in condensed matter physics*. USA: Oxford University Press, 2 ed., 2002.

[109] H. Feshbach, "A unified theory of nuclear reactions. II," *Annals of Physics*, vol. 19, pp. 287–313, Aug. 1962.

[110] S. Inouye, M. R. Andrews, J. Stenger, H.-J. Miesner, D. M. Stamper-Kurn, and W. Ketterle, "Observation of Feshbach resonances in a BoseEinstein condensate," *Nature*, vol. 392, pp. 151–154, Mar. 1998. Number: 6672 Publisher: Nature Publishing Group.

[111] E. J. Mueller and G. Baym, "Finite-temperature collapse of a Bose gas with attractive interactions," *Physical Review A*, vol. 62, p. 053605, Oct. 2000. Publisher: American Physical Society.

[112] W. Ketterle and N. J. van Druten, "Bose-Einstein condensation of a finite number of particles trapped in one or three dimensions," *Physical Review A*, vol. 54, pp. 656–660, July 1996.

[113] S. Giovanazzi and D. H. J. ODell, "Instabilities and the roton spectrum of a quasi-1D Bose-Einstein condensed gas with dipole-dipole interactions," *The European Physical Journal D - Atomic, Molecular, Optical and Plasma Physics*, vol. 31, pp. 439–445, Nov. 2004.

[114] H. L. C. Couto, A. T. Avelar, and W. B. Cardoso, "Effective equations for repulsive quasi-1D BECs trapped with anharmonic transverse potentials," *Annalen der Physik*, vol. 530, p. 1700352, Apr. 2018. arXiv: 1707.03260.

[115] M. Krmer, L. Pitaevskii, and S. Stringari, "Macroscopic Dynamics of a Trapped Bose-Einstein Condensate in the Presence of 1D and 2D Optical Lattices," *Physical Review Letters*, vol. 88, p. 180404, Apr. 2002.

[116] A. Grlitz, J. M. Vogels, A. E. Leanhardt, C. Raman, T. L. Gustavson, J. R. Abo-Shaeer, A. P. Chikkatur, S. Gupta, S. Inouye, T. Rosenband, and W. Ketterle, "Realization of Bose-Einstein Condensates in Lower Dimensions," *Physical Review Letters*, vol. 87, p. 130402, Sept. 2001. Publisher: American Physical Society.

[117] B. L. Tolra, K. M. OHara, J. H. Huckans, W. D. Phillips, S. L. Rolston, and J. V. Porto, "Observation of Reduced Three-Body Recombination in a Correlated 1D Degenerate Bose Gas," *Physical Review Letters*, vol. 92, p. 190401, May 2004. Publisher: American Physical Society.

[118] E. P. Gross, "Structure of a quantized vortex in boson systems," *Il Nuovo Cimento (1955-1965)*, vol. 20, pp. 454–477, May 1961.

[119] E. P. Gross, "Hydrodynamics of a Superfluid Condensate," *Journal of Mathematical Physics*, vol. 4, pp. 195–207, Feb. 1963. Publisher: American Institute of Physics.

[120] L. Pitaevskii, "Vortex Lines in an imperfect Bose gas," *Soviet Physics JETP*, vol. 13, pp. 451–454, Aug. 1961.

[121] S. Strogatz, *Nonlinear Dynamics and Chaos*. New York: Perseus Books, 1 ed., 1994.

[122] D. S. Petrov, D. M. Gangardt, and G. V. Shlyapnikov, "Low-dimensional trapped gases," *Journal de Physique IV (Proceedings)*, vol. 116, pp. 5–44, Oct. 2004. Publisher: EDP Sciences.

[123] R. J. Marshall, G. H. C. New, K. Burnett, and S. Choi, "Exciting, cooling, and vortex trapping in a Bose-condensed gas," *Physical Review A*, vol. 59, pp. 2085–2093, Mar. 1999. Publisher: American Physical Society.

[124] M. J. Davis, S. A. Morgan, and K. Burnett, "Simulations of Bose Fields at Finite Temperature," *Physical Review Letters*, vol. 87, p. 160402, Sept. 2001. Publisher: American Physical Society.

[125] D. J. Griffiths, *Introduction to Quantum Mechanics*. New Jersey: Pearson Education, 2 ed., 2005.

[126] Y. Castin and R. Dum, "Low-temperature Bose-Einstein condensates in time-dependent traps: Beyond the $U(1)$ symmetry-breaking approach," *Physical Review A*, vol. 57, pp. 3008–3021, Apr. 1998. Publisher: American Physical Society.

[127] J. Mathews and R. L. Walker, *Mathematical Methods of Physics*. California: Addison-Wesley Publishing Company, 2 ed., 1969.

[128] A. Recati, N. Pavloff, and I. Carusotto, "Bogoliubov theory of acoustic Hawking radiation in Bose-Einstein condensates," *Physical Review A*, vol. 80, p. 043603, Oct. 2009. Publisher: American Physical Society.

[129] J. Meng, H. Toki, S. G. Zhou, S. Q. Zhang, W. H. Long, and L. S. Geng, "Relativistic continuum Hartree Bogoliubov theory for ground-state properties of exotic nuclei," *Progress in Particle and Nuclear Physics*, vol. 57, pp. 470–563, Oct. 2006.

[130] C. Gaul and C. A. Muller, "Bogoliubov excitations of disordered Bose-Einstein condensates," *Physical Review A*, vol. 83, p. 063629, June 2011.

[131] M. Edwards, P. A. Ruprecht, K. Burnett, R. J. Dodd, and C. W. Clark, "Collective Excitations of Atomic Bose-Einstein Condensates," *Physical Review Letters*, vol. 77, pp. 1671–1674, Aug. 1996. Publisher: American Physical Society.

[132] F. Dalfovo, S. Giorgini, L. P. Pitaevskii, and S. Stringari, "Theory of Bose-Einstein condensation in trapped gases," *Reviews of Modern Physics*, vol. 71, pp. 463–512, Apr. 1999.

[133] W. Ketterle, D. S. Durfee, and D. M. Stamper-Kurn, "Making, probing and understanding Bose-Einstein condensates," p. 87.

[134] G. Baym and C. J. Pethick, "Ground-State Properties of Magnetically Trapped Bose-Condensed Rubidium Gas," *Physical Review Letters*, vol. 76, pp. 6–9, Jan. 1996.

[135] S. Simon, *The Oxford Solid State Basics*. Oxford: Oxford University Press, 1 ed., 2005.

[136] A. D. Martin and J. Ruostekoski, "Nonequilibrium quantum dynamics of atomic dark solitons," *New Journal of Physics*, vol. 12, p. 055018, May 2010.

[137] K. Xu, Y. Liu, D. E. Miller, J. K. Chin, W. Setiawan, and W. Ketterle, "Observation of Strong Quantum Depletion in a Gaseous Bose-Einstein Condensate," *Physical Review Letters*, vol. 96, p. 180405, May 2006.

[138] T. D. Lee, K. Huang, and C. N. Yang, "Eigenvalues and Eigenfunctions of a Bose System of Hard Spheres and Its Low-Temperature Properties," *Physical Review*, vol. 106, pp. 1135–1145, June 1957.

[139] R. Lopes, C. Eigen, N. Navon, D. Clment, R. P. Smith, and Z. Hadzibabic, "Quantum depletion of a homogeneous Bose-Einstein condensate," *Physical Review Letters*, vol. 119, p. 190404, Nov. 2017. arXiv: 1706.01867.

[140] A. Miller, D. Pines, and P. Nozires, "Elementary Excitations in Liquid Helium," *Physical Review*, vol. 127, pp. 1452–1464, Sept. 1962. Publisher: American Physical Society.

[141] L. Landau, "Theory of the Superfluidity of Helium II," *Physical Review*, vol. 60, pp. 356–358, Aug. 1941. Publisher: American Physical Society.

[142] M. Isoard and N. Pavloff, "Departing from Thermality of Analogue Hawking Radiation in a Bose-Einstein Condensate," *Physical Review Letters*, vol. 124, p. 060401, Feb. 2020. Publisher: American Physical Society.

[143] J. R. Muoz de Nova, K. Golubkov, V. I. Kolobov, and J. Steinhauer, "Observation of thermal Hawking radiation and its temperature in an analogue black hole," *Nature*, vol. 569, pp. 688–691, May 2019. Number: 7758 Publisher: Nature Publishing Group.

[144] A. I. Vdovin and A. A. Dzhioev, "Thermal Bogoliubov transformation in nuclear structure theory," *Physics of Particles and Nuclei*, vol. 41, pp. 1127–1131, Dec. 2010.

[145] A. L. Goodman, "Hartree–Fock–Bogoliubov theory with applications to nuclei," *Adv. Nucl. Phys.; (United States)*, vol. 11:1, June 1979. Institution: Department of Physics, Tulane University, New Orleans, Louisiana.

[146] N. P. Proukakis, S. Gardiner, M. Davis, and M. Szymanska, *Quantum Gases: Finite Temperature and Non-Equilibrium Dynamics*, vol. 1 of *Cold Atoms*. London: Imperial College Press, 1 ed., 2013.

[147] C. W. Gardiner, "Particle-number-conserving Bogoliubov method which demonstrates the validity of the time-dependent Gross-Pitaevskii equation for a highly condensed Bose gas," *Physical Review A*, vol. 56, pp. 1414–1423, Aug. 1997. Publisher: American Physical Society.

[148] M. Girardeau and R. Arnowitt, "Theory of Many-Boson Systems: Pair Theory," *Physical Review*, vol. 113, pp. 755–761, Feb. 1959. Publisher: American Physical Society.

[149] S. A. Gardiner and S. A. Morgan, "Number-conserving approach to a minimal self-consistent treatment of condensate and noncondensate dynamics in a degenerate Bose gas," *Physical Review A*, vol. 75, p. 043621, Apr. 2007. Publisher: American Physical Society.

[150] M. Lewenstein and L. You, "Quantum Phase Diffusion of a Bose-Einstein Condensate," *Physical Review Letters*, vol. 77, pp. 3489–3493, Oct. 1996. Publisher: American Physical Society.

[151] K. Jacobs and D. A. Steck, "A straightforward introduction to continuous quantum measurement," *Contemporary Physics*, vol. 47, pp. 279–303, Sept. 2006. Publisher: Taylor & Francis _eprint: https://doi.org/10.1080/00107510601101934.

[152] C. W. Gardiner and P. Zoller, *Quantum Noise*. Heidelberg, Germany: Springer, 3 ed., 2004.

[153] D. Manzano, "A short introduction to the Lindblad master equation," *AIP Advances*, vol. 10, p. 025106, Feb. 2020.

[154] K. Jacobs, *Stochastic Processes for Physicists: Understanding Noisy Systems*. New York: Cambridge University Press, 1 ed., 2010.

[155] C. W. Gardiner, *Handbook of Stochastic Methods: for Physics, Chemistry and the Natural Sciences*. Boca Raton, Florida: Springer, 2 ed., 1997.

[156] P. E. Kloeden and E. Platen, *Numerical Solution of Stochastic Differential Equations*. Berlin, Heidelberg: Springer Berlin Heidelberg, 1992.

[157] J. Stewart, *Essential Calculus*. Belmont, CA: Brooks/Cole, 2 ed., 2013.

[158] H. M. Wiseman and G. J. Milburn, *Quantum Measurement and Control*. New York: Cambridge University Press, 1 ed., 2010.

[159] R. v. Handel, J. K. Stockton, and H. Mabuchi, "Modelling and feedback control design for quantum state preparation," *Journal of Optics B: Quantum and Semiclassical Optics*, vol. 7, pp. S179–S197, Sept. 2005. Publisher: IOP Publishing.

[160] G. J. Milburn and D. F. Walls, *Quantum Optics*. Berlin, Heidelberg: Springer, 2 ed., 2008.

[161] S. S. Szigeti, S. J. Adlong, M. R. Hush, A. R. R. Carvalho, and J. J. Hope, "Robustness of system-filter separation for the feedback control of a quantum harmonic oscillator undergoing continuous position measurement," *Physical Review A*, vol. 87, p. 013626, Jan. 2013. Publisher: American Physical Society.

[162] L. Bouten, R. Van Handel, and M. R. James, "An Introduction to Quantum Filtering," *SIAM Journal on Control and Optimization*, vol. 46, pp. 2199–2241, Jan. 2007.

[163] G. Gauthier, I. Lenton, N. M. Parry, M. Baker, M. J. Davis, H. Rubinsztein-Dunlop, and T. W. Neely, "Direct imaging of a digital-micromirror device for configurable microscopic optical potentials," *Optica*, vol. 3, pp. 1136–1143, Oct. 2016. Publisher: Optical Society of America.

[164] S. D. Wilson, A. R. R. Carvalho, J. J. Hope, and M. R. James, "Effects of measurement backaction in the stabilization of a Bose-Einstein condensate through feedback," *Physical Review A*, vol. 76, p. 013610, July 2007.

[165] A. S. Bradley, S. J. Rooney, and R. G. McDonald, "Low-dimensional stochastic projected Gross-Pitaevskii equation," *PHYSICAL REVIEW A*, p. 13, 2015.

[166] C. W. Gardiner and M. J. Davis, "The stochastic GrossPitaevskii equation: II," *Journal of Physics B: Atomic, Molecular and Optical Physics*, vol. 36, pp. 4731–4753, Dec. 2003.

[167] M. Le Bellac, *Quantum Physics*. Cambridge: Cambridge University Press, 1 ed., 2006.

[168] A. Hopkins, K. Jacobs, S. Habib, and K. Schwab, "Feedback cooling of a nanomechanical resonator," *Physical Review B*, vol. 68, p. 235328, Dec. 2003.

[169] M. Koch, C. Sames, A. Kubanek, M. Apel, M. Balbach, A. Ourjoumtsev, P. W. H. Pinkse, and G. Rempe, "Feedback Cooling of a Single Neutral Atom," *Physical Review Letters*, vol. 105, p. 173003, Oct. 2010.

[170] M. Iwasaki, T. Yotsuya, T. Naruki, Y. Matsuda, M. Yoneda, and K. Aikawa, "Electric feedback cooling of single charged nanoparticles in an optical trap," *Physical Review A*, vol. 99, p. 051401, May 2019.

[171] P. L. Knight and P. W. Milonni, "The Rabi frequency in optical spectra," *Physics Reports*, vol. 66, pp. 21–107, Dec. 1980.

[172] M. Plancherel and M. Leffler, "Contribution tude de la reprsentation Dune fonction arbitraire par des intgrales dfinies," *Rendiconti del Circolo Matematico di Palermo (1884-1940)*, vol. 30, pp. 289–335, Dec. 1910.

[173] G. Auletta, M. Fortunato, and G. Parisi, *Quantum Mechanics*. Cambridge: Cambridge University Press, 1 ed., 2009.

[174] O. Morizot, Y. Colombe, V. Lorent, H. Perrin, and B. M. Garraway, "Ring trap for ultracold atoms," *Physical Review A*, vol. 74, p. 023617, Aug. 2006. Publisher: American Physical Society.

[175] T. P. Meyrath, F. Schreck, J. L. Hanssen, C.-S. Chuu, and M. G. Raizen, "Bose-Einstein condensate in a box," *Physical Review A*, vol. 71, p. 041604, Apr. 2005. Publisher: American Physical Society.

[176] A. Zangwill, *Modern Electrodynamics*. Cornwall: Cambridge University Press, 1 ed., 2018.

[177] T.-L. Ho and M. Ma, "Quasi 1 and 2d Dilute Bose Gas in Magnetic Traps: Existence of Off-Diagonal Order and Anomalous Quantum Fluctuations," p. 10.

[178] K. Damle, T. Senthil, S. N. Majumdar, and S. Sachdev, "Phase transition of a Bose gas in a harmonic potential," *Europhysics Letters (EPL)*, vol. 36, pp. 7–12, Oct. 1996.

[179] W. J. Mullin, "Bose-Einstein condensation in a harmonic potential," *Journal of Low Temperature Physics*, vol. 106, pp. 615–641, Mar. 1997.

[180] P. B. Blakie, A. S. Bradley, M. J. Davis, R. J. Ballagh, and C. W. Gardiner, "Dynamics and statistical mechanics of ultra-cold Bose gases using c-field techniques," *Advances in Physics*, vol. 57, pp. 363–455, Sept. 2008. Publisher: Taylor & Francis _eprint: https://doi.org/10.1080/00018730802564254.

[181] G. R. Dennis, J. J. Hope, and M. T. Johnsson, "XMDS2: Fast, scalable simulation of coupled stochastic partial differential equations," *Computer Physics Communications*, vol. 184, pp. 201–208, Jan. 2013.

[182] M. J. Werner and P. D. Drummond, "Robust Algorithms for Solving Stochastic Partial Differential Equations," *Journal of Computational Physics*, vol. 132, pp. 312–326, Apr. 1997.

[183] J. R. Cash and A. H. Karp, "A variable order Runge-Kutta method for initial value problems with rapidly varying right-hand sides," *ACM Transactions on Mathematical Software*, vol. 16, pp. 201–222, Sept. 1990.

[184] C. Rackauckas and Q. Nie, "Adaptive methods for stochastic differential equations via natural embeddings and rejection sampling with memory," *Discrete and continuous dynamical systems. Series B*, vol. 22, no. 7, pp. 2731–2761, 2017.

[185] C. Rackauckas and Q. Nie, "Stability-Optimized High Order Methods and Stiffness Detection for Pathwise Stiff Stochastic Differential Equations," *arXiv:1804.04344 [math]*, Apr. 2018. arXiv: 1804.04344.

[186] S. S. Szigeti, *Controlled Bose-Condensed Sources for Atom Interferometry*. PhD Thesis, Australian National University, Canberra, 2013.

[187] I. Danshita and P. Naidon, "Bose-Hubbard ground state: Extended Bogoliubov and variational methods compared with time-evolving block decimation," *Physical Review A*, vol. 79, p. 043601, Apr. 2009. Publisher: American Physical Society.

[188] T. Hashizume, J. C. Halimeh, and I. P. McCulloch, "Hybrid infinite time-evolving block decimation algorithm for long-range multidimensional quantum many-body systems," *Physical Review B*, vol. 102, p. 035115, July 2020. Publisher: American Physical Society.

[189] R. Ors and G. Vidal, "Infinite time-evolving block decimation algorithm beyond unitary evolution," *Physical Review B*, vol. 78, p. 155117, Oct. 2008. Publisher: American Physical Society.

[190] S. R. White, "Density-matrix algorithms for quantum renormalization groups," *Physical Review B*, vol. 48, pp. 10345–10356, Oct. 1993. Publisher: American Physical Society.

[191] J. Dukelsky and S. Pittel, "The density matrix renormalization group for finite fermi systems," *Reports on Progress in Physics*, vol. 67, pp. 513–552, Mar. 2004. Publisher: IOP Publishing.

[192] C. Zhao, L. Jiang, X. Liu, W. M. Liu, X. Zou, and H. Pu, "Hartree-Fock-Bogoliubov theory of dipolar Fermi gases," *Physical Review A*, vol. 81, p. 063642, June 2010.

[193] A. Altland and B. Simons, *Condensed Matter Field Theory*. Cambridge: Cambridge University Press, 2 ed., 2010.

[194] G. Adesso, S. Ragy, and A. R. Lee, "Continuous Variable Quantum Information: Gaussian States and Beyond," *Open Systems & Information Dynamics*, vol. 21, p. 1440001, June 2014.

[195] L. F. Lafuerza and R. Toral, "On the Gaussian Approximation for Master Equations," *Journal of Statistical Physics*, vol. 140, pp. 917–933, Sept. 2010.